HIGH-PRESSURE COMPLIANT SYNTACTIC FOAM FOR HYDRAULIC NOISE CONTROL

A Dissertation
Presented to
The Academic Faculty

by

Elliott Gruber

In Partial Fulfillment
Of the Requirements for the Degree
Doctor of Philosophy in Mechanical Engineering

Georgia Institute of Technology

December 2016

HIGH-PRESSURE COMPLIANT SYNTACTIC FOAM FOR HYDRAULIC NOISE CONTROL

Approved by:

Dr. Kenneth A. Cunefare, Advisor
School of Mechanical Engineering
Georgia Institute of Technology

Dr. Lawrence Jacobs
College of Engineering
Georgia Institute of Technology

Dr. Michael Leamy
School of Mechanical Engineering
Georgia Institute of Technology

Dr. William Koros
School of Chemical and Biomolecular Engineering
Georgia Institute of Technology

Dr. Karim Sabra
School of Mechanical Engineering
Georgia Institute of Technology

Date Approved: November 11, 2016

ACKNOWLEDGEMENTS

At many time completing a doctoral degree feels like a solo endeavor; however, it is an undertaking which requires a great deal of support and encouragement from a variety of people. First, I must thank my parents who have raised me into the person I am today. Often times, I was willing to settle for good enough in high school but they were always there pushing me to fulfill my capabilities. This led to a few visits to Georgia Tech, first in the spring of 2006 and then the winter of 2007; those visits lead to my matriculation as a Bachelor's of Science and the onwards to the current graduate program. It is because of my parents that I was able to complete all of my degrees. I must also thank my advisor Dr. Cunefare. The first time I met Dr. Cunefare was during his introductory lecture in my Senior Design section. He described the difference between a technician and an engineer, emphasizing the need to understand all aspects of a technical problem. During his time as my advisor, he demonstrated how to understand all aspects of a problem and how to pursue solutions. His guidance has greatly developed my technical and communication skills. Next, I must also thank my reading committee. They all provided valuable insight following my proposal which led to successful completion of the research. Specifically, Dr. Koros's advice and knowledge about permeation and fluorination helped greatly with all the following research. I also need to thank Dr. Yao's lab group, specifically Adam Maffe, for allowing me to use their fume hoods repeatedly. Furthermore, Adrian Samaniego at Inhance products provided very helpful assistance with both setting up the fluorinator and how to safely and successfully conduct a fluorination.

It is also very important to thank the people who paid for everything, Danfoss Power Solutions. I interned with them for the summer of 2013 after which the picked up the project the following Spring have continued to support me and the project since then.

I was also fortunate to have excellent support from my peers through my entire time at grad school. When I first moved into my office, it was occupied by Nick Earnhart and Ben Beck, both of whom were on the final stages of their dissertation. The knowledge they passed down about the process greatly eased my time in grad school. Next is Ellen Skow who started with the group at the same time as me. Together, we progressed through grad school often lending support to each other when graduation felt years away. There were many other officemates through the years who also deserve gratitude: Ryan Salmon, Rene Roberts, Kamil Kocak, Matt Edwards, Jamie Burdell, John McGrael, Aprameya Satish, Nathan Pedigo, Ken Marek and Man Gupta. There are also countless other friends who all helped in their own way throughout my time here who are too numerous to name. I would also be remiss if I forgot to thank the Dunkin Donuts in the student center for serving the most delicious iced coffee and filling my caffeine needs.

To the future graduate student looking for a very specific answer to a semi-related problem, try Chapter 5 the answer is always in Chapter 5. Also, check out the reference list, which is where I learned everything anyway.

TABLE OF CONTENTS

LIST OF TABLES

LIST OF FIGURES

NOMENCLATURE

A	Area	ρ	Density
C	Capacitance, Concertation gradient, Coherence	Π	Acoustic power
D	Diffusion coefficient	λ	Wavelength, Lame's parameter
E	Young's modulus	ω	radial frequency
F	Rate of transfer per unit area	ν	Poisson's ratio
G	Shear modulus, Spectral density	σ	Stress
K	Bulk Modulus	ε	Strain
L	Inductance	δ	Phase angle
M	Mach number	γ	Ratio of specific heats
P	Pressure	IMP	Internal Microsphere Pressure
Q	Flow rate	TL	Transmission Loss
R	Resistance, Universal gas constant	$*$	Effective
S	Cross sectional area		
T	Power transmission coefficient, Temperature		
U	Strain energy		
V	Volume, Mean flow rate		
X	Material Modulus		
Z	Impedance		
c	speed of sound, damping, volume fraction		
e	Deviatoric strain		
f	Frequency		
i	inner		
j	Extrema of bessel functions		
k	spring stiffness, wavenumber		
m	mass		
o	outer		
r	Radius		
s	Deviatoric stress		
t	Thickness, transfer matrix elements		
u	Particle velocity		
v	Specific volume		
z	Compressibility factor		

SUMMARY

Pressure fluctuations within a hydraulic system, commonly known as noise, create problems, such as leaks and breakout noise, within the system and necessitate treatment. Prior work has demonstrated the effectiveness of a flow-through expansion chamber with a syntactic foam liner; the device is known as a suppressor. Syntactic foam is a term of art which refers to a material fabricated from a host matrix and specifically selected inclusions to alter the engineering properties of the composite body. The syntactic foam used to treat noise is a voided polymer; the voids are created by hollow microspheres which collapse when exposed to a critical value of hydrostatic pressure. The voids within the host polymer increase the effective compliance to the foam; the increase in compliance decreases the noise within the system. As the system pressure increases, the voids within the foam shrink, reducing the compliance of the foam and its noise control effectiveness. The current work seeks to find a method to limit the voids from contracting with increasing system pressure. The work is conducted by increasing the internal pressures of the microspheres and fluorinating their surface to inhibit loss of internal pressure before fabrication. The increased pressure within the microspheres prevents voids created by the collapsed microspheres from losing volume as drastically as unpressurized voids at higher pressures. The result is functional noise control at elevated pressure, up to the maximum system operating pressure of 35 MPa.

CHAPTER 1

INTRODUCTION

Pressure ripple within hydraulic circuits can cause significant problems for the system and its operator; effective treatment of the pressure ripple will reduce the severity of these problems – improving system functionality, longevity and operator comfort. Pressure ripple, more commonly known as fluid-borne noise, is treated in a hydraulic system by a specific acoustic impedance change within the flow circuit; the impedance change is caused by either resonance, such as an alternate flow path, or a change in the dimensions or boundaries of the waveguide – generally referred to as changing the compliance of the waveguide. Generally, altering the compliance is a more effective method for broadband noise treatment than devices which employ resonance as their primary noise control phenomena for devices of similar volume [1-4]. Prior work has demonstrated effective noise control within a variety of traditional noise-control devices which employ syntactic foam to increase the compliance within the device [4, 5]. It has been demonstrated that increasing compliance within a confined single device effectively treats noise for the entire hydraulic system, i.e. the compliance does not need to be distributed throughout the system for noise control. The drawback to the current generation of syntactic foam is the reduction of noise control effectiveness at pressures above 7 MPa because the foam loses compliance at these pressures.

Syntactic foam is a term of art which covers any host material with specifically selected inclusions to alter the engineering properties of the host; common examples of syntactic foams are concrete, fiberglass and the dielectric materials used as filler in capacitors. The syntactic foam under examination is a polymer host matrix with hollow

microsphere inclusions; the microspheres collapse at a critical elevated system pressure; the collapsed spheres form voids causing the compliance of the foam to increase. The compliance of the foam is a function of the void fraction created by the collapsed microspheres; as systems pressure rise, voids shrink and the foam is less effective at treating noise. This dissertation will analyze how to prevent the voids from losing their volume as precipitously with increasing system pressure without making the microspheres or voids prohibitively stiff. Effective noise control is especially desirable as system pressure increases because acoustic energy is generally proportional to the system pressure; therefore, it is imperative to effectively treat noise at elevated system pressures, up to a maximum system pressure of 35 MPa.

1.1 Research Motivation

The dynamic portion of pressure, akin to the AC component of an electrical signal, causes several problems within a hydraulic system. The pressure variation within the fluid places additional stress on sealing surfaces potentially overriding their rated sealing pressure and causing leakage. Fluid-borne noise can also cause difficulty in accurately positioning end-effectors, whose position and velocity is determined by pressure and flow. In addition, the fluid-borne noise couples with the structural components of the system (pipes, hoses, flanges, panels, etc.) to vibrate these components, also known as structure-borne vibration. The cyclical nature of the stress creates fatigue cycles on components, shortening their lifetimes. The structure-borne vibrations may also shake the machine operator via a coupling with his chair within the cab for mobile applications. This creates a twofold problem. First, this condition may be very uncomfortable for an operator to spend an eight-hour work day, more rapidly

fatiguing the operator which both reduces his efficiency and increasing the likelihood of operational mistakes. Second, it may also create a biodynamic feed-through loop: a loop where the vibration of the machine causes the operator to shake the controls further vibrating the machine, which can destabilize the entire machine [6]. Furthermore, the vibrating structural elements may couple with the surrounding airborne environment to create breakout noise. The noise may reach hazardous levels, necessitating the usage of hearing protection; at lower levels, the noise may still disrupt communication between on-site workers, which is necessary to operate a safe work environment around heavy machinery [7]. New Holland Agriculture, a large manufacturer of hydraulic equipment, found in a survey of their customers that cabin noise is the third most important factor for users purchasing a new piece of equipment, ahead of reliability and price, and behind adequate horsepower and good fuel economy [8]. Treating the fluid-borne noise will reduce the severity of all associated problems in the fluid, structure and air, potentially eliminating some of them – including quieting the cabin environment [9].

The operating range of system pressure in many hydraulic systems is from system idling pressure, slightly above atmospheric pressure depending on system, to 35 MPa; the current generation of foam loses effectiveness at pressures above 7 MPa; hence, a new solution is needed [4, 10]. If it is assumed the energy lost to heat and noise is proportional to pressure, it follows that higher system pressures have more acoustic energy. Furthermore, it is essential to effectively treat noise at these pressures as the problems associated with noise are most severe at high pressure. It is hypothesized that increasing the initial internal pressure of the microspheres will improve the noise control effectiveness at high pressure. The aim of this work is to determine how to raise the

internal pressure of the microspheres; to determine what pressure is necessary to achieve effective noise control over the entire pressure range, up to 35 MPa; and to develop a foam which is comprised of specifically prepared microspheres; in addition, the host polymer will be analyzed to determine the optimal host for effective noise control.

An effective noise control solution must treat fluid-borne noise in the frequencies which carry the most acoustic energy. Figure 1-1 and Figure 1-2 show example power spectra for two system pressures, 10.3 and 20.7 MPa. The peak acoustic pressure for both systems pressure is on the order of MPa, which is several orders of magnitude large than any airborne acoustic event. It is important to note that the overall acoustic power increases with increasing system pressure. A pump typically produces noise in the piston-passing frequency as well as its harmonics; for the system shown the pump passing frequency is 225 Hz and the energy associated harmonics up to 3 kHz is non-negligible. Therefore, an effective noise control solution needs to be broadband in order to treat noise across the enter frequency range of interest. Other hydraulic systems will generate different spectral content because the pump passing frequency may be different or the pumping unit may change either in number of pistons or in pumping mechanism entirely; as a result, it will be essential to treat noise at these frequencies which now carry acoustic energy. Digital hydraulics is a developing system architecture and control scheme using extremely quick opening and closing valves to create an impulse-like pressure pulse in the system [11] which carry acoustic energy across all frequencies, necessitating a broadband noise control solution. It has been shown from prior work that a flow-through suppressor treats noise effectively across a broad frequency band [1, 2, 12, 13].

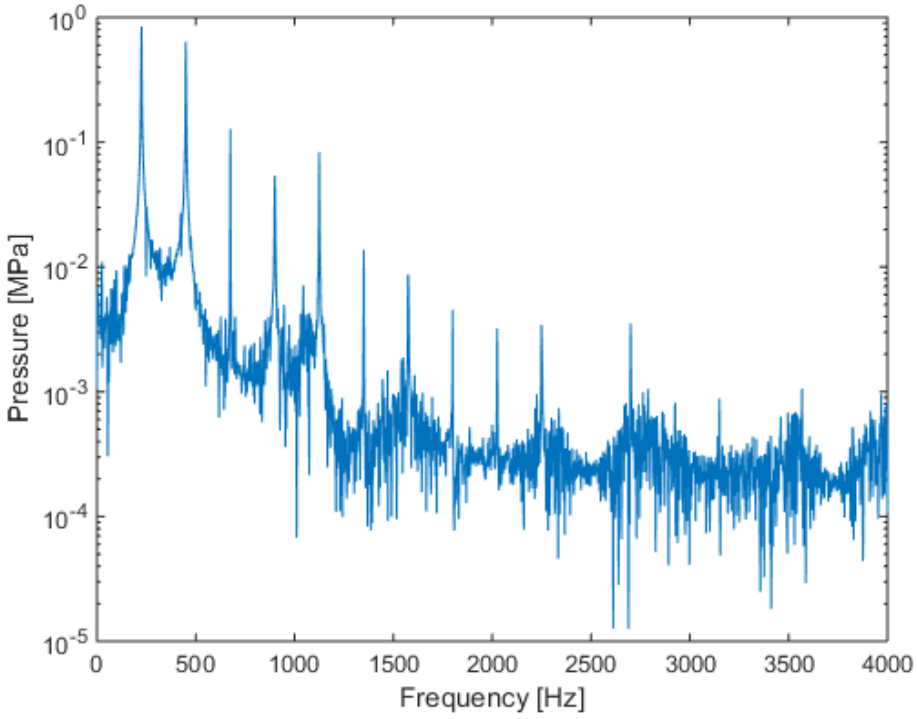

Figure 1-1: Power spectrum of pressure ripple at a system pressure of 10.3 MPa

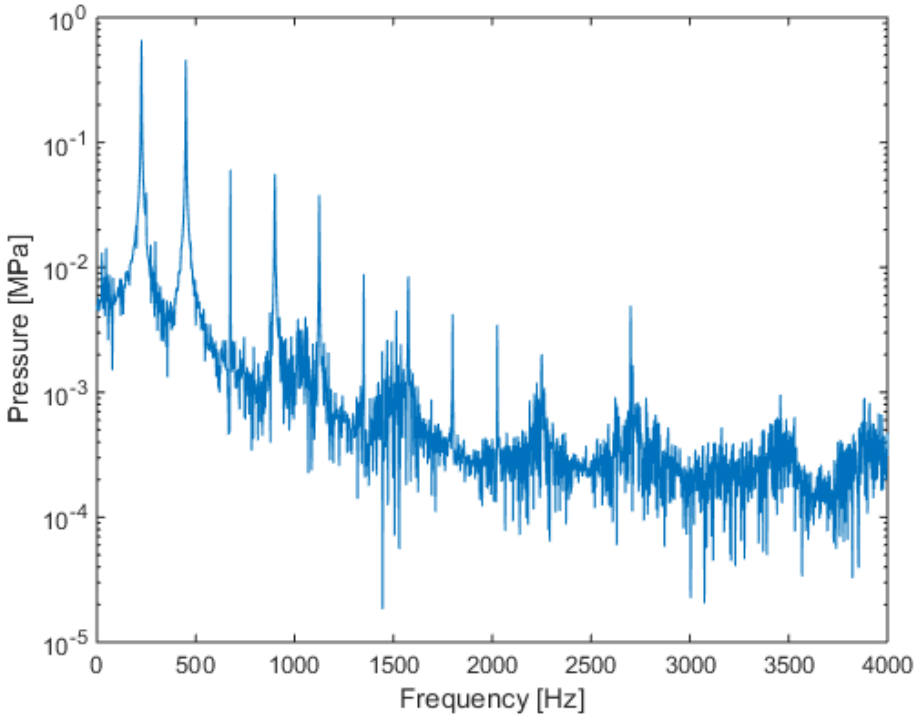

Figure 1-2: Power spectrum of pressure ripple at a system pressure of 20.7 MPa

1.2 Research Objectives

The objective of the research discussed within is to develop a syntactic foam which effectively treats noise over the pressure range of interest, from zero to 35 MPa, and accurately model its mechanical properties. It is beneficial to predict the mechanical properties of the composite foam for prediction and optimization. Accurate prediction of the material properties will allow for other modeling efforts to be utilized in order to predict the effect that inclusion of the foam will have on the system. The modeling of the syntactic foams is conducted through multiphase modeling, techniques which use the properties of the element and relative volumes to predict effective moduli [14-17]. Models for predicting the noise control effectiveness have been developed for several noise control devices which employ syntactic foam, such as quarter- and half- wave resonators, Helmholtz resonators and flow-through suppressors [3-5, 18-20]. If the material properties of the foam are known, these models can be used to predict the behavior of a device with the developed foam. Furthermore, implementation of the models will inform design decisions to determine the optimal mechanical properties for effective noise treatment.

1.3 Research Approach

It is hypothesized that by altering the voids created by collapsed microspheres so the voids do not lose their volume at higher pressure, the composite foam will remain compliant at higher pressures, increasing its effectiveness for noise control at those pressures. The voids behave as gas bubbles; therefore, it is predicted increasing the internal pressure of the void will decrease its volumetric loss at elevated pressures. At present, the author was unable to find microspheres with an initial pressure above

atmospheric pressure or any literature published on increasing the internal pressure of a microsphere.

Microspheres are on the order of hundreds of microns in diameter or smaller and have a monolithic wall, presenting no apparent way to increase the mass of gas with in microsphere. The mass of gas is considered because the volume of gas fluctuates with ambient conditions such as pressure and temperature; while mass is independent of either quantity and increased mass will lead to higher pressures in a fixed volume. One potential mechanism to increase the internal pressure is to permeate a gas across the microsphere wall and then alter the chemistry of the microsphere material to prevent the gas from permeating out of the microsphere when the exterior pressure is released.

Once the pressurized microspheres have been prepared, they are incorporated into a host matrix of a specifically selected host polymer. The foam is subjected to a variety of tests to both measure the mechanical properties and measure the noise control effectiveness of the foam. The noise control data is compared against previously measured data to determine the improvement in noise control effectiveness over the previous generation of foam. The measured mechanical data is also used to validate the material modeling conducted.

1.4 Overview of Dissertation

The following chapters will outline the background of the work, and discuss the current state of the art of the syntactic foam, both in terms of modeling its physical properties and construction. Then a method for measuring the wavefield in a hydraulic test circuit will be presented as a means for determining noise control effectiveness. The dissertation will finish with conclusions. The background of the work will discuss the

source of the noise as well as prior work done to treat noise and discuss their shortcomings. The modeling chapter will discussed which modeling techniques are used and how they are applied to model the foam. The following chapter discusses how to prepare the foam both the microspheres and the host polymer. Next, the methodology of how to determine the wave fields both theoretically and experimentally will be discussed. Finally, experimental measurements will presented and then the dissertation will close with conclusions.

CHAPTER 2

BACKGROUND AND MOTIVATION

This chapter will review the current literature pertaining to hydraulic noise control and syntactic foam. The chapter will begin with an overview of the current state of the art in hydraulic noise control. The next section will discuss the current status of syntactic foam for the purpose of hydraulic noise control. The gaps within the literature will be presented as research opportunities for high pressure noise control in hydraulic systems in the final section.

2.1 Hydraulic Noise Control

Hydraulic noise control devices primarily function by creating an acoustic impedance mismatch within the hydraulic circuit which reduces the transmission of acoustic energy past the mismatch. Dissipative devices, similar to a car muffler, are not effective and will be discussed later. The devices are classified by the primary method employed to create the impedance mismatch and treat noise. The first type of device is resonant-style devices and the second type of device is compliant-style devices. Acoustic energy transmitted across an interface is a function of the specific acoustic impedance at the interface. At an interface with an alternate flow path, called a side branch, the transmitted acoustic energy is

$$T_{\Pi} = \frac{Z_b^2}{\left(\frac{\rho_0 c}{2S} + Z_b\right)^2}, \tag{2.1}$$

where ρ_0 is the ambient density of the medium, c is the speed of sound in the medium, S is cross sectional area of the primary flow path and Z_b is the impedance of the branch [21]. No acoustic energy is transmitted when Z_b is zero; furthermore, noise is significantly reduced for low values of Z_b. A zero impedance condition arises when a branch reaches one of its resonance frequencies [21]. In addition, noise will be reasonably well treated for low values of side-branch impedances.

The second type of hydraulic noise control changes the specific acoustic impedance at an interface by either changing the flow area or the material properties of the flow path. At a single interface with changing material properties or cross-sectional area the transmitted acoustic energy is

$$T_{\Pi} = \frac{4 \, Z_1/S_1 \; Z_2/S_2}{\left(Z_1/S_1 + Z_2/S_2 \right)^2}, \tag{2.2}$$

where Z is the acoustic impedance and S is the cross sectional area, and the subscript labels denote which media, where 1 is upstream and 2 is downstream of the impedance change [21]. In equation (2.2), noise is perfectly treated when the numerator is zero. Since the impedance and cross-sectional area of medium 1 are fixed, the only two parameters which can be altered are the impedance and cross-sectional area of medium 2. If the downstream cross sectional area, S_2, goes to infinity the numerator in equation (2.2) goes to zero and is significantly reduced for large values. Available volume for a noise control device on a mobile hydraulic application limits cross-sectional area from becoming sufficiently large and being an effective noise control option. The other option is to have zero impedance in the second media. Acoustic impedance is a function of bulk

modulus; a material with zero bulk modulus will have zero impedance. Similarly, a material with low bulk modulus will have low impedance and will treat noise effectively.

The side branch devices are analogous to resonant style devices with a proper selection of branch impedance shown in equation (2.1), Z_b, while compliant devices can be partially described by the changing media case. Flow-through compliant-style devices are not wholly described by equation (2.2) because they have a second media change at the downstream port of the device. Applying equation (2.2) at both ports individually is not sufficient to model a suppressor because this approach neglects any resonant behavior of a finite device. A relation for a device with two media and two area changes, i.e. flow from a pipe into a lined expansion chamber then back into a pipe, cannot be succinctly shown; however, equation (2.2) provides a general background to allow the problem to be understood.

A common metric used to classify noise control effectiveness is transmission loss. Transmission loss is the ratio of the incident acoustic energy to transmitted acoustic energy at an interface; it varies across frequency and is usually presented in a decibel quantity. Transmission loss is related to the acoustic power transmission coefficient through

$$TL = 10 \log\left(\frac{1}{T_{\Pi}}\right) = 10 \log\left(\frac{\Pi_i}{\Pi_t}\right) \tag{2.3}$$

where Π is the acoustic power, i is incident and t is transmitted. If the acoustic power transmission coefficient was zero, the transmission loss would be infinite and the noise would be perfectly controlled.

2.1.1 Resonant-style Noise Control Devices

Resonant-style noise control devices treat noise by using a resonant behavior to create the zero impedance condition necessary to treat noise. Common examples of such devices are Quincke-tubes, tuning cables and Helmholtz resonators. Quincke-tubes and tuning cables are often used interchangeably in commercial applications to refer to both quarter- and half-wave resonators. In order to prevent confusion, only quarter- and half-wave resonators will be used to refer to these devices.

Quarter-wave resonators support the resonance of a wavelength four times as long as the device; schematics of two types of this device, side branch and inline, are shown in Figure 2-1. Both device types function similarly; the branch path has a rigid end and an open end which support resonance at frequencies, *f*, corresponding to the odd integer multiples, *n*, of the length, *L*, of the branch,

$$f = \frac{nc}{4L}, n = 1, 3, 5, 7 \ldots . \tag{2.4}$$

An example transmission loss curve for a quarter-wave resonator is shown in Figure 2-2 with the dimensions of the device shown in Table 2-1. The device does not exhibit broadband noise control, which makes the device undesirable for hydraulic noise control. Figure 1-1 and Figure 1-2 show the power spectrum of noise found in a hydraulic system. It is most important to treat the noise at the frequencies with the highest acoustic energy. The noise presented in the figures has energy in the harmonics of the pump passing frequency of 225 Hz. It would seem a simple solution would be to create a quarter-wave resonator which treats noise at the harmonics. However, many practical systems will change the pumping frequency to adjust flow rate or achieve optimal fuel efficiency,

shifting the noise spectrum which will render a quarter-wave resonator inefficient at treating noise for all but a single usage condition. In addition, the size of the device scales in proportion to the wavelength of interest, which is proportional to the frequency which carries the largest amount of acoustic energy. For a nine piston pump operating at 1500 RPM, a typical pump in a typical operating condition, the frequency of interest is 225 Hz as shown in Figure 1-1 and Figure 1-2. Frequency and wavelength are related through

$$c = f\lambda\,, \tag{2.5}$$

where c is the speed of sound, f is the frequency and λ is the wavelength. In a hydraulic system, the speed of sound is approximately 1400 m/s which means the wavelength of interest is approximately 6 meters long. A quarter-wave resonator would need to be 1.5 meters long, which is too long for a practical hydraulic system.

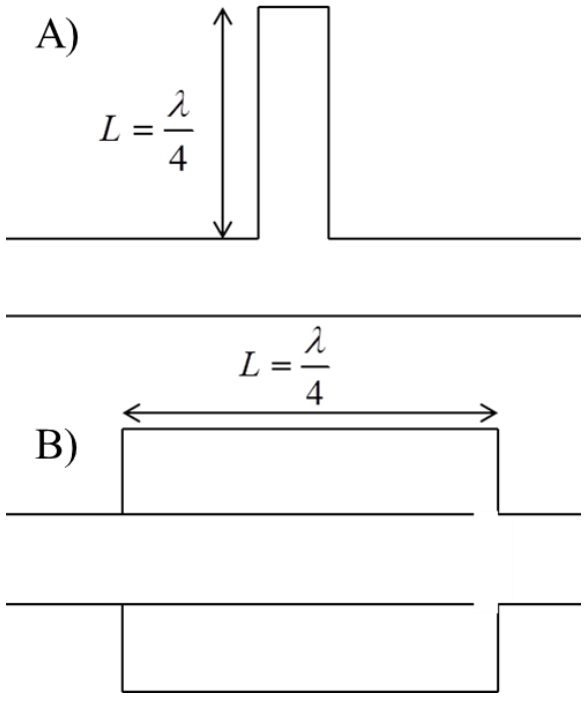

Figure 2-1: Quarter-wave resonator schematic A) Side-branch B) In-line (cross sectional views)

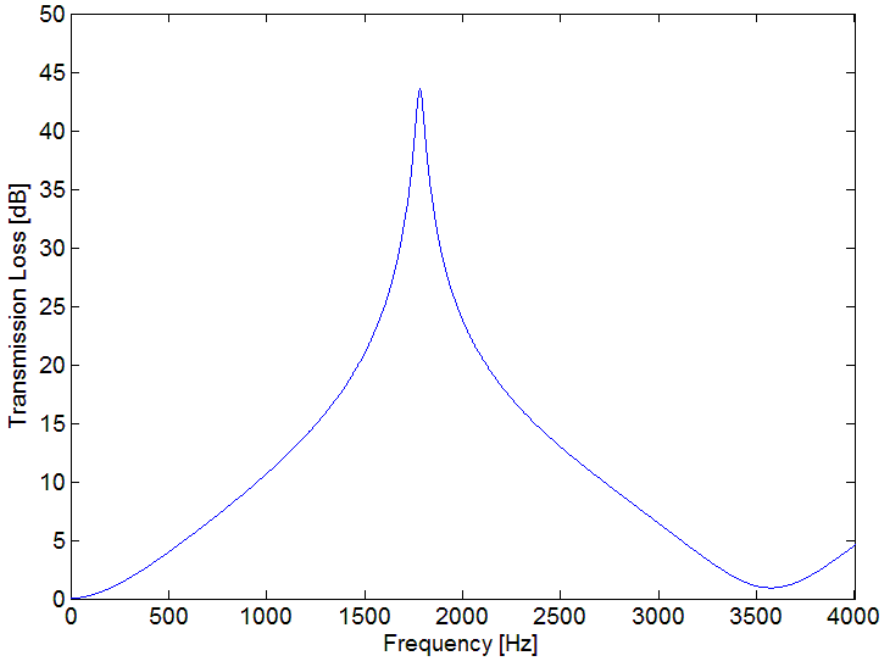

Figure 2-2: Transmission Loss curve for 1/4 wave resonator, with corresponding dimensions in Table 2-1

Table 2-1: Dimensions of quarter-wave resonator, dimensions match devices presented in Earnhart [4]

Dimension	Quantity
L	97.28 mm
r	31.75 mm
S_{pipe}	3.33 cm^2

Half-wavelength resonators function similarly to quarter-wavelength devices, but instead treating noise in the frequencies corresponding to half-wavelengths. Schematics of two half-wavelength resonators are shown in Figure 2-3. The dual open end conditions support the integer multiples of the half-wavelengths,

$$f = \frac{nc}{2L}, n = 1, 2, 3 \ldots . \tag{2.6}$$

The noise within the system is treated at the frequencies corresponding to these wavelengths. The drawbacks to a half-wave resonator are similar to the quarter-wave

resonator: narrowband noise control and relatively large size for frequencies of interest in a hydraulic system, on the order of three meters. The transmission loss curve of a half-wave resonator is narrow band, similar to the transmission loss curve for the quarter-wave resonator shown in Figure 2-2, scaling in frequency depending on the size of the alternate flow path for a half-wave resonator.

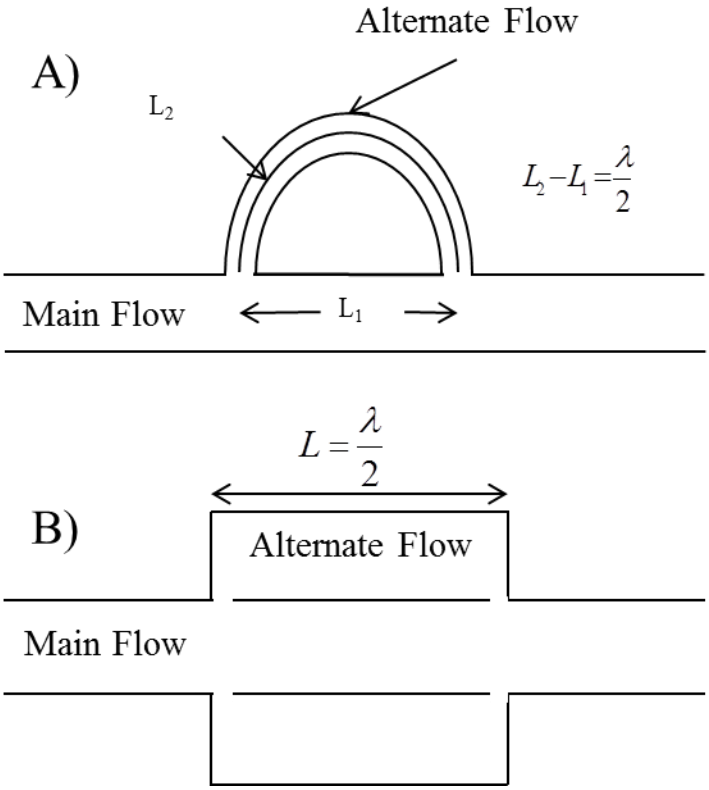

Figure 2-3: Half-wavelength resonator schematic

A third type of resonant-style noise control device commonly employed in a hydraulic system is a Helmholtz resonator; a schematic is shown in Figure 2-4. The important geometric features of the device are labeled. A Helmholtz resonator functions as a single degree-of-freedom system, analogous to an electrical RLC circuit or a mechanical spring-mass-damper system. The geometry of the resonator is used to find the analogous terms shown in Table 2-2, where ρ_0 is the density of the fluid, c is the speed of

sound in the fluid, S is the cross-sectional area of the neck, L' is the effective length of the neck, V is the volume of the chamber, R_r is the radiation resistance and R_w is the thermoviscous resistance [21]. The device only treats noise effectively at or near its resonance frequency,

$$\omega = \sqrt{k/m} = \sqrt{LC} = c\sqrt{\frac{S}{VL_n}}. \tag{2.7}$$

In equation (2.7), the resonance frequency scales with the speed of sound. The high speed of sound in hydraulic fluid would require a large volume and neck length. Alternatively, a small neck area can be used to reduce natural frequency but a small neck will also reduce noise control performance. A study by Ijas and Virvalo conducted an optimization for Helmholtz resonator geometry and found the optimal size to be a 40 cm long neck and a cavity with dimension of 8 cm by 50 cm; the selected geometry is too cumbersome for usage on a mobile hydraulic application [22]. Therefore, a Helmholtz resonator is not a suitable noise treatment solution for broadband noise control.

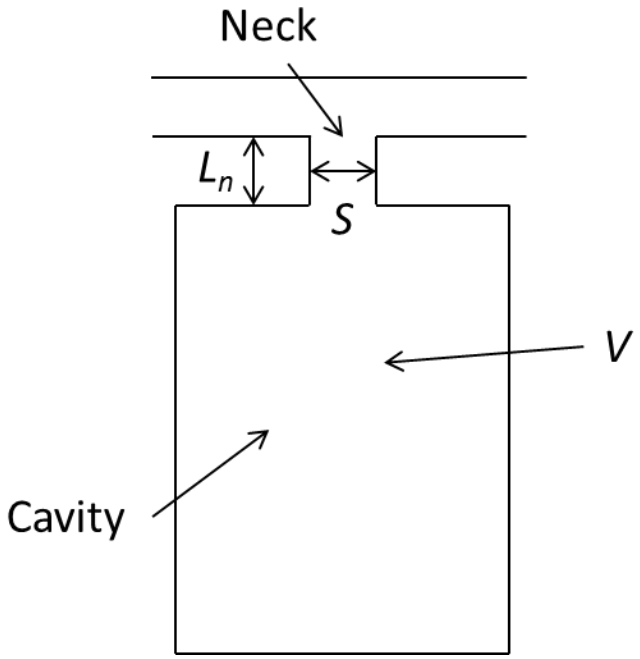

Figure 2-4: Helmholtz resonator schematic

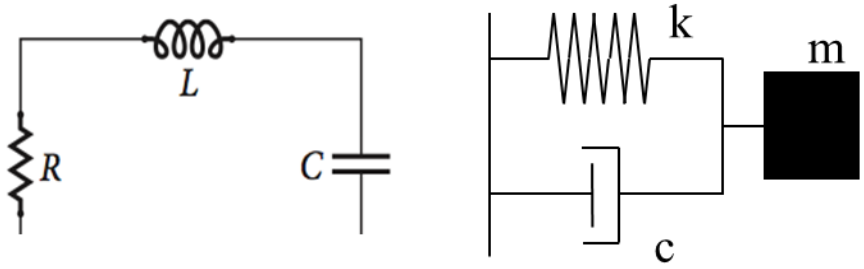

Figure 2-5: Equivalent electrical circuit and spring-mass-damper system

Table 2-2: Electric and mechanical quantities for a Helmholtz Resonator

Electric Quantity	Mechanical Quantity	Acoustic Relation
Inductance, L	Mass, m	$L = m = \rho_0 S L_n'$ (2.8)
Capacitance, C	Spring Stiffness, k	$\frac{1}{C} = k = \frac{\rho_0 c^2 S^2}{V}$ (2.9)
Resistance, R	Damping, c	$R = c = R_r + R_w$ (2.10)

Prior research has demonstrated that inclusion of syntactic foam will change the behavior of a resonant-style noise control device by reducing the effective sound speed within the device [4]. The reduction in sound speed means the device can be reduced in

size and still treat noise in the relatively low frequencies which carry the majority of acoustic energy in a hydraulic system, as seen in Figure 1-1 and Figure 1-2. This follows from the analysis above; if the speed of sound in the hydraulic system is reduced from 1400 m/s, the wavelength associated with a given frequency will also be proportionally reduced. Furthermore, the syntactic foam used has a lossy component which also alters the noise control performance by absorbing acoustic energy [4]. The lossiness dulls the transmission loss peaks and valleys in the frequency regime, i.e. the magnitude of transmission loss for the frequencies with the highest transmission loss is less but the converse is true for the frequencies with the lowest transmission loss. However, inclusion of the foam does not change the repeated narrowband behavior of the resonant-style devices, so this class of devices does not clear the threshold of effective noise treatment for a hydraulic system. In addition, the properties of the foam change with system pressure, which will change the effective speed of sound within the chamber. Since resonant-style device performance changes based on speed of sound, the frequencies of high noise control will shift with system pressure if syntactic foam is included. Even for a system operating at a fixed speed, the resonant style device employing syntactic foam cannot be tuned for optimal performance over all pressures.

2.1.2 Compliant-style Noise Control Devices

Compliant-style devices create a change in specific acoustic impedance by altering cross-sectional area or propagation media. A common compliant-style noise control device used in airborne systems is a muffler on a car. The simplest compliant-style device used in hydraulic noise control is an expansion chamber, shown in Figure 2-6 [13]. Many other compliant-style devices are modifications to an expansion chamber.

A commercially-available device is the bladder-style suppressor; in addition, its prototypical analogue is the liner style suppressor [2, 12, 23-27]. The noise control behavior of both of these devices, as well as a plain expansion chamber, can be altered with: inlet and outlet extensions, a perforated diffuser and multiple chambers of varying dimensions [13].

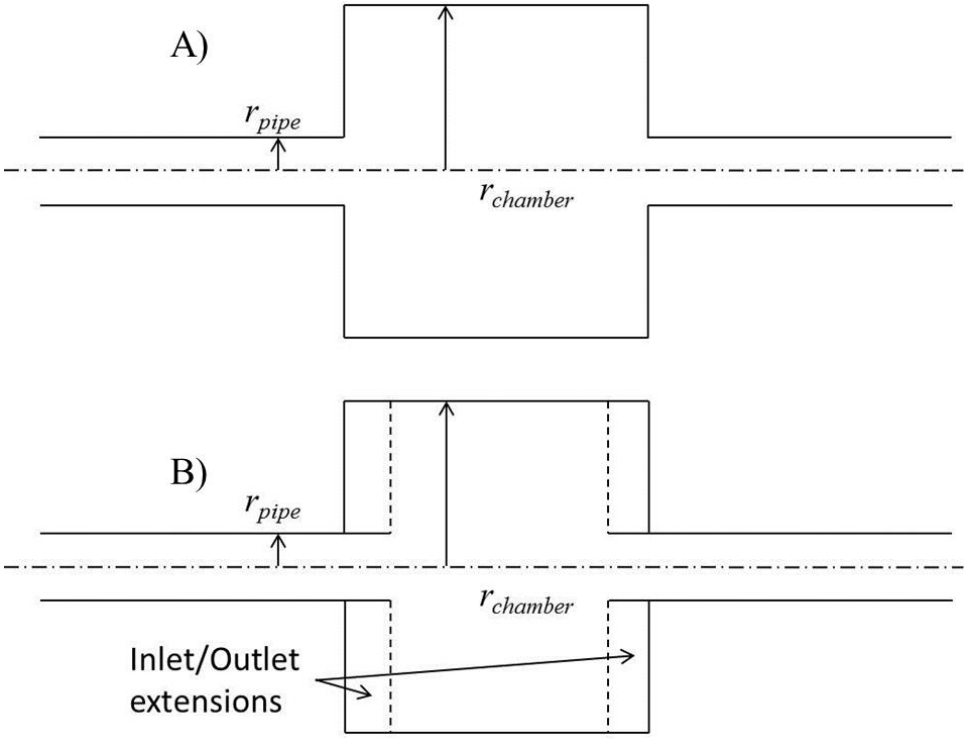

Figure 2-6: Expansion chamber, a) Without inlet/outlet extensions b) With inlet/outlet extensions

As stated previously, the simplest type of compliant-style noise control device is an expansion chamber, shown in Figure 2-6. The change in cross sectional area between the pipe, S_{pipe}, and the chamber, $S_{chamber}$, defined by the radii, r_{pipe} of the inlet pipe and $r_{chamber}$ of the chamber, changes the specific acoustic impedance which reduces the magnitude of acoustic energy transmitted through the device. From a noise treatment perspective, it does not matter if the area of the chamber is larger or smaller than the flow area; however, reducing the cross sectional area of the flow path may induce turbulent

flow which would induce flow noise negating the effectiveness of the device. The acoustic power transmission coefficient of an expansion chamber for low frequencies is given by

$$T_{\Pi} = \frac{1}{1 + \left(\frac{S_1 - S}{2S} kL \right)^2} \tag{2.11}$$

where S is the cross-sectional area, S_1 is the cross sectional area of the chamber, k is the wave number and L is the length of the chamber. equation (2.11) is only valid for $kL<<1$; for larger values of kL, a different modeling technique is necessary [21]. For a 30 cm long device in a hydraulic system, equation (2.11) begins to lose accuracy at approximately 74 Hz – far too low for the purposes of predicting hydraulic noise control. Furthermore, the cross-sectional area of the device needs to be small enough to not support non-planar modes for the frequency range of interest if it is to be modeled in this way. In addition, equation (2.11) neglects any losses within the fluid.

The performance of a traditional expansion chamber can be improved by including inlet/outlet extensions, multiple chambers and inclusion of a compliant media. Erikson presents an extensive discussion about the effect of inlet and outlet extensions, as well as multiple chambered expansion chambers [28]. Altering geometry allows for the noise control performance of the device to be shaped differently in the frequency domain to target noise. In general, the predicted performance scales with cross sectional area ratio; a larger change between the device and the flow path will more effectively treat noise. There is an upper limit of feasibility as a large change in cross-sectional area will occupy a large volume within a machine. For many mobile applications the change in

cross sectional area necessary for effective noise control is too large to be accommodated. One method to shrink the necessary cross-sectional area is to include additional compliance within the cavity of the device.

A commercially available expansion chamber style device with included additional compliance is a bladder-style suppressor; a schematic is shown in Figure 2-7 [1, 2, 23-27, 29-31]. A bladder-style suppressor functions by containing a pressurized volume of gas within the bladder of the device, known as charge pressure; the gas enters the bladder via the charging valve. The gas is several orders of magnitude more compliant than oil which creates a large impedance mismatch at the end caps of the device, reducing the level of noise transmitted through the device. The pressure of the gas is known as the charge pressure; the ratio between the operating pressure of the system and the charge pressure will determine how effectively the device treats noise [1, 31]. In cases when the charge pressure of the device is less than system pressure, known as the under-charged case, the device treats noise effectively. The noise control effectiveness improves as the charge pressure approaches system pressure from below up to a ratio of approximately 90%. In the case when charge pressure is greater than or equal to system pressure, known as the overcharged case, the bladder does not separate from the annulus. In this charge case, a bladder-style suppressor behaves as an expansion chamber with chamber cross-sectional area determined by the annulus, and is not an effective noise treatment option [1]. The drastic difference in behavior between the under-charged and overcharged cases creates a charge pressure selection problem. Correct selection of a charge pressure requires foreknowledge of the system usage [1, 29, 31]. Furthermore, charge pressure within the device will decrease over time as gas permeates through the

bladder, leaks around the bladder edges or leaks through the valve. The most desirable location for a noise treatment device is adjacent to the pump outlet to reduce the fluid borne noise produced from propagating into the system. However, in many commercial systems the pump is located centrally within the machine. If a bladder style suppressor was located centrally in the machine as well access would be difficult which may reduce the frequency of bladder recharges – reducing the overall effectiveness of the device.

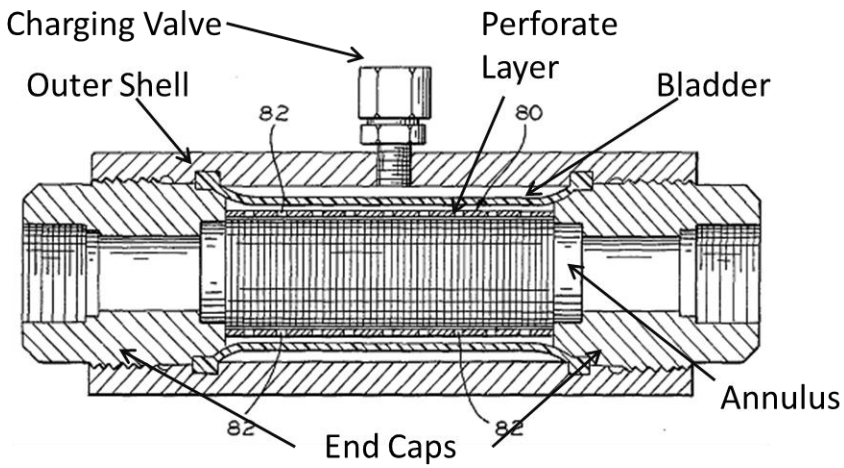

Figure 2-7: Bladder Style Suppressor [23]

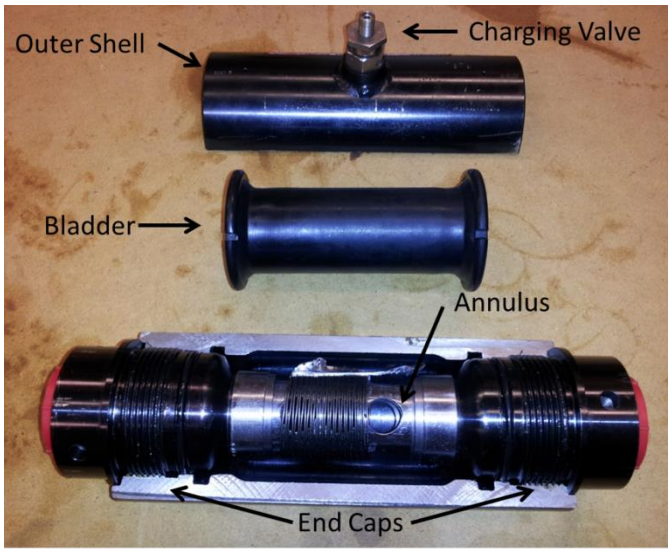

Figure 2-8: Cross-section of WM-3081 Suppressor

2.2 Syntactic Foam for Usage in Hydraulic Noise Control

Another type of a compliant-style noise control device is the liner-style suppressor [3, 12]. The compliance within the device comes from the syntactic foam liner. Syntactic foam is a term of art for any host matrix with inclusions specifically selected to alter the effective properties of the composite foam. In general, inclusions can be selected to alter mechanical properties, strength to weight ratio, thermal resistance or a multitude of other factors. The syntactic foam under examination is a voided polymer. The voids within the polymer are created by collapsed, hollow microspheres. When the microspheres are spherical, they serve to raise the bulk modulus of the composite which is detrimental to noise control. The voids created by the collapsed spheres are very soft and improve noise control. The microspheres collapse at a critical pressure differential across the microsphere wall, given by

$$P_{cr} = \frac{2Et^2}{r^2\sqrt{3\left(1-\nu^2\right)}}, \tag{2.12}$$

where E and ν are the Young's modulus and Poisson's ratio of the sphere material and t and r are the thickness and radius of the sphere [32]. The critical pressure is a pressure difference across the shell; the collapse pressure is the sum of the critical pressure of the shell and the pressure inside the microsphere,

$$P_{col} = P_{cr} + P_{int}. \tag{2.13}$$

Figure 2-9 shows the microspheres above and below collapse pressure. The device performance is dependent on the system pressure; with noise control effectiveness decreasing with increasing system pressure after collapse pressure has been exceeded.

However, no maintenance is possible during the life of the device which allows it to be positioned within the system for optimal noise control, most often near the outlet of the pump.

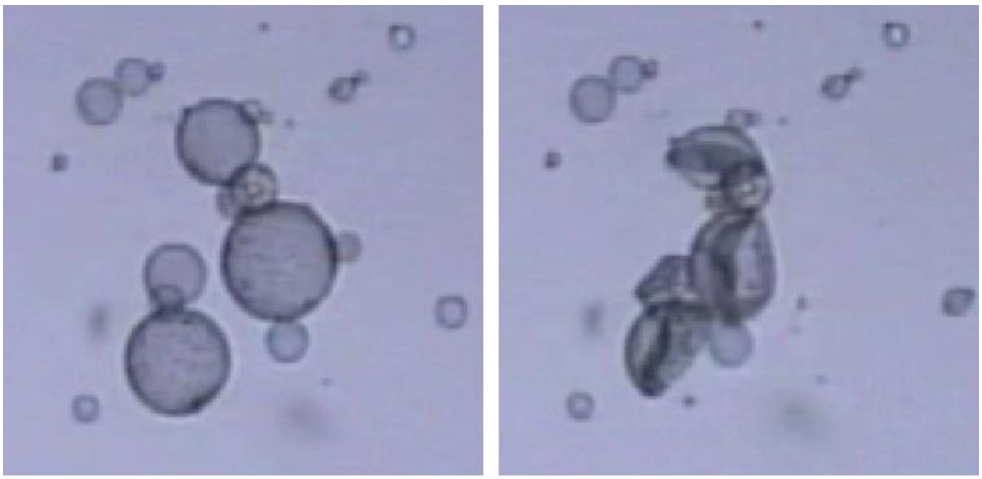

a) b)

Figure 2-9: Collapse of microspheres, picture from AkzoNobel. a) Pre-collapse b) Post-collapse

2.3 Research Opportunities

A noise control device using a syntactic foam liner can be developed which treats noise effectively over the entire range of system pressures. The transmission loss curves in Figure 2-10 show that as system pressure increases, the noise control effectiveness of the foam decreases [4]. Figure 2-11 shows the measured bulk modulus over part of the pressure range of interest up to 25 MPa. The full pressure range, up to 35 MPa, was not measured because the o-rings on the test fixture ruptured at approximately 25 MPa over a series of tests. The data point at a system pressure of approximately 21 MPa is higher because of an error in the measurement technique. For the current generation of foam, the bulk modulus increases rapidly with increasing system pressure which diminishes its noise control effectiveness. The bulk modulus is primarily a function of the volume fraction of the voids with in the host polymer. The microspheres may be altered in order

to allow for the foam to retain its compliance. The alteration will need to prevent the voids created by collapsed microspheres from losing their volume while remaining compliant. An analysis of Boyle's law suggests increasing the initial pressure of the microspheres will ensure the voids have a higher volume at elevated pressures. The larger void volume will increase the compliance of the foam and increase its effectiveness as a noise control option at elevated pressures. Boyle's law calculates the change in an isothermal process, $PV=k$ where k is a constant or $P_1V_1 = P_2V_2$, where 1 represents the initial state and 2 represents the final – elevated pressure – state. Figure 2-12 shows the decreasing void fraction and increasing bulk modulus of the first generation foam with increasing system pressure. Something that is non-intuitive about Figure 2-12 is the volume fraction decreases very rapidly with increasing system pressure but the bulk modulus does not increase by a similar fraction, i.e. at a void fraction of 1% the bulk modulus is not 99% of the value of the host. It will be shown in Chapter 3 that this is a characteristic of the host polymer having a relatively high Poisson's ratio approaching the upper limit of 0.5.

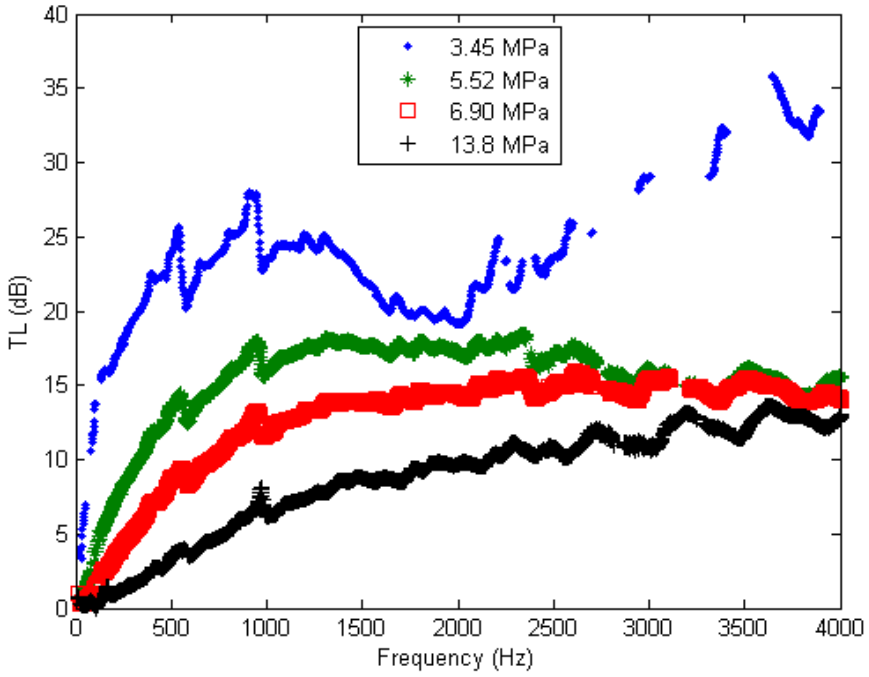

Figure 2-10: Transmission Loss for a first generation foam for several system pressures [4]

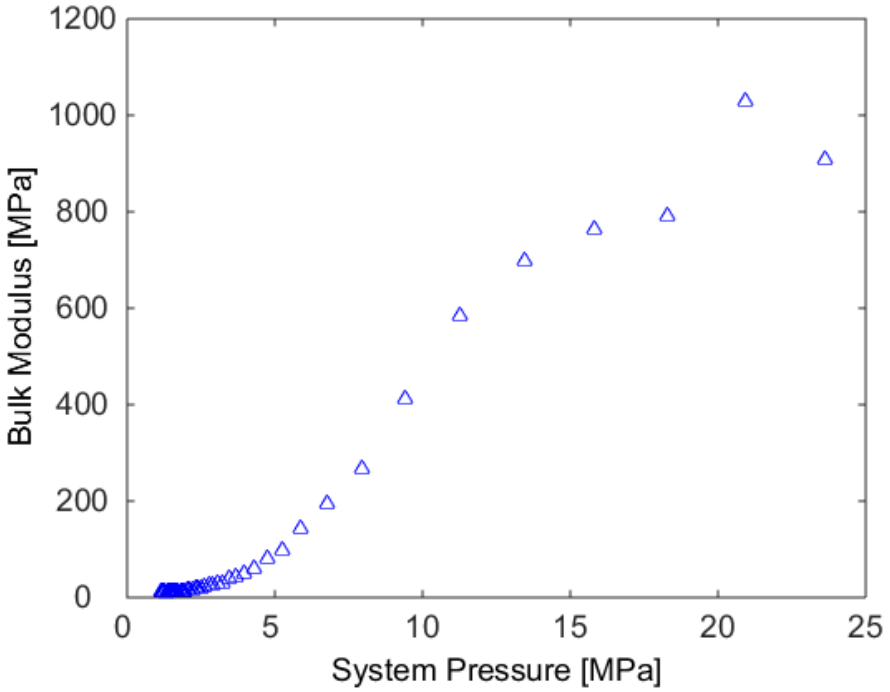

Figure 2-11: Bulk Modulus as a function of system pressure

It is hypothesized that by increasing the internal pressure of the voids, they will better retain their volume at elevated system pressure. Figure 2-13 shows the predicted

volume fractions for three initial microsphere pressures (IMP). An atmospheric IMP rapidly compresses with increasing system pressure while higher IMPs do not compress as drastically. For instance, the atmospheric IMP reaches a void fraction of 1% at approximately 5 MPa, while an IMP of 1 MPa does not decrease to that void fraction at a system pressure less than 35 MPa. The curves for the void fractions do not start at zero system pressure because the microspheres would not have collapsed at that pressure, which limits their noise control effectiveness. In general, a larger void fraction means a more compliant foam which will increase noise control effectiveness.

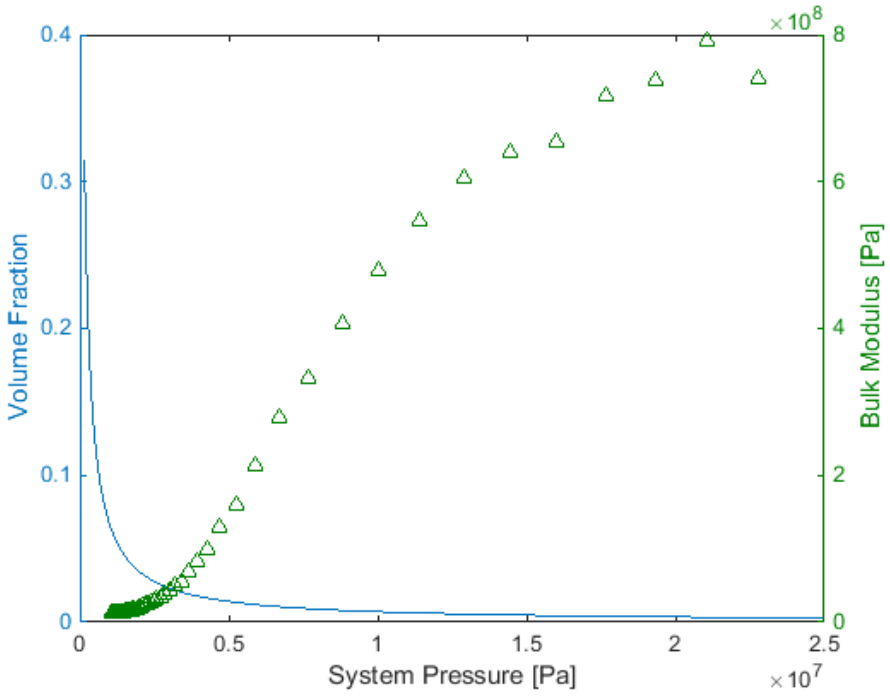

Figure 2-12: Calculated void fraction and measured bulk modulus for first generation foam over range of system pressure

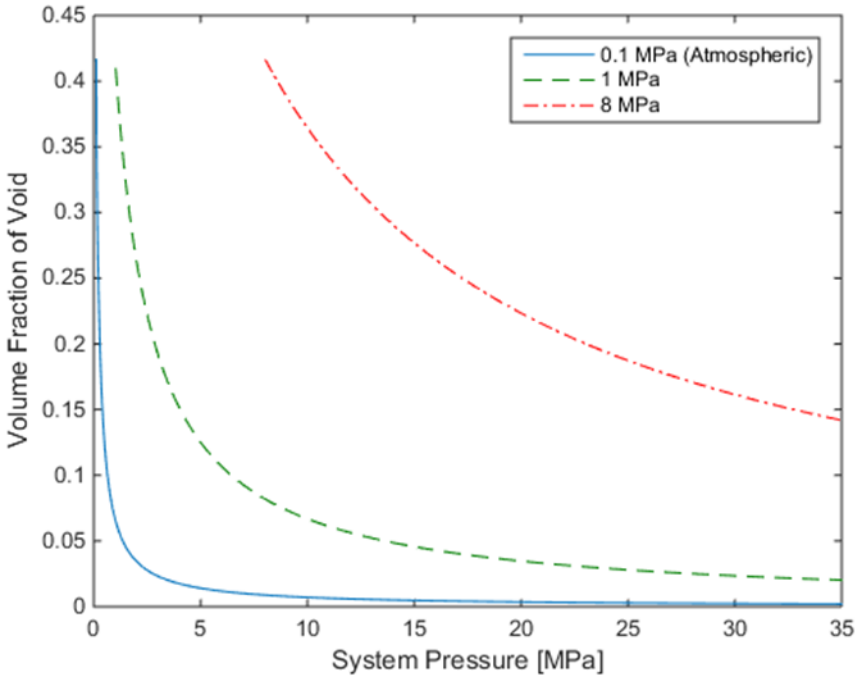

Figure 2-13: Void fractions for several IMPs over the pressure range of interest

CHAPTER 3

SYNTACTIC FOAM MODELING

Syntactic foam is a term of art applying to any host material matrix with inclusions specifically selected to alter the effective material properties of the composite in order to make the material more suitable for a desired engineering application. Some of the effective properties which can be altered are the material moduli, the thermal and electric resistance as well as strength-to-weight ratio. Some common examples of syntactic foam are fiberglass, where the fibers provide additional strength to the composite; concrete, where the stones are the inclusions to improve the strength characteristics of the cement; and as the dielectric material between capacitors due to its ability to accurately achieve very low dielectric constants [33]. The syntactic foam under examination in this work is a voided polymer where the voids are used to increase the compliance of the foam. The voids are created by collapsed hollow microspheres. A thin-walled hollow sphere, such as a microsphere, will collapse when exposed to external hydrostatic pressure if the pressure difference across the shell exceeds the critical pressure, as shown in equation (2.12). At pressure differentials less than the critical pressure the inclusion of thin-walled hollow microspheres serve to increase the compliance of the foam but to a much lesser degree than their collapsed voids; the bulk modulus will be further discussed in Section 3.7.1.

The effective mechanical properties of composites, such as syntactic foams, can be modeled from the properties of their constituents and relative volumes by multiphase modeling techniques [15, 34]. The small scale constituents are known as the microscale while the large scale body is known as the macroscale. The process of using the

properties of each constituent to calculate the composite process is known as homogenization, shown schematically in Figure 3-1. In order for the homogenized properties to be accurate, the characteristic dimension of constituent phases must be several orders of magnitude smaller than the composite body. In addition, for lumped parameter acoustic modeling the wavelength of interest needs to be much larger than the inclusions for accurate modeling in dynamic applications. For the syntactic foam under examination, the inclusions are on the order of micrometers while the composite body is generally on the order of centimeters. The four order of magnitude shift in length is sufficient for accurate material moduli prediction. In addition, the wavelengths of concern in hydraulic systems are on the order of meters which are large enough to not invalidate the modeling assumptions.

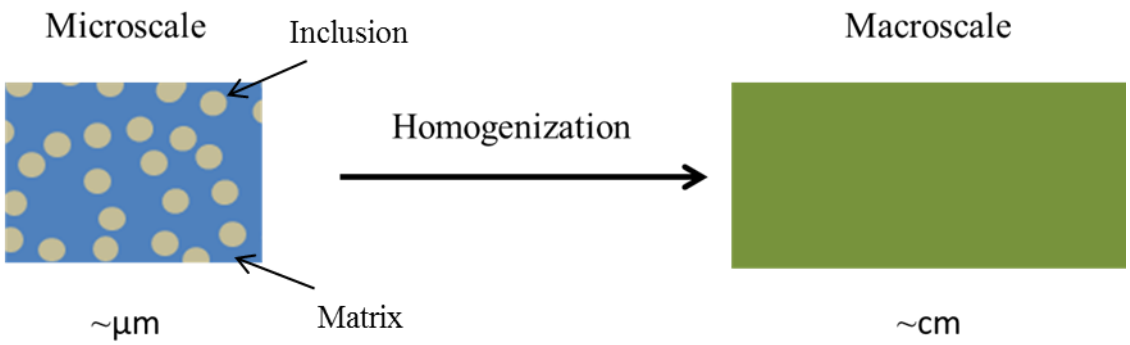

Figure 3-1: Microscale to macroscale homogenization

The simplest method for calculating the effective modulus of a composite is to add the moduli of its constituents as if they were springs in either parallel or in series while weighting the moduli for the relative volumes of each component. Adding springs in parallel is done by

$$k_{eff} = k_1 + k_2 + \ldots \tag{3.1}$$

where k is a given spring constant. This can be expanded upon to find equivalent moduli using the relative volume of all phases and it is known as the Voigt bound [35],

$$X_{eff} = c_1 X_1 + c_2 X_2 + \ldots \tag{3.2}$$

where X is the desired moduli and c is the volume fraction of each material. By definition

$$\sum_{n=1}^{N} c_n = 1, \tag{3.3}$$

where N is the number of phases – types of material – in the composite. Springs are added in series by

$$\frac{1}{k_{eff}} = \frac{1}{k_1} + \frac{1}{k_2} + \ldots. \tag{3.4}$$

This can be expanded to find the equivalent moduli with volume fractions, known as the Reuss bound [36],

$$\frac{1}{X_{eff}} = \frac{c_1}{X_1} + \frac{c_2}{X_2} + \ldots. \tag{3.5}$$

Equivalent moduli are calculated using the two methods for a material with gas void inclusions at an initial volume fraction of 50% and an isothermal change in volume of the gas over the system pressure range of interest. The results of two calculations, for two different host bulk moduli, are shown in Figure 3-2 and Figure 3-3. The predictions converge at higher system pressures because the void fraction approaches zero and the material properties of the composite are dominated by the host polymer. The large

difference between the bounds means that both cannot be correct for a real isotropic material such as the syntactic foam. For example, at a system pressure of 5 MPa in the 1000 MPa host bulk modulus simulation, there is a difference of approximately 80% in predicted moduli, which is too large for precise modeling. The difference is not as prominent for the softer host modulus but the bounds still differ by a large margin at lower pressures. Further model development is necessary for the accuracy level required.

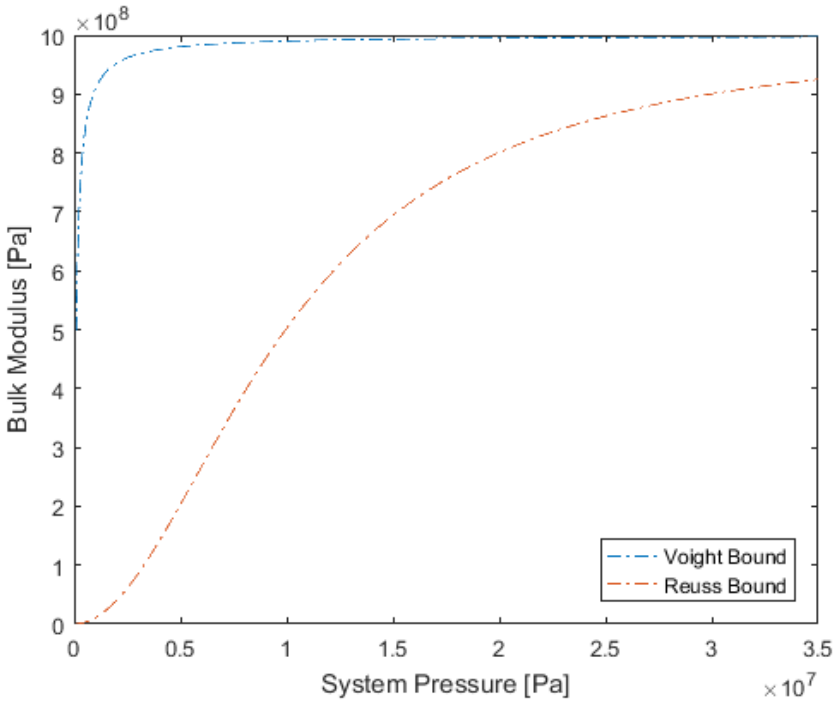

Figure 3-2: Voigt and Reuss bounds for bulk modulus, host polymer bulk modulus 1000 MPa

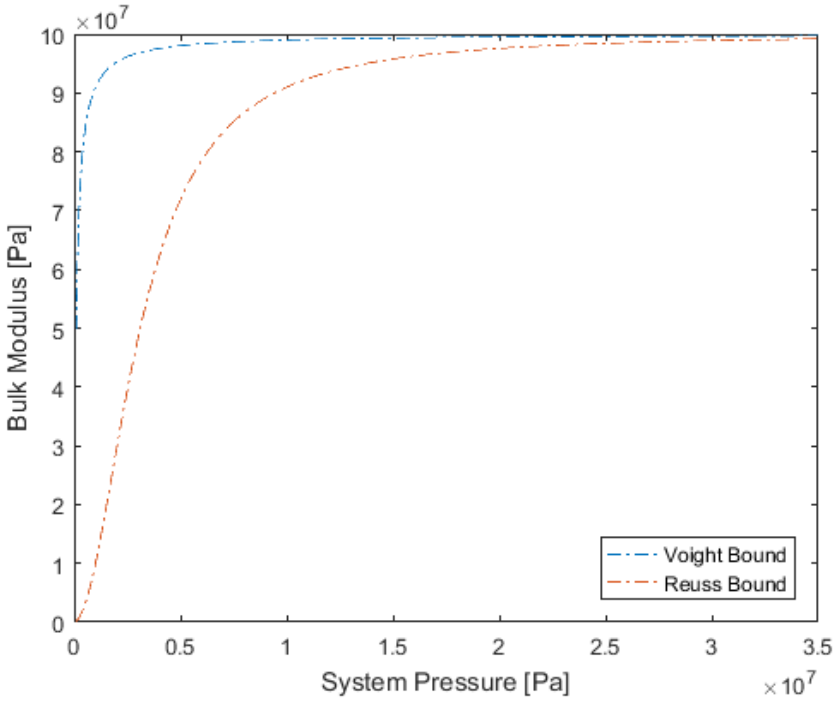

Figure 3-3: Voigt and Reuss bounds for bulk modulus, host polymer bulk modulus 100 MPa

More accurate modeling than the simple volume weighting can be conducted by multiphase modeling techniques; these techniques use the material properties of the constituents and their relative volume ratios to predict the effective property of the composite. Multiphase modeling traces its roots primarily to the work conducted by Einstein and Eshelby. Einstein analyzed the effect of Brownian motion of particles within a viscous fluid as well as how spherical inclusions affect the viscosity of a fluid [14, 37, 38]. This analysis is the foundation for models which calculate the effective shear modulus of materials with inclusions. Eshelby conducted the foundational work for proving the viability of homogenization techniques and calculating effective bulk modulus [15, 34]. The work analyzes a hypothetical volume of homogenous material which is misfit compared to a void in a larger volume of the same homogenous material. A surface traction deforms the first volume so it fits within the void of the second, the

two volumes are perfectly bonded and the traction is released. The release of the traction causes a stress and associated strain within the material. Eshelby provides a method to find the local stress and strain fields within the material which allows for calculation of the strain energy. This provides basis for models which calculate the effective bulk modulus, many of which depend on the strain energy within the composite.

Several multiphase models based on Einstein and Eshelby have been developed; some of the more popular models are the differential method [39, 40], the Mori-Tanaka method [41, 42], the composite spheres method [16, 43-45] and the self-consistent method [17, 46], all of which have some similarities. One fundamental similarity of all techniques is the use of a representative volume element (RVE). An example RVE is shown in Figure 3-4; the RVE is a single inclusion surrounded by host matrix. The volume of host material is such that the volume fraction of the RVE matches that of overall composite. RVEs have no required geometry; however, most are selected to have either spherical or cubic shape for geometric simplicity. For a spherical inclusion within a spherical RVE as shown in Figure 3-4, the volume ratio is that of the cube of the radii, $r_{inclusion}^3 / r_{matrix}^3$. Eshelby has demonstrated that simulating the composite properties of the RVE is equivalent to the composite properties of the entire composite [15]. This process of using the properties on the RVE, the microscale, to predict the properties of the composite, the macroscale, is known as homogenization.

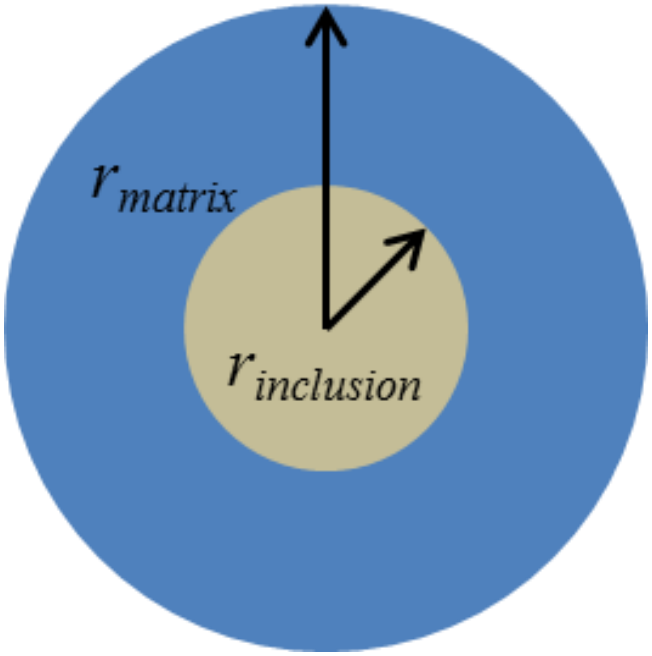

Figure 3-4: Representative Volume Element [15]

Each multiphase modeling method has advantages and disadvantages. The differential method is only accurate for dilute concentrations, which does not fit the syntactic foam under examination. The Mori-Tanaka method derives the effective moduli by determining the average strain from a far field stress and then algebraically manipulating stress, strain and material properties to find the equivalent moduli. The Mori-Tanaka method is very simple to use; however, it has been found to be inaccurate [41, 42, 46]. The composite spheres method accurately predicts the effective bulk modulus, but only provides bounds for the effective shear modulus [16, 43-45]. The self-consistent method will accurately predict shear modulus but uses the same derivation as the composite spheres model to predict effective bulk modulus [17, 46]. The remaining material properties will be found using linear material relations at several points under the assumption of local linearity at each calculation point.

3.1 Modulus Normalization

Traditionally in modeling literature, results of modulus predictions are normalized to the stiffest constituent; however, normalization may lead to false conclusions with a syntactic foam. The shape of the normalized modulus with respect to increasing system pressure will change depending on the value of the host modulus. The Voigt bound representative of low Poisson's ratios, shown in equation (3.2), can be calculated to find the effective bulk modulus and be normalized to the bulk modulus of the polymer,

$$K_{norm} = \frac{K_{eff}}{K_p} = c\,\frac{K_v}{K_p} + (1 - c)\,. \tag{3.6}$$

The first term in equation (3.6) will always be significantly less than the second term. At low pressures, the ratio of the bulk moduli will be very low as the polymer is significantly stiffer than gas. At higher pressures, the volume fraction approaches zero. The second term is not dependent on the bulk modulus of the polymer, so it follows that the normalized predictions would not vary greatly with a change in host. A slight difference in normalized prediction for two values of host modulus can be seen in Figure 3-5. The prediction of the Reuss bound, first shown in equation (3.5) and representative of host polymers with high Poisson's ratios, changes more drastically with increasing host bulk modulus. The normalized bulk modulus for the Reuss bound is

$$K_{norm} = \frac{K_{eff}}{K_p} = \frac{K_v}{(K_p - K_v)\,c + K_p}\,. \tag{3.7}$$

Changing the bulk modulus of the host will drastically change the shape of the curve with respect to system pressure; predictions for two values of host bulk modulus are shown in

Figure 3-6. Therefore, conclusions drawn from normalized modulus curves cannot be generalized to all cases and normalization has no benefit.

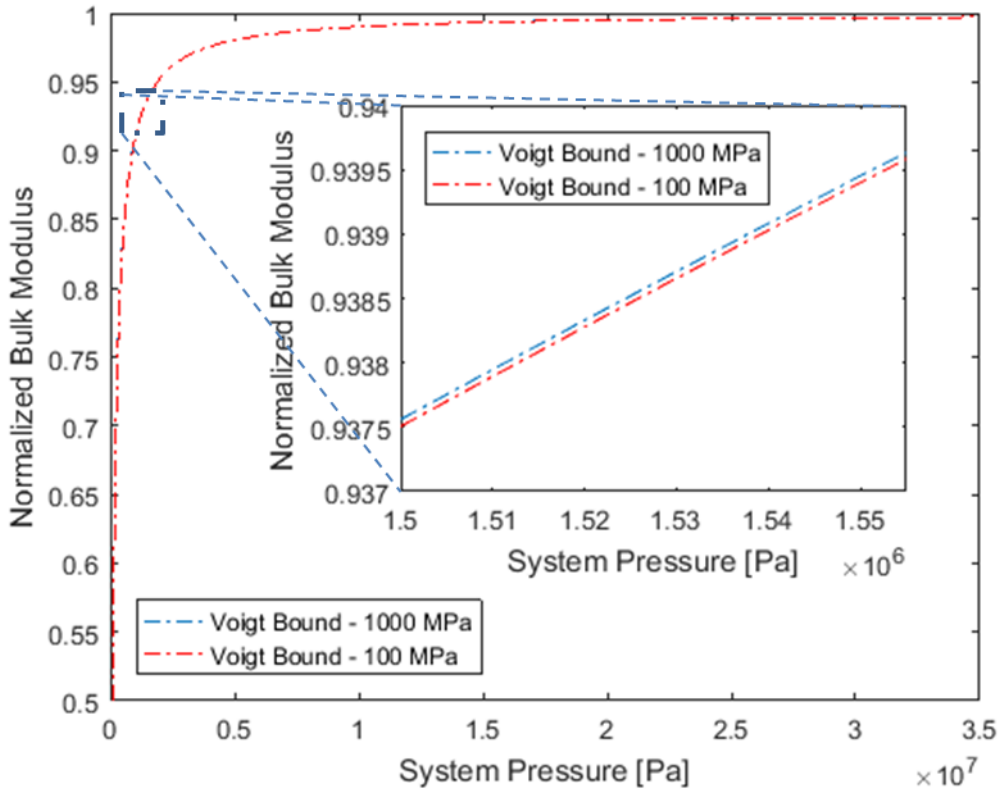

Figure 3-5: Normalized bulk modulus using Voigt Bound with two different host bulk moduli

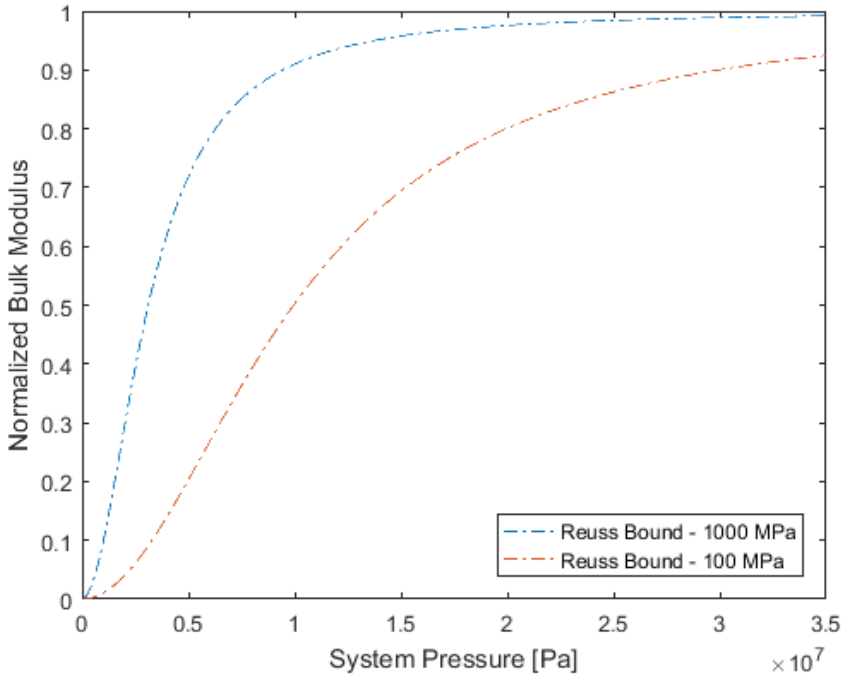

Figure 3-6: Normalized bulk modulus using Reuss Bound with two different host bulk moduli

3.2 Composite Spheres Method

The composite spheres method was developed by Hashin to calculate the effective bulk modulus of composite materials [16, 43-45]. As the name of the model suggests the model analyzes a RVE of a spherical inclusion surrounded by a sphere of host material, as shown in Figure 3-7. As with the spherical RVE example above, the radii are selected to match the appropriate volume ratio of the sample. In order to calculate the effective bulk modulus, a hypothetical stress tensor, T_i, is applied to the surface of the RVE, as shown in Figure 3-7. Strain energy is calculated by

$$U_0 = \frac{1}{2}\int_V \sigma_{ij}^{(0)} \varepsilon_{ij}^{(0)} dV \ , \tag{3.8}$$

where σ_{ij} is stress and ε_{ij} is strain. Hooke's law in three-dimensions relates stress and strain,

$$\sigma_{ij}^{(0)} = \lambda_m \varepsilon_{kk}^{(0)} \delta_{ij} + 2G_m \varepsilon_{ij}^{(0)}, \tag{3.9}$$

where λ_m is Lame's first parameter and G_m is the shear modulus. The bounds for composite bulk modulus are found by putting equation (3.8) in terms of only stress related terms,

$$U_0^{\sigma} = \frac{1}{2} \int_{(V)} \left(\frac{\sigma^{(0)^2}}{9K_m} + \frac{s_{ij}^{(0)} s_{ij}^{(0)}}{2G_m} \right) dV, \tag{3.10}$$

where $\sigma^{(0)}$ is the isotropic part of stress and $s^{(0)}_{ij}$ is the deviatoric part of stress, or strain related terms,

$$U_0^{(\varepsilon)} = \frac{1}{2} \int_{(V)} \left(K_m \varepsilon^{(0)^2} + 2G_m e_{ij}^{(0)} e_{ij}^{(0)} \right) dV, \tag{3.11}$$

where $\varepsilon^{(0)}$ is the isotropic part of strain and $e^{(0)}_{ij}$ is the deviatoric part of strain. The isotropic portions of stress and strain are related through

$$\sigma^{(0)} = 3K_m \varepsilon^{(0)}, \tag{3.12}$$

where K_m is the bulk modulus, and the deviatoric parts of stress and strain are related through

$$s_{ij}^{(0)} = 2G_m e_{ij}^{(0)}, \tag{3.13}$$

where

$$\sigma^{(0)} = \sigma_{kk}^{(0)},\ e^{(0)} = e_{kk}^{(0)},\ s_{ij}^{(0)} = \sigma_{ij}^{(0)} - \frac{1}{3}\sigma^{(0)}\delta_{ij} \text{ and } e_{ij}^{(0)} = \varepsilon_{ij}^{(0)} - \frac{1}{3}\varepsilon^{(0)}\delta_{ij}. \tag{3.14}$$

For a body with inclusions the total strain energy is given by

$$U^{(\sigma)} = U_0 + \delta U^{(\sigma)} \tag{3.15}$$

or

$$U^{(\varepsilon)} = U_0 + \delta U^{(\varepsilon)}, \tag{3.16}$$

where

$$\delta U^{(\sigma)} = \frac{1}{2}\int_{(\bar{V}_n)} \left(\frac{K_m - K_p}{9K_m K_p}\sigma^{(0)}\sigma + \frac{G_m - G_p}{2G_m G_p} s_{ij}^{(0)} s_{ij} \right) dV \tag{3.17}$$

and

$$\delta U^{(\varepsilon)} = \frac{1}{2}\int_{(\bar{V}_n)} \left(\left(K_m - K_p\right)\varepsilon^{(0)}\varepsilon + 2\left(G_m - G_p\right) e_{ij}^{(0)} e_{ij} \right) dV \ . \tag{3.18}$$

Furthermore the total strain energy of a given RVE is

$$U^{(\sigma)} = \frac{1}{2}\left(\frac{\sigma^{(0)^2}}{9K^*} + \frac{s_{ij}^{(0)} s_{ij}^{(0)}}{2G^*} \right) V \tag{3.19}$$

and

$$U^{(\varepsilon)} = \frac{1}{2}\left(K^* \varepsilon^{(0)^2} + 2G^* e_{ij}^{(0)} e_{ij}^{(0)} \right) V \ , \tag{3.20}$$

where the superscript * designates a composite property. equations (3.15) and (3.16) are used with the substitutions from equations (3.10), (3.11), (3.17) and (3.18) to calculate the effective material moduli.

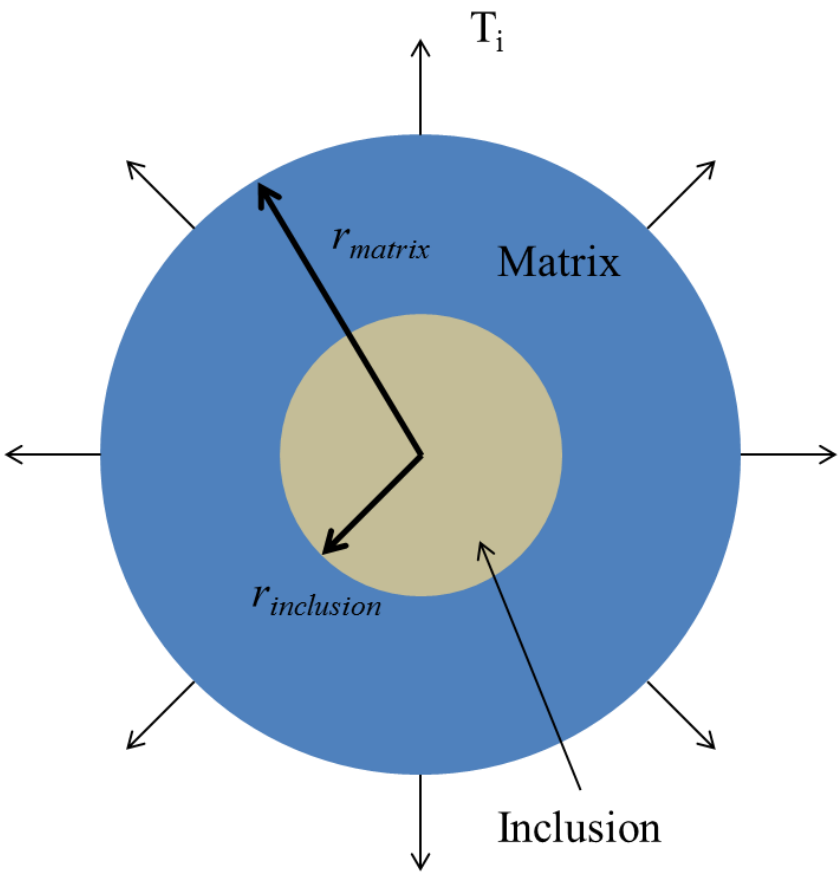

Figure 3-7: RVE with surface stress tensor for use with composite spheres method

The equivalent bulk modulus, K^*, is found by manipulating the preceding equations and enforcing continuity of stress and displacement at the boundary between host and insert. First, a hypothetical tensor of hydrostatic stress is applied to the outer surface of the RVE. The selection of the loading tensor allows for the strain energy bounds in equations (3.17) and (3.18) to be calculated. Manipulating the above equations gives two expressions for equivalent bulk modulus; however, the relations can be shown to be mathematically equivalent. The effective bulk modulus, K^*, is given by

$$K^* = K_m + (K_i - K_m)\frac{(4G_m + 3K_m)c}{4G_m + 3K_i + 3(K_m - K_i)c}, \tag{3.21}$$

where K is the bulk modulus, G is the shear modulus, c is the volume fraction and subscripts m and i represent the matrix and inclusions, respectively.

The model is calculated for an example host and gaseous inclusions with the results shown in Figure 3-8, the collapsed microsphere wall is assumed to have a negligible contribution to the overall properties of the foam. In addition, Reuss and Voigt bounds are shown for comparison. As discussed previously, there is significant difference between the Voigt and Reuss bounds, especially at low system pressures. These bounds and composite sphere predictions converge at higher system pressures where the void fraction approaches zero. Figure 3-8 plots the predicted bulk modulus by the composite spheres method for multiple different hosts with the only variance between hosts being their respective Poisson's ratios. A different Poisson's ratio will manifest in different predicted bulk moduli as it will change the shear modulus of the host, which is used by the composite spheres method to predict bulk modulus. The relation between host bulk modulus and shear modulus is given by

$$G = \frac{3K(1 - 2\nu)}{2(1 + \nu)}, \tag{3.22}$$

a function of Poisson's ratio. In Figure 3-8 the selected range of Poisson's ratios cover the range of Poisson's ratios found in practical materials, from 0 to 0.4995. The lower values are very close to the Voigt bound and the highest value approaches the Reuss bound. This follows logically as the bounds define loading in series or parallel; a low Poisson's ratio would lead to little non-axial deformation that is loading in series and a

high Poisson's ratio would lead to high non-axial deformation that is similar to loading in parallel. The Poisson's ratios are usually above 0.4 for many of the polymers used to fabricate foams under analysis. This means the Voigt bound is insufficient to predict the bulk modulus of syntactic foam. Furthermore, if the Poisson ratio is approximately 0.49 the predicted modulus is no longer near the Reuss bound. Therefore, in order to accurately model the bulk modulus of a syntactic foam, the composite spheres method will be used. The predictions shown assume a Poisson's ratio of 0.5 for the gaseous voids because it is assumed the gas has a finite bulk modulus and an idealized shear modulus of 0. The composite spheres method can also be used to find the effective shear modulus; however, the bounds for the effective shear modulus are not equivalent for all cases [43]; therefore an alternate modeling technique is necessary.

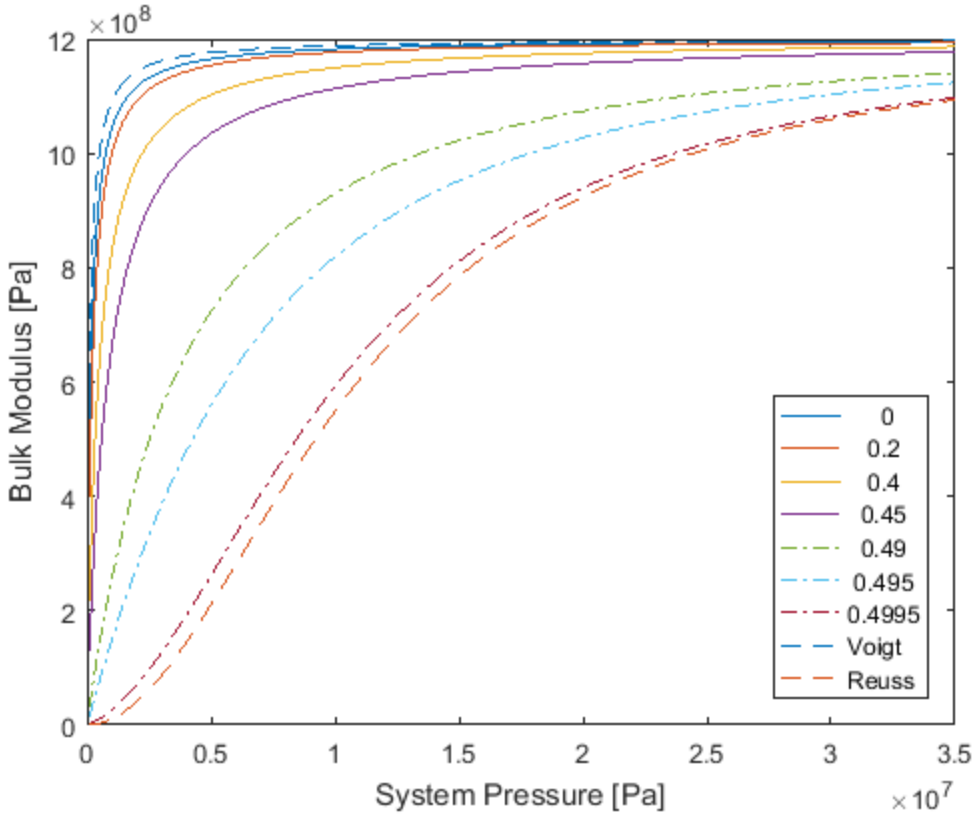

Figure 3-8: Normalized bulk modulus for Voigt and Reuss bounds as well as compositsite spheres method with seven host material Poisson's ratios. Host Bulk Modulus of 1.2 GPa.

3.3 Self-Consistent Method

The self-consistent model utilizes an RVE within an infinite volume of composite material with unknown properties to calculate the effective shear modulus; this is schematically shown in Figure 3-9 [17, 46]. The properties of the homogenous media are initially unknown, but defined to be equivalent to the effective properties of the RVE. The effective shear modulus is calculated by first defining a spherical coordinate system which is then defined in all three regions: inclusions, host and homogenous media. Continuity of stress and strain is enforced at the boundaries between the media; this creates a set of eight equations with nine unknowns. A final boundary condition of pure torsion is assumed at an infinite distance to the origin to resolve the final unknown. This defines the stress and strain fields through the composite, and by following a similar

procedure as the composite spheres method to calculate the strain energy within the composite the effective shear modulus can be found. The effective modulus is found by the quadratic relation,

$$\left(\frac{G^*}{G_m}\right)^2 A + \left(\frac{G^*}{G_m}\right) B + D = 0 \tag{3.23}$$

where G^* is effective shear modulus, G_m is the shear modulus of the host, and

$$\begin{aligned} A = {} & 8\left[\frac{G_i}{G_m} - 1\right](4 - 5\nu_m)\eta_1 c^{10/3} - 2\left[63\left(\frac{G_i}{G_m} - 1\right)\eta_2 + 2\eta_1\eta_3\right]c^{7/3} \\ & + 252\left[\frac{G_i}{G_m} - 1\right]\eta_2 c^{5/3} - 25\left[\frac{G_i}{G_m} - 1\right](7 - 12\nu_m + 8\nu_m^2)\eta_2 c \\ & + 4(7 - 10\nu_m)\eta_2\eta_3 \end{aligned} , \tag{3.24}$$

$$\begin{aligned} B = {} & -4\left[\frac{G_i}{G_m} - 1\right](1 - 5\nu_m)\eta_1 c^{10/3} + 4\left[63\left(\frac{G_i}{G_m} - 1\right)\eta_2 + 2\eta_1\eta_3\right]c^{7/3} \\ & - 504\left[\frac{G_i}{G_m} - 1\right]\eta_2 c^{5/3} + 150\left[\frac{G_i}{G_m} - 1\right](3 - \nu_m)\nu_m\eta_2 c \\ & + 3(15\nu_m - 7)\eta_2\eta_3 \end{aligned} , \tag{3.25}$$

and

$$\begin{aligned} D = {} & 4\left[\frac{G_i}{G_m} - 1\right](5\nu_m - 7)\eta_1 c^{10/3} - 2\left[63\left(\frac{G_i}{G_m} - 1\right)\eta_2 + 2\eta_1\eta_3\right]c^{7/3} \\ & + 252\left[\frac{G_i}{G_m} - 1\right]\eta_2 c^{5/3} + 25\left[\frac{G_i}{G_m} - 1\right](\nu_m^2 - 7)\eta_2 c \\ & - (7 + 5\nu_m)\eta_2\eta_3 \end{aligned} , \tag{3.26}$$

where

$$\eta_1 = \left[\frac{G_i}{G_m} - 1\right](49 - 50\nu_i\nu_m) + 35\left(\frac{G_i}{G_m}\right)(\nu_i - 2\nu_m) + 35(2\nu_i - \nu_m)$$

$$\eta_2 = 5\nu_i\left[\frac{G_i}{G_m} - 8\right] + 7[G_i + G_m + 4] \quad , \qquad (3.27)$$

$$\eta_3 = \left(\frac{G_i}{G_m}\right)(8 - 10\nu_m) + (7 - 5\nu_m)$$

where G_i is the shear modulus of the inclusion, ν_i is the Poisson's ratio of the inclusion and ν_m is the Poisson's ratio of the host. A quadratic equation has two solutions and an isotropic material cannot simultaneously have two shear moduli; one of the moduli must be rejected using rejection criteria: a) the predicted modulus is negative or b) the predicted modulus is outside of the bounds of the two constituents. Generally, one of the predicted moduli is negative and therefore immediately rejected.

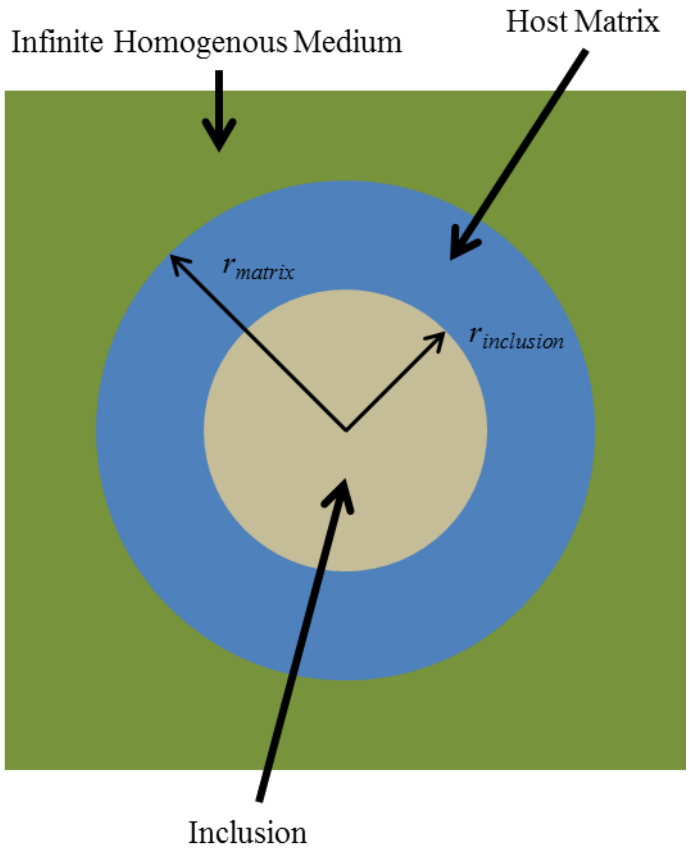

Figure 3-9: Schematic of RVE for use with self-consistent method

Figure 3-10 shows predicted shear modulus from the self-consistent method as well as the Voigt and Reuss bounds for shear modulus. The Reuss bound predicts a shear modulus of zero for the entire pressure range. This follows mathematically from equation (3.5), if X_1 is zero, as is the case for the shear modulus of a gaseous bubble, X_{eff} will also be zero. It is plain to see a foam sample supports shear and therefore has a non-zero shear modulus; therefore, the Reuss bound is inaccurate for this application. The shear moduli predicted by Voigt bound and the shear moduli predicted by the self-consistent method almost completely agree. An analysis of differing Poisson's ratios, similar to the analysis presented in Figure 3-8 for the composite spheres method, will not be presented for the self-consistent method. If the bulk modulus of the host is assumed constant, i.e. variable

Poisson's ratio, normalizing to the shear modulus of the host gives identical curves. If the shear modulus of the host is assumed constant, the bulk modulus of the host can such that the foam compresses to a volume less than zero when loaded, which is non-physical and the foam would behave nonlinearly which invalidates the assumptions of the model. For a physical version of such a material with low bulk modulus, the bulk modulus would increase with increasing system pressure which is not captured within the current model. Because of their similarity, either the Voigt bound or the self-consistent method can be used to predict the effective shear modulus of a polymer with gas voids. However, the Voigt bound predicts an incorrect shear modulus value in the pre-collapsed regime. Figure 3-11 shows the results of calculations for the shear modulus if the inclusions are solid spheres, i.e. uncollapsed microspheres. In addition, the predicted modulus is above a normalized value of unity because the normalization is with respect to the host shear modulus and the shear modulus of the inclusion is higher than the modulus of the host. For this case, the self-consistent method very nearly matches the Reuss bound. Because neither bound predicts both collapsed and uncollapsed regimes closely, the self-consistent method will be used.

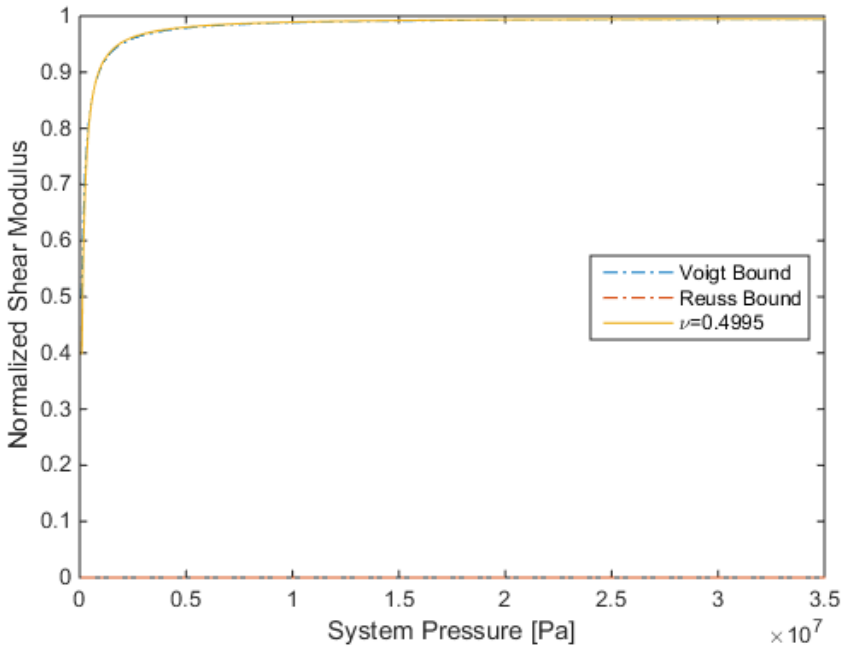

Figure 3-10: Normalized shear modulus for Voigt and Reuss bounds as well as self-consistent method with voids

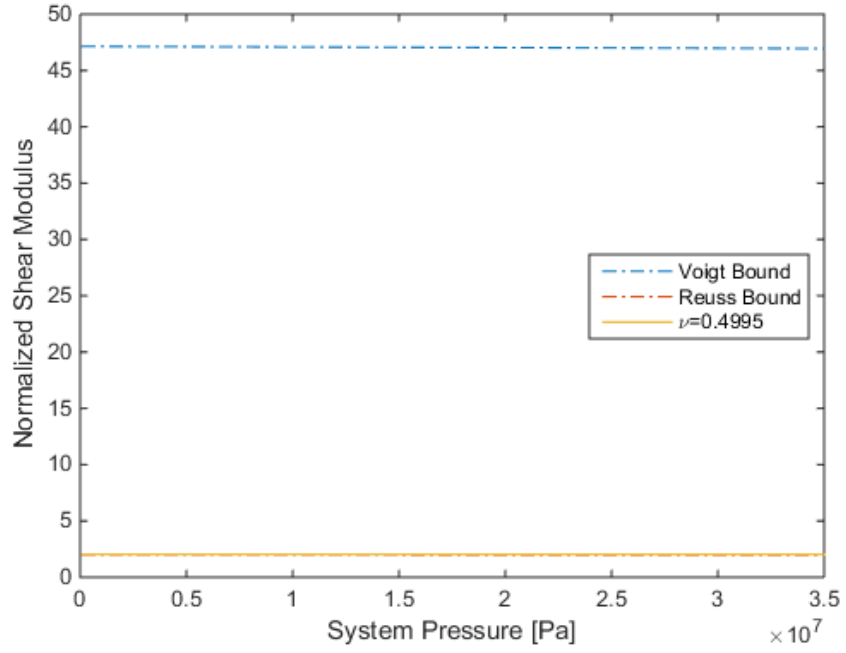

Figure 3-11: Normalized shear modulus for Voigt and Reuss bounds as well as self-consistent method with solid inclusions

3.4 Complex Material Properties

The host material used to create the syntactic foam has loss characteristics, and its lossiness affects the noise control behavior of the foam and must be adequately captured within the material modeling. A further discussion of frequency-dependent properties will occur in the next section. The development of both the composite spheres method and self-consistent method do not require real material properties to remain valid; therefore, the models can be extended to predict the complex material properties [45, 46]. The storage and loss modulus are calculated simultaneously for both models.

A common method to represent the loss characteristic is the use of complex material properties,

$$X = X' + iX'', \tag{3.28}$$

where X is the material modulus under examination, X' is the storage modulus and X'' is the loss modulus. It is common to present material properties as a loss fraction, generally known as the tangent of the phase angle, δ,

$$\tan\delta = \frac{X''}{X'}. \tag{3.29}$$

For many polymers, the value of the loss fraction is between 0.1 and 0.7, with some polymers reaching 1.5, with higher values indicating a material with a higher relative value of damping. The loss fraction will not be presented in this work because the host changes properties over frequency and pressure, making it non-intuitive to draw conclusions from this ratio. An example tan δ plot is shown Figure 3-12. Both the storage and loss modulus increase monotonically with increasing frequency and system pressure;

however, the calculated tan δ does not match this pattern, as shown by the area of high tan δ for low system pressures and high frequencies. This area represents an area of high relative lossiness rather than high absolute lossiness. Absolute lossiness is of greater concern to hydraulic noise control; therefore, the material properties will be presented separately as a storage modulus and loss modulus.

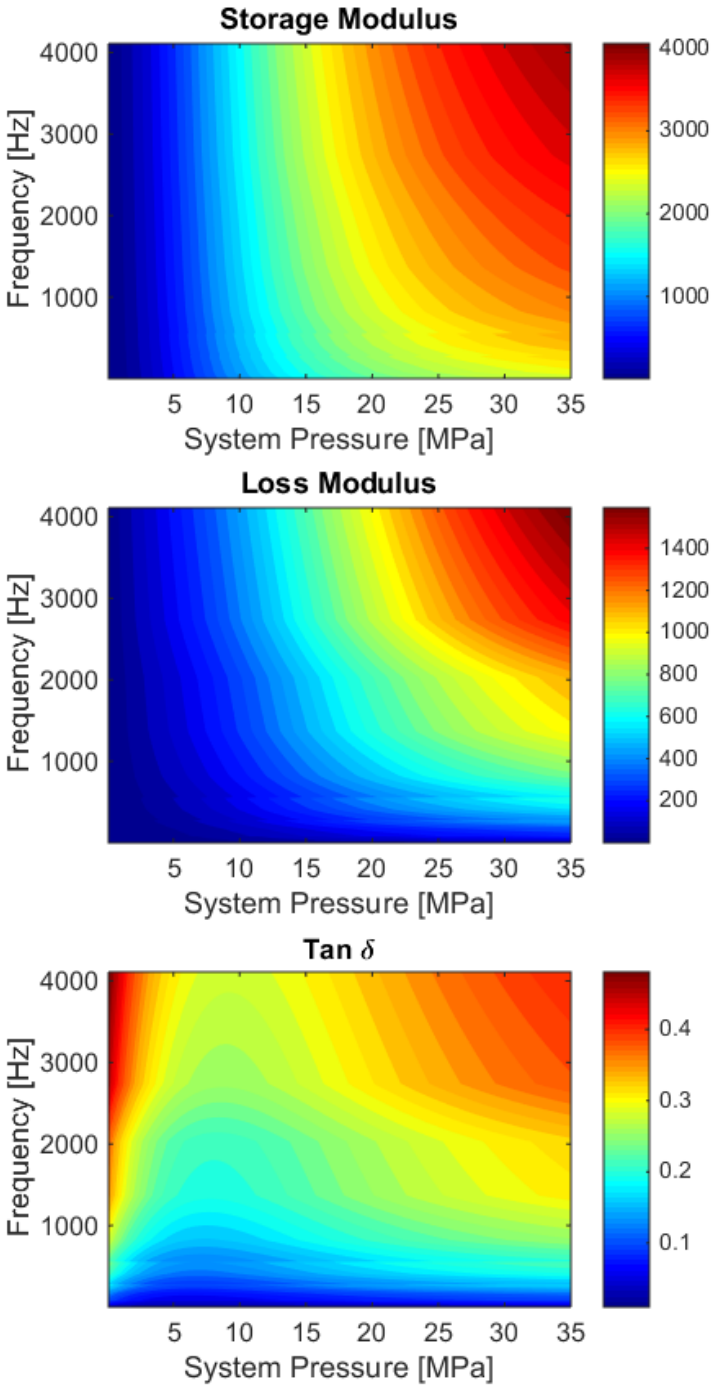

Figure 3-12: Predicted storage modulus, loss modulus and tan delta for example foam

A hydraulic suppressor is commonly, yet incorrectly, referred to as a pulsation absorber; this implies that the device prevents the acoustic energy transfer primarily through a loss mechanism, however in actuality; noise is primarily treated with

compliance. As discussed above, the foam will have some lossiness; however, the particle velocity in a liquid media, such as hydraulic oil, is not high enough for damping alone to be an effective means of noise control. Acoustic particle velocity is related to acoustic pressure by impedance, and for a plane wave the relation is

$$u = \frac{P}{\rho_0 c} \tag{3.30}$$

where ρ_0 is the ambient density of the medium, approximately 990 kg/m^3 for hydraulic oil, and c is the speed of sound, approximately 1400 m/s in hydraulic oil. For an acoustic wave in hydraulic oil, the particle velocity will be approximately six orders of magnitude less than the pressure. The particle velocity will be on the order of 1 m/s for the range of pressure ripple seen in hydraulic systems this particle velocity would require a series of small pores to dissipate acoustic energy. Salmon measured the noise control effectiveness of liner-style suppressors with and without a porous diffusing surface; the treatment of noise was similar across four different device configurations suggesting the additional damping was not highly effective as a noise control technique [47].

3.5 Dynamic Material Properties

Many polymers have frequency dependent moduli; an example of the modulus change over frequency for a host polymer is shown in Figure 3-13. It is seen that the material becomes stiffer and lossier at higher frequencies, albeit at different rates. The stiffening of the foam is detrimental to noise control. The change in modulus with respect to frequency is large enough to necessitate capture in the modeling. Similar to complex

material modeling, the multiphase modeling techniques are not invalidated by modeling frequency dependent properties, allowing it to be used for modeling the syntactic foam.

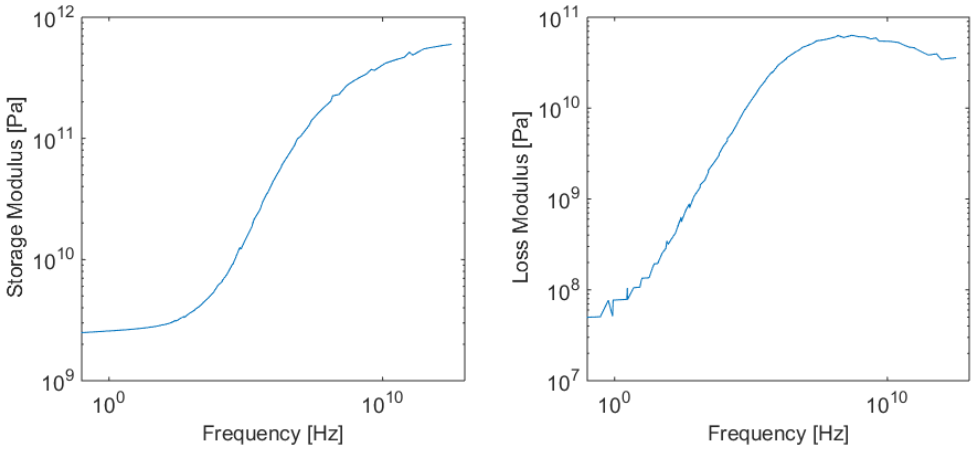

Figure 3-13: Frequency dependent properties of first generation host, provided by manufacturer

3.6 Thermal and Pressure Dependent Properties

The material moduli of many polymers in commercial use today are dependent on the temperature and pressure. Different host properties can be input into the relevant equation to represent the host at different pressure and temperature conditions.

Empirical measurements for the effect of temperature on the polymer of the first generation of foam are shown in Figure 3-14. Both the storage and loss modulus change significantly from 20° C to 45° C. However, in the frequency range of interest, from 0 to 4000 Hz, the change in storage modulus is less drastic, approximately 2 GPa at the higher frequencies, as seen in Figure 3-15, while the loss modulus changes by almost an order of magnitude for a similar temperature shift. The modulus shift in frequency for polymers is known as the time-temperature superposition and can be modeled using the equation set forth by Williams et al. [48].

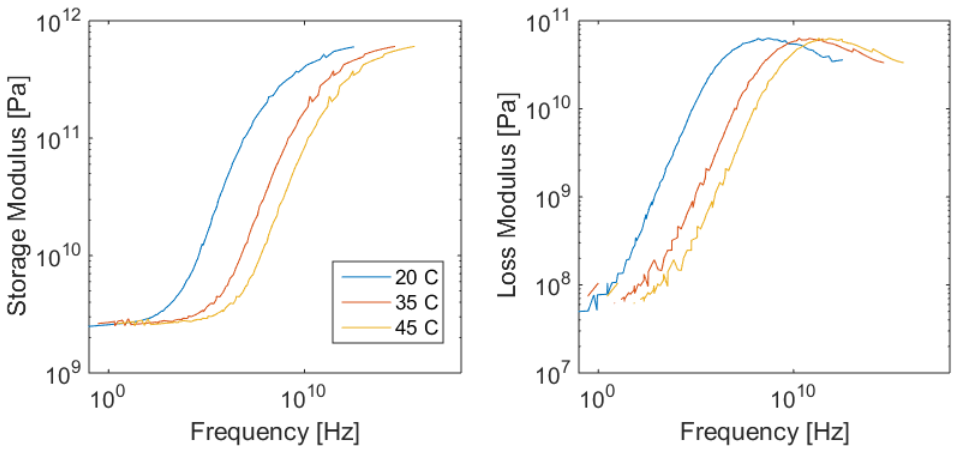

Figure 3-14: Temperature dependence of bulk modulus of first generation polymer

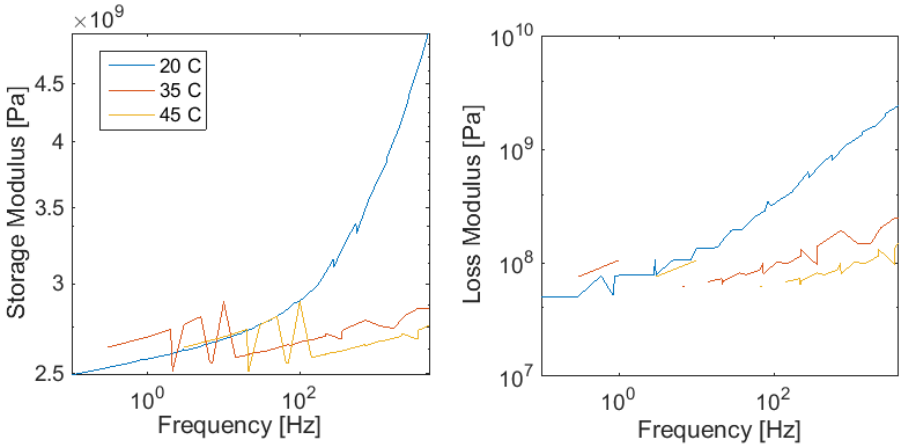

Figure 3-15: Temperature dependence of bulk modulus of first generation polymer, 0 to 4000 Hz

The moduli of the host polymer are not independent of system pressure and the polymer may stiffen with increasing pressure. In order to accurately simulate the composite properties of the foam, the relevant material moduli will need to be input into the pertinent model. The material properties at elevated pressure may either be found from experimentation or theory. The stiffening of the host polymer with increasing pressure will be overall detrimental to noise control.

3.7 Modeling of Syntactic Foam for Hydraulic Noise Control

The material property model employs the composite spheres method to calculate the dynamic complex bulk modulus and the self-consistent method to calculate the dynamic complex shear modulus. Both moduli are calculated in two system pressure regimes based on the state of the microsphere, the pre-collapsed and the post-collapsed regime. The physical foam will have a small range of pressures where the microspheres collapse due to distribution of sphere geometry, both in terms of radius and in terms of sphericalness which will determine how well the model predicts critical behavior. For the purpose of modeling, the collapse of the microspheres is assumed to happen at a single discrete pressure. A thin-walled spherical shell is not rigid; the method to calculate the bulk modulus of a thin-walled spherical shell will be discussed in the following section. In the post collapsed regime, the voids are assumed to behave as gas bubbles with initial pressure equivalent to their internal pressure; any stiffness contribution from the collapsed sphere wall is neglected. The gas bubbles are assumed to have a bulk modulus proportional to pressure, and to not be able to support shear as an idealized fluid, i.e. the shear modulus is zero. The volume of the gas bubble exposed to elevated system pressure is modelled by isothermal compression. The compression of the host polymer is modelled using its static bulk modulus. Once the compressed volume of each phase is found, the volume fraction of the RVE is recalculated to be used for material moduli prediction. The dynamic properties are modelled over the range of frequencies of interest, usually up to 4000 Hz.

3.7.1 Pre-buckled Microsphere Behavior

The bulk modulus of a thin-walled microsphere is found from calculating its radial deformation at elevated pressure,

$$\Delta r = \frac{P r^2 (1-\nu)}{2 E t} \tag{3.31}$$

and applying the definition of bulk modulus gives the effective bulk modulus of a thin-walled microsphere as

$$K = \frac{-8 E^3 t^3}{r\left(\left(12\nu t^2 - 12 t^2\right) E^2 + \left(6\nu^2 rt - 12\nu rt + 6rt\right) PE + \left(\nu^3 r^2 - 3\nu^2 r^2 + 3\nu r^2 - r^2\right) P^2\right)}. \tag{3.31}$$

The bulk modulus changes with system pressure, as shown in Figure 3-17, but the modulus is generally less than most host polymers.

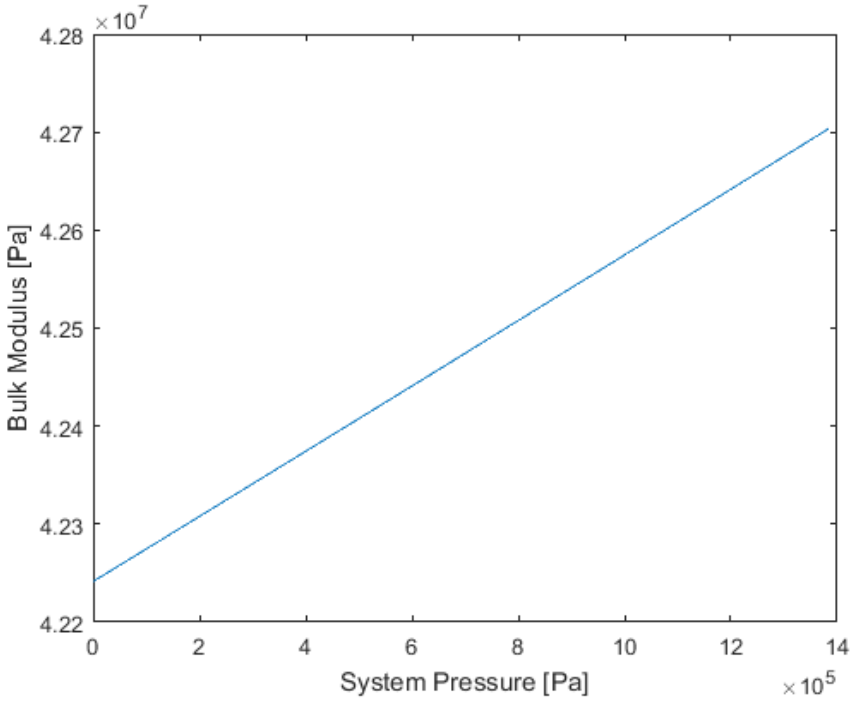

Figure 3-16: Bulk modulus of a spherical shell at pressures less than collapse pressure

Some predictions of the bulk and shear modulus for pressurized microsphere are shown in Figure 3-17, Figure 3-18, Figure 3-19 and Figure 3-20. It is important to note the predicted material moduli vary over frequency and system pressure and recall that lower bulk moduli treat noise most effectively. The dependency is different for both moduli in both pressurization cases. In general, the shear modulus is predicted to be a much weaker function of system pressure. Figure 3-19 and Figure 3-20 demonstrate the effect of collapse on the material modulus. In the pre-collapsed region, both the shear and bulk modulus have no dependency on system pressure. At pressures higher than the collapse pressure, the microspheres collapse and the bulk modulus is drastically reduced. In addition, the post-collapse bulk modulus varies very weakly in frequency. The collapse also happens at the atmospheric IMP but cannot be seen in the figures because it happens at a relatively low pressure.

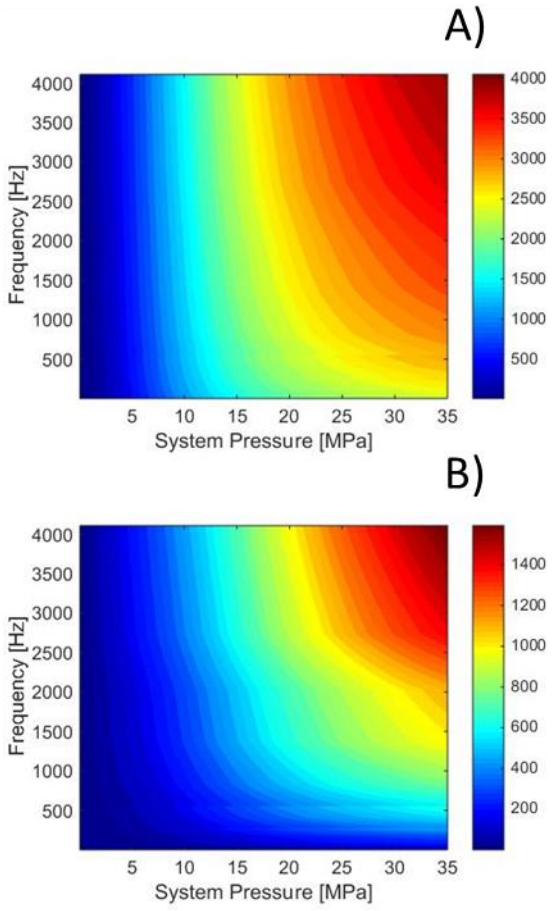

Figure 3-17: Bulk modulus of syntactic foam 50% initially microsphere by volume, atmospheric IMP. A) Storage modulus, B) Loss modulus

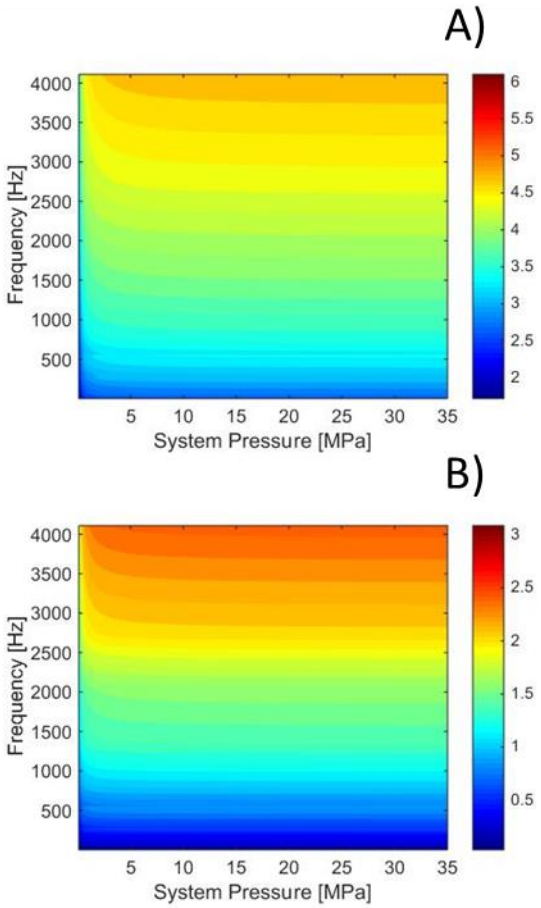

Figure 3-18: Shear modulus of syntactic foam, 50% initially microsphere by volume, atmospheric IMP. A) Storage modulus, B) Loss modulus

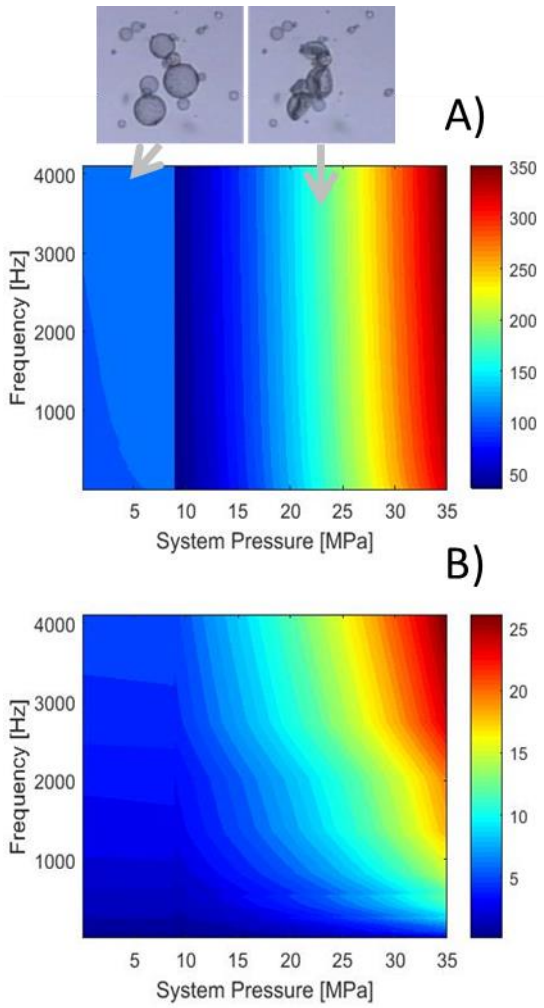

Figure 3-19: Bulk modulus with pressurized microsphere to 8 MPa, 50% initially microsphere by volume, state of microspheres shown. A) Storage modulus, B) Loss modulus

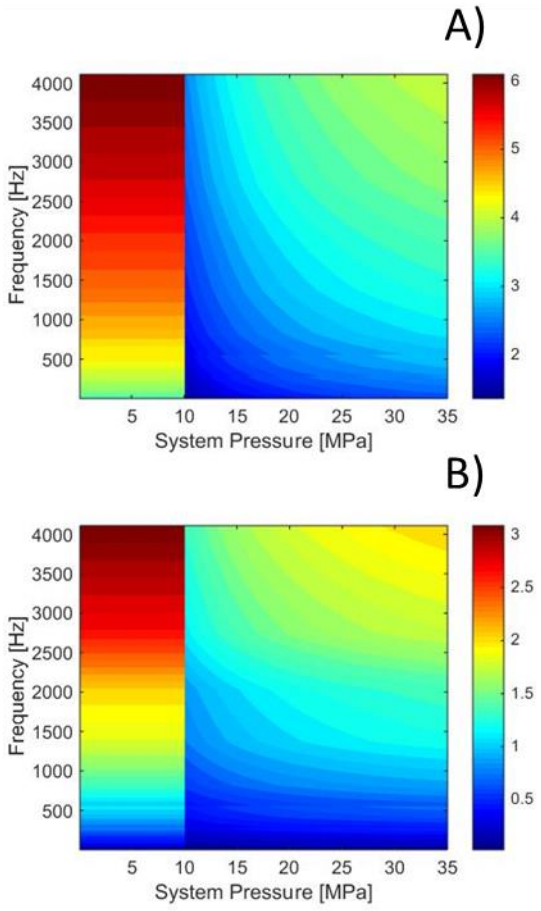

Figure 3-20: Shear modulus with pressurized microspheres to 8 MPa, 50% initially microsphere by volume. A) Storage modulus, B) Loss modulus

3.7.2 Deformed Volume under Hydrostatic Pressure

After the material properties are calculated, it is also necessary to calculate the reduced volume of foam at a given pressure to perform further calculations, specifically transmission loss predictions. The material properties are functions of pressure; therefore, the deformation of a foam annulus cannot accurately be calculated with a single linear relation. The total deformation is calculated using a superposition of an externally loaded capped annulus and an internally loaded, uncapped annulus. The relations for the deformations of the three relevant dimensions are presented in Table 3-1. Since the material properties of the foam change with pressure, the desired pressure is divided into

increments and the deformation is calculated by iterating through each pressure increment. The deformed dimensions from the prior iteration are used to calculate the following iteration. A convergence study was conducted to see the number iterations necessary to achieve an accurate prediction. Figure 3-22 shows the deformed volume as a fraction of the predicted deformed volume for one million iterations. The predicted normalized volume approaches unity for relatively low number of iterations; therefore, Figure 3-23 is used to show the predicted volume up to 50,000 iterations. In Figure 3-23, the predicted volume seems to oscillate with changing iteration number. The reason for the oscillation is what fraction of pressure iterations occur at system pressures which are pre- or post-microspheres collapse. The relative maxima have a larger fraction of precollapsed iterations while the relative minima have a lower fraction of precollapsed iterations. The exact behavior of the local extrema will shift depending on the exact conditions of the foam, i.e. the dimensions of the microspheres and the predicted usage conditions. However, the general trend suggests 10,000 iterations are sufficient to find a deformed volume of foam; the predicted volume is above 99.99% of the predicted volume for 1,000,000 iterations while being less computationally expensive.

Table 3-1: Deformations of an annulus for interior and exterior loading, dimensions shown in Figure 3-21

Dimension	Deformation due to inner loading	Deformation due to outer loading
r_i	$\Delta r_i = \frac{P r_i}{E}\left(\frac{r_o^2 + r_i^2}{r_o^2 - r_i^2} - \nu\right)$ (3.32)	$\Delta r_i = \frac{-P r_i}{E}\frac{r_o^2(2-\nu)}{r_o^2 - r_i^2}$ (3.33)
r_o	$\Delta r_o = \frac{P}{E}\frac{2 r_o r_i^2}{r_o^2 - r_i^2}$ (3.34)	$\Delta r_o = \frac{-P r_o}{E}\frac{r_o^2(1-2\nu) + r_i^2(1+\nu)}{r_o^2 - r_i^2}$ (3.35)
L	$\Delta L = \frac{-P\nu L}{E}\frac{2 r_i^2}{r_o^2 - r_i^2}$ (3.36)	$\Delta L = \frac{-P L}{E}\frac{r_o^2(1-2\nu)}{r_o^2 - r_i^2}$ (3.37)

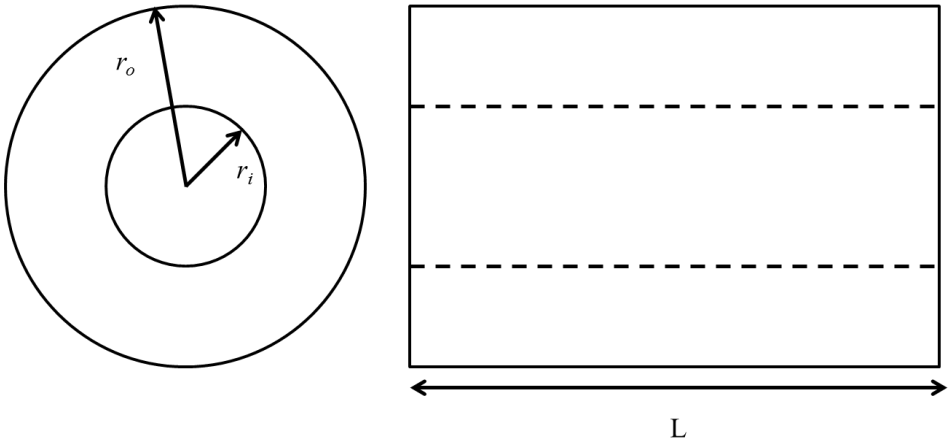

Figure 3-21: Dimensions of foam annulus

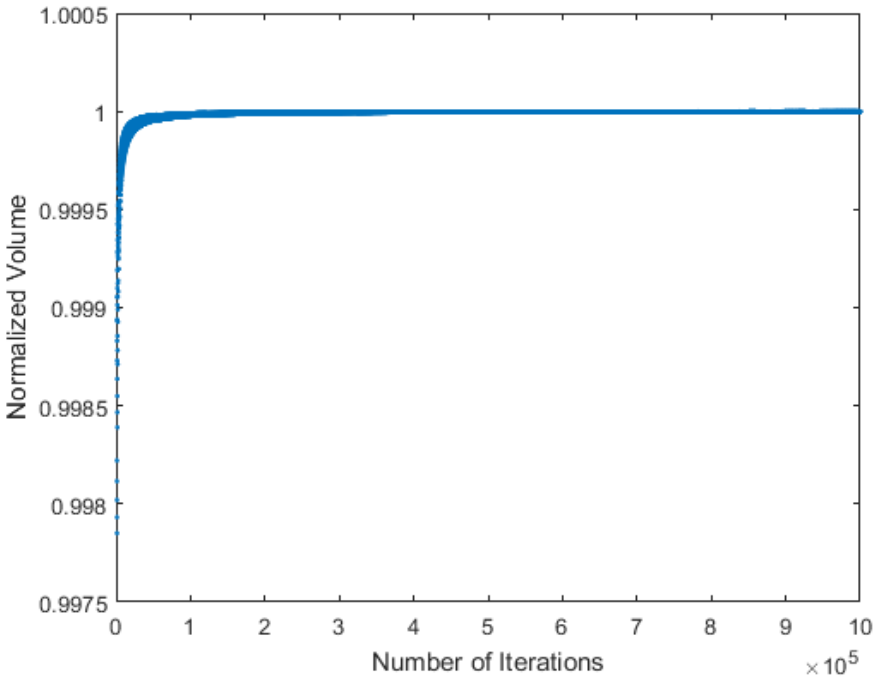

Figure 3-22: Convergence of predicted deformed volume over number of iterations. Volume normalized to deformed volume after one million iterations.

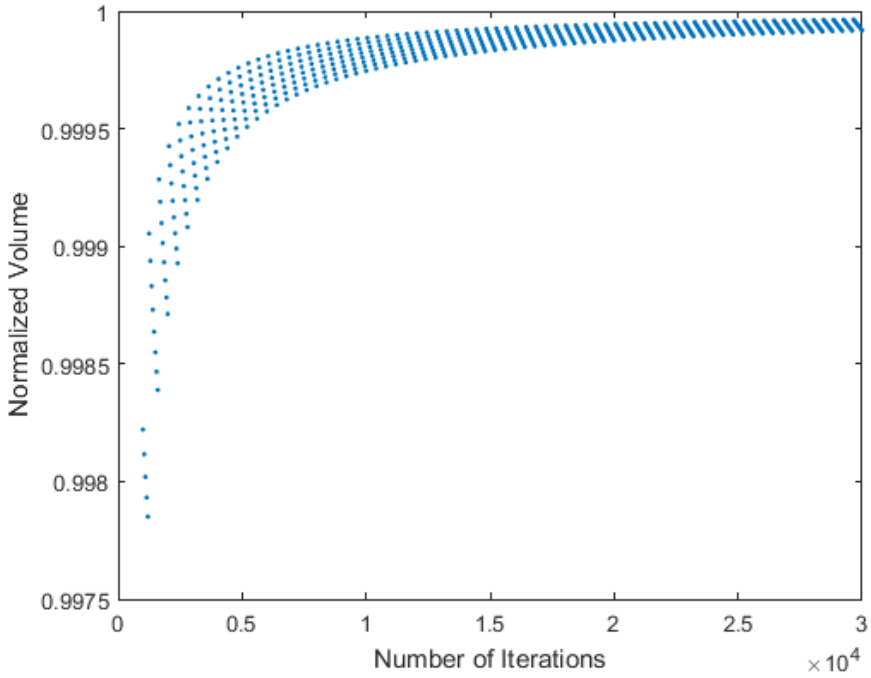

Figure 3-23: Convergence of predicted deformed volume over number of iterations. Volume normalized to deformed volume with one million iterations. Predicted volume shown up to 30,000 iterations.

3.7.3 Remaining Material Properties

In order to calculate the remaining material properties – Young's modulus, Poisson's ratio and Lame's parameter – linear material relations are used for each simulated frequency and system pressure under the assumption of local linearity in terms of deformed state for the system pressure and dynamic properties for the frequency. The material moduli relations are given by

$$E^* = \frac{9K^*G^*}{3K^* + G^*}, \tag{3.38}$$

$$\lambda^* = K^* - \frac{2G^*}{3}, \tag{3.39}$$

and

$$\nu^* = \frac{3K^* - 2G^*}{2\left(3K^* + G^*\right)}, \tag{3.40}$$

where E is Young's modulus, K is bulk modulus, G is shear modulus, ν is Poisson's ratio, λ is Lame's parameter and the * superscript denotes the effective parameter of the entire foam composite. Calculation of the full set of material parameters allows for more complete modeling usages; most importantly Lame's parameter is necessary for simulating transmission loss of a suppressor employing syntactic foam.

3.8 Non-ideal Gas Behavior

The ideal gas law only holds for gases of lower temperature or pressure and a more complete model may be necessary for precise predictions outside of these conditions. The compressibility factor, z, is defined by

$$z = \frac{P v}{R T}, \tag{3.41}$$

where P is the absolute pressure, v is the specific volume, R is the specific gas constant and T is the absolute temperature. For an ideal gas, the compressibility factor is unity; however, for non-ideal gases compressibility factor can deviate as shown in Figure 3-24. Compressibility factor is a function of pressure, specific volume and temperature and can be solved through a derivation of the Van der Waals gas relation, which accounts for the interaction of molecules in a gas unlike the ideal gas law,

$$P = \frac{R T}{v - b} - \frac{a}{v^2}, \tag{3.42}$$

where P is pressure, R is the specific gas constant, v is specific volume, a is a constant which accounts for the force of attraction between molecules and b accounts for the finite volume occupied by the molecules [49]. equation (3.42) can be analyze at the critical point of the gas to remove the unknown constants,

$$a = \frac{27}{64}\frac{R^2 T_c^2}{P_c} \tag{3.43}$$

$$b = \frac{R T_c}{8 P_c} \tag{3.44}$$

where the subscript c denotes the critical value of the quantity for a specific gas. The pressure, specific volume and temperature are often given in their reduced form, i.e. in ratio to their critical values,

$$P_r = \frac{P}{P_c}, v_r = \frac{v}{v_c}, T_r = \frac{T}{T_c}. \tag{3.45}$$

equations (3.43) and (3.44) are substituted into equation (3.43) and then simplified with the reduced parameters to

$$\left(p_r + \frac{3}{v_r^2}\right)(3v_r - 1) = 8T_r \tag{3.46}$$

which allows for calculation of volume at elevated pressure and temperature. For nitrogen, the critical pressure is 3.4 MPa, the critical temperature is 126 K and the critical volume is 0.00322.

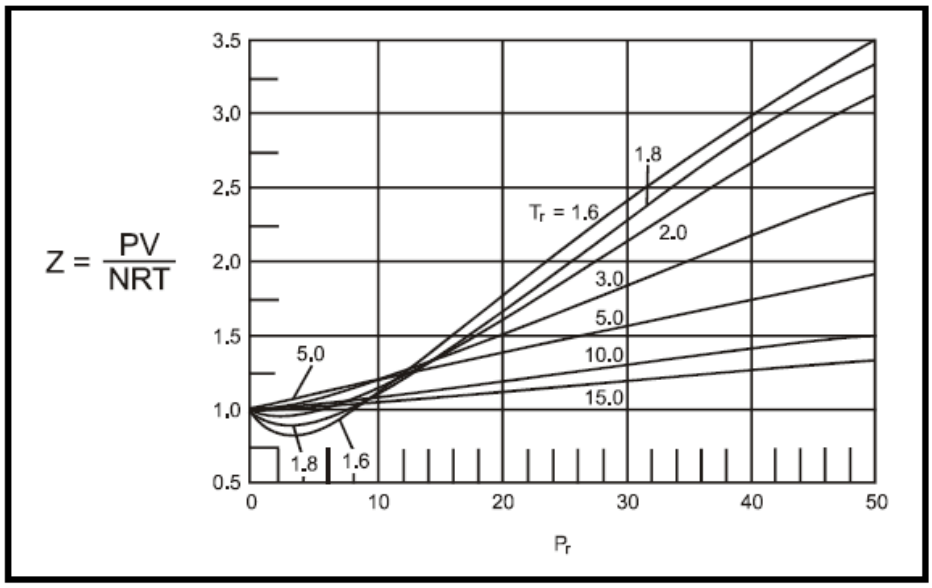

Figure 3-24: Compressibility factor of a gas [50]

Figure 3-25 shows the predicted volumes for the volume created by a collapsed microsphere over the system pressure range under consideration. For the entire pressure range Boyle's law predicts a larger volume than Van der Waals compressibility by between 4 and 35% with the two predictions converging at higher pressures. If the system pressure continues to be increased, eventually the Van der Waals prediction will be larger. Figure 3-26 shows the bulk modulus of the void across system pressures. For an ideal gas the bulk modulus may be calculated with either an isothermal or adiabatic assumption; an isothermal assumption predicts the bulk modulus is equivalent to the system pressure and an adiabatic assumption predicts the bulk modulus to be the ratio of specific heats multiplied by the system pressure. The bulk modulus for the Van der Waals compressibility is calculated through the definition of bulk modulus and modelled volume. The isothermal assumption is the lowest bulk modulus for the entire pressure range. The adiabatic assumption predicts a higher bulk modulus until 25 MPa when the Van der Waals assumption becomes the high bulk modulus.

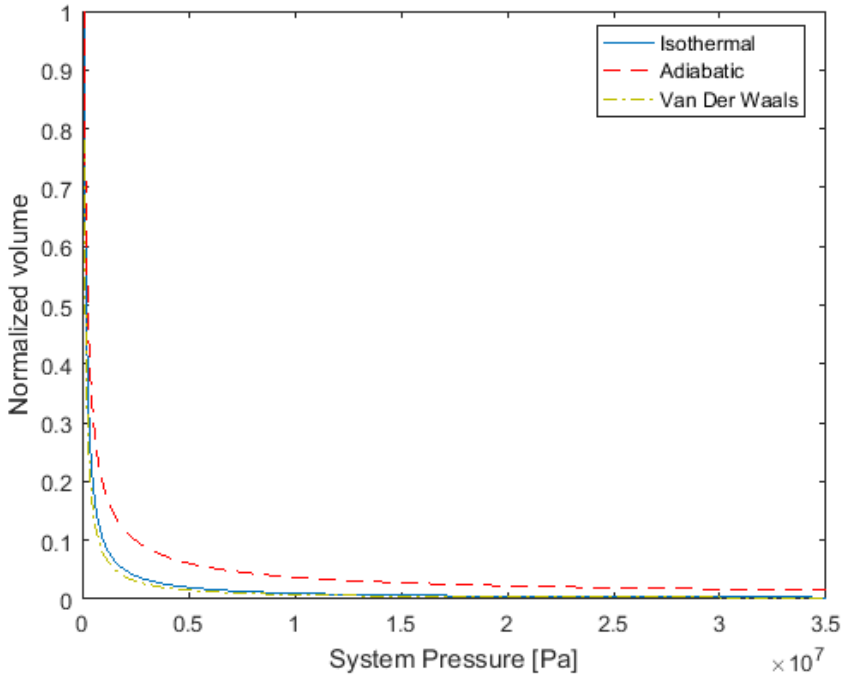

Figure 3-25: Volume of a representative microsphere for Boyle's law compression and Van der Waal's prediction at 25 °C

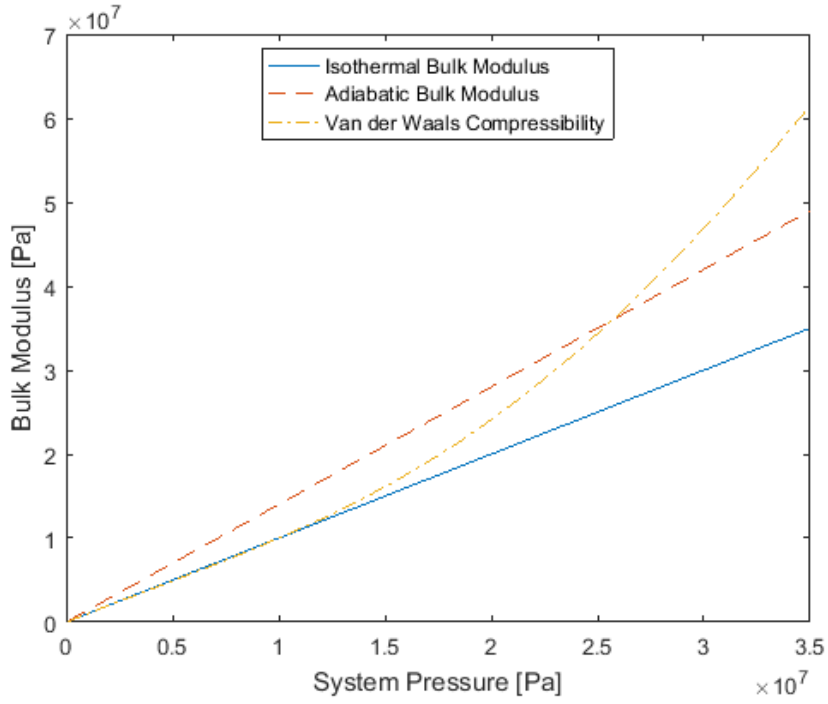

Figure 3-26: Bulk modulus for gas using different compression assumptions at 25 °C

The difference in void volume and bulk modulus of the gas over different assumptions will change the effective bulk modulus of the composite foam. Figure 3-27 shows the effective bulk modulus of atmospheric IMP microspheres at -40 °C for the three different assumptions of compression behavior and Figure 3-28 shows the adiabatic and Van der Waals predictions normalized to an Isothermal assumption as well as the Van der Waals assumption normalized to adiabatic. Similar to Figure 3-26, the bulk modulus of an adiabatic assumption is highest at lower system pressures and the Van der Waals assumption is highest at high system pressure. Figure 3-29 and Figure 3-30 show the absolute and relative bulk moduli for the three assumptions with atmospheric IMP at a temperature of 100 °C. The deviation from ideal gas behavior is higher at elevated temperature and it follows logically the Van der Waals prediction deviates from the other two assumptions more at higher temperature as seen in Figure 3-30. The same analysis was conducted for microspheres with 8 MPa IMP at both -40 °C and 100 °C, with the predicted bulk modulus shown in Figure 3-31 to Figure 3-34. Similar conclusions can be drawn that at higher temperature the deviation between predictions is larger at high temperatures. The difference in IMP also affects the predicted modulus, which is most evident in the Van der Waals to Isothermal comparison in Figure 3-32. Other cases of IMP and temperature are shown in Appendix C.1.

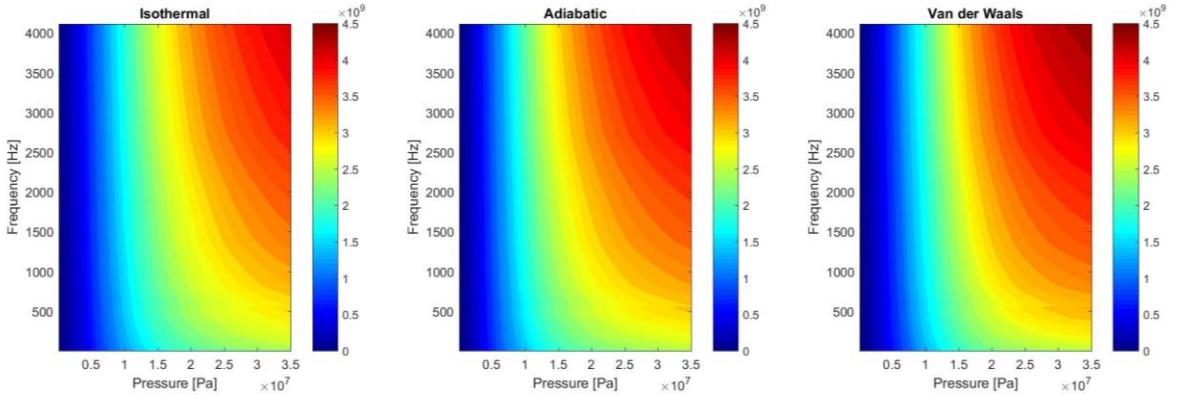

Figure 3-27: Absolute bulk modulus for atmospheric IMP microspheres at -40 °C for three gas compression assumptions

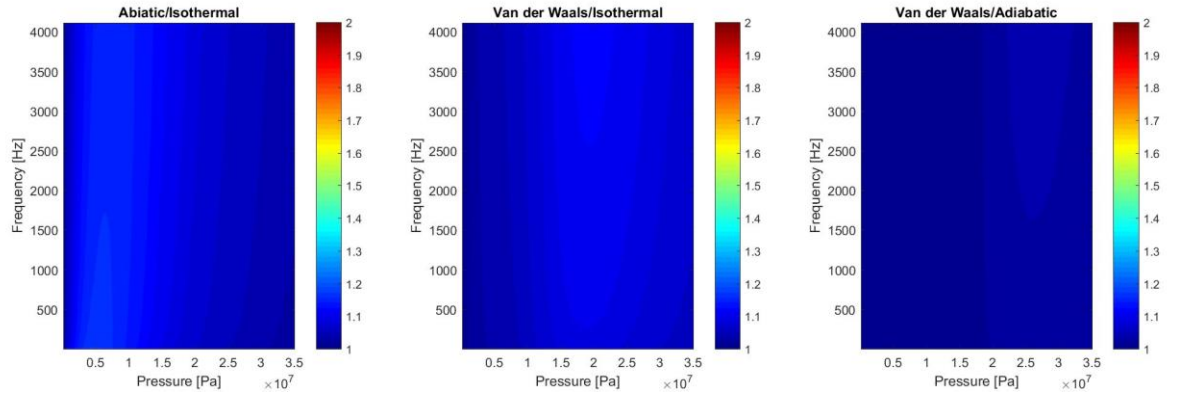

Figure 3-28: Relative bulk modulus for atmospheric IMP microspheres at -40 °C for three gas compression assumptions

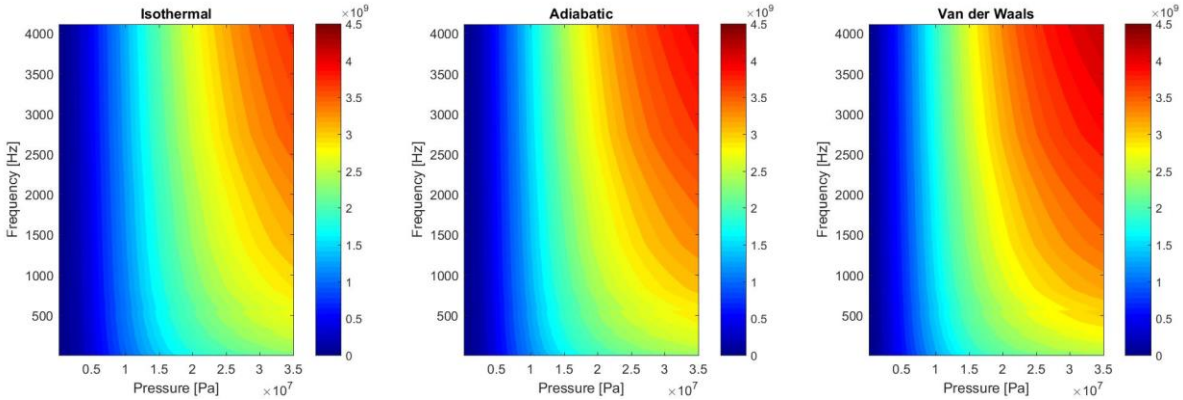

Figure 3-29: Absolute bulk modulus for atmospheric IMP microspheres at 100 °C for three gas compression assumptions

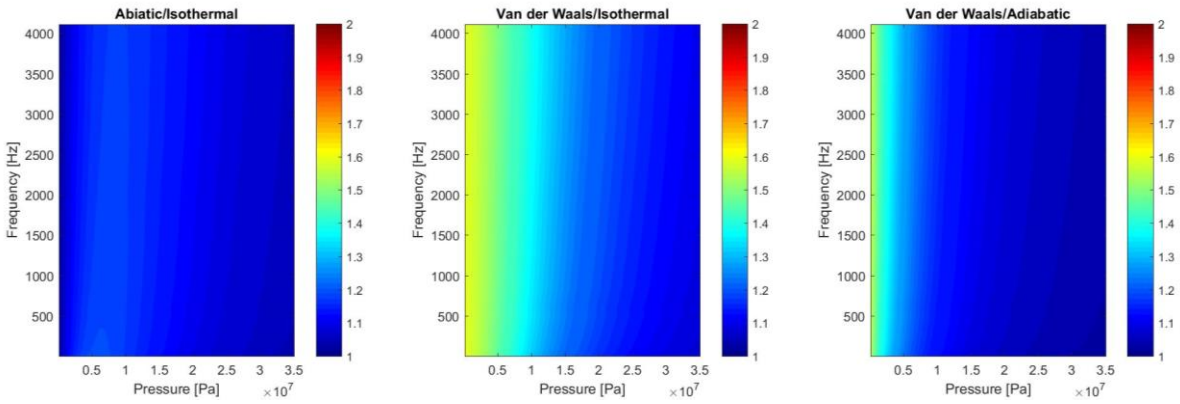

Figure 3-30: Relative bulk modulus for atmospheric IMP microspheres at 100 °C for three gas compression assumptions

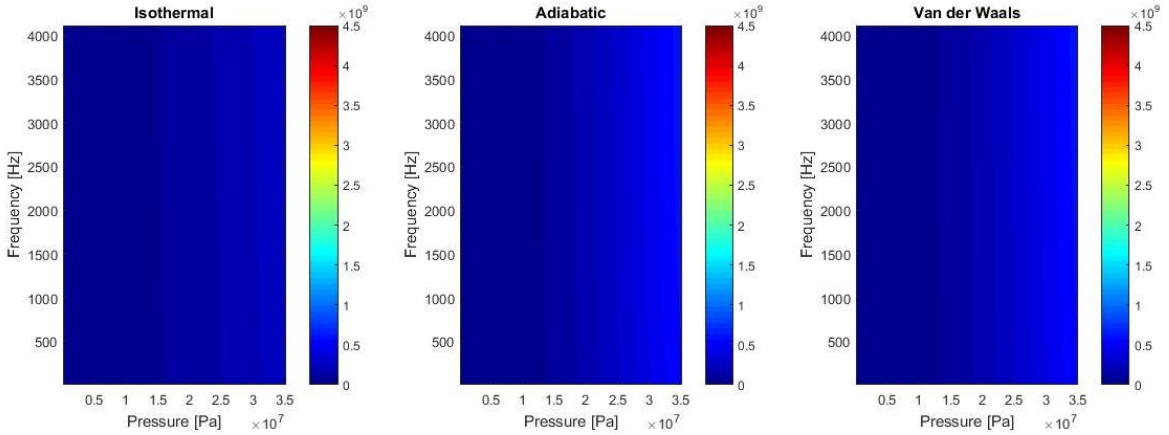

Figure 3-31: Absolute bulk modulus for 8 MPa IMP microspheres at -40 °C for three gas compression assumptions

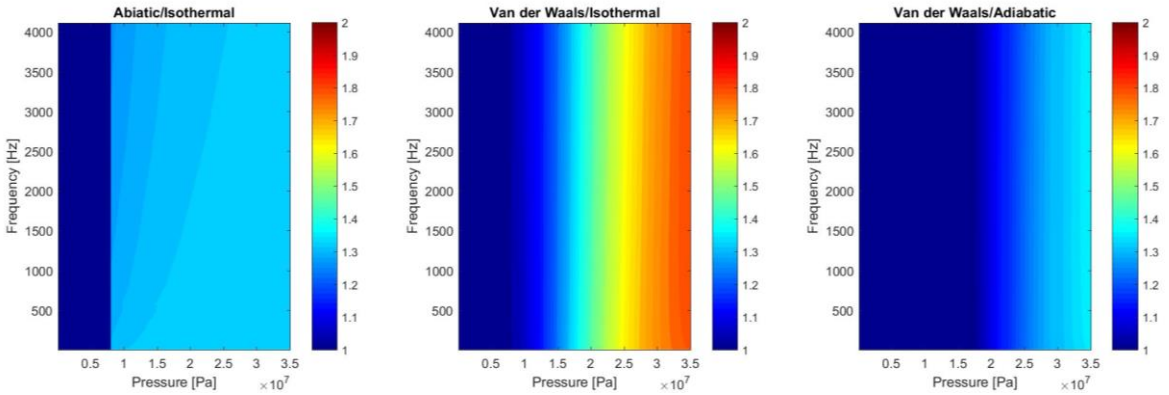

Figure 3-32: Relative bulk modulus for 8 MPa IMP microspheres at -40 °C for three gas compression assumptions

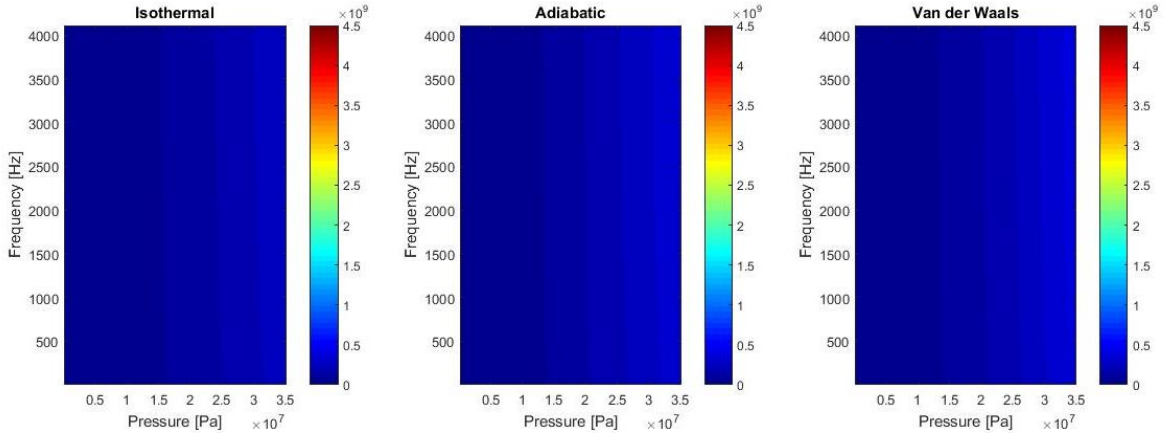

Figure 3-33: Absolute bulk modulus for 8 MPa IMP microspheres at 100 °C for three gas compression assumptions

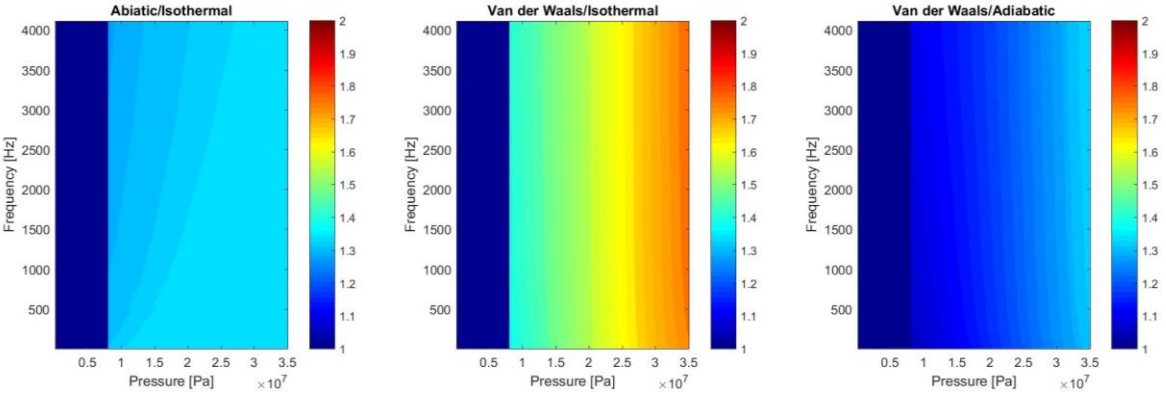

Figure 3-34: Relative bulk modulus for 8 MPa IMP microspheres at 100 °C for three gas compression assumptions

The slight difference in predicted bulk modulus may manifest itself in difference in noise control effectiveness as predicted by transmission loss. The transmission loss is modeled for a several system pressures; some predictions are shown in Figure 3-35 to Figure 3-39 all with the host from the first generation of foam. In general there are slight differences in transmission loss for almost all cases. The largest differences are seen between the isothermal bulk modulus assumption and Van der Waals compression are on the order of two decibels in certain frequency ranges. The difference between an isothermal bulk modulus prediction and a Van der Waals assumption are typically on the

order of less than one decibel. In general, neither difference is very large – the assumption made for gaseous compression does not materially affect the predictions.

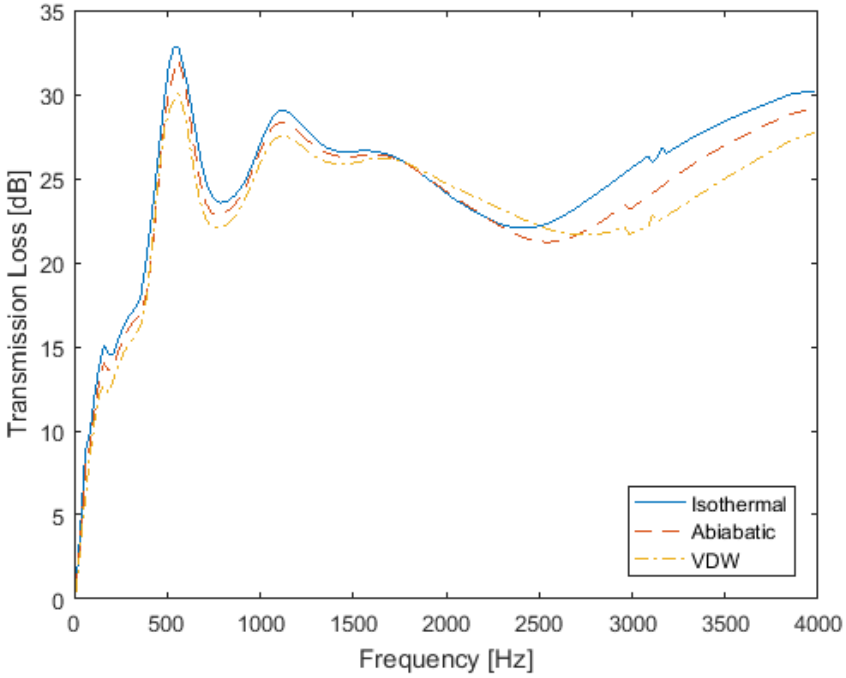

Figure 3-35: Transmission loss prediction for multiple gas compression assumptions, system pressure 2 MPa

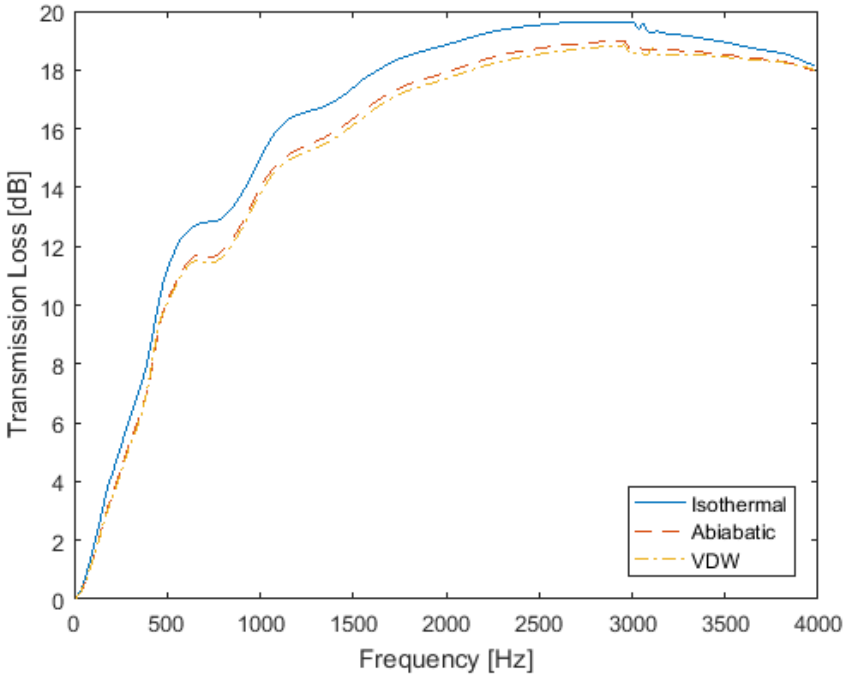

Figure 3-36: Transmission loss prediction for multiple gas compression assumptions, system pressure 8 MPa

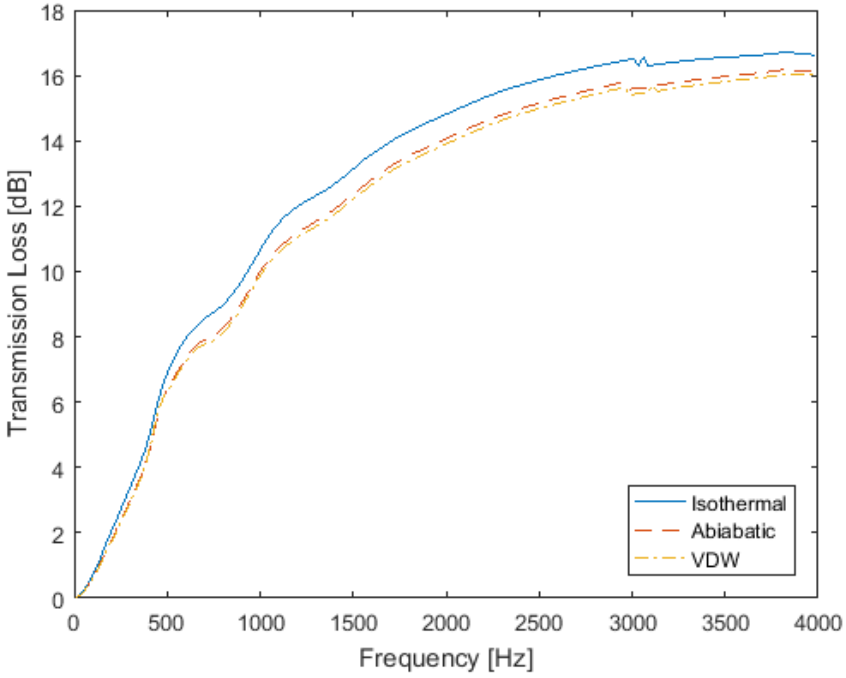

Figure 3-37: Transmission loss prediction for multiple gas compression assumptions, system pressure 15 MPa

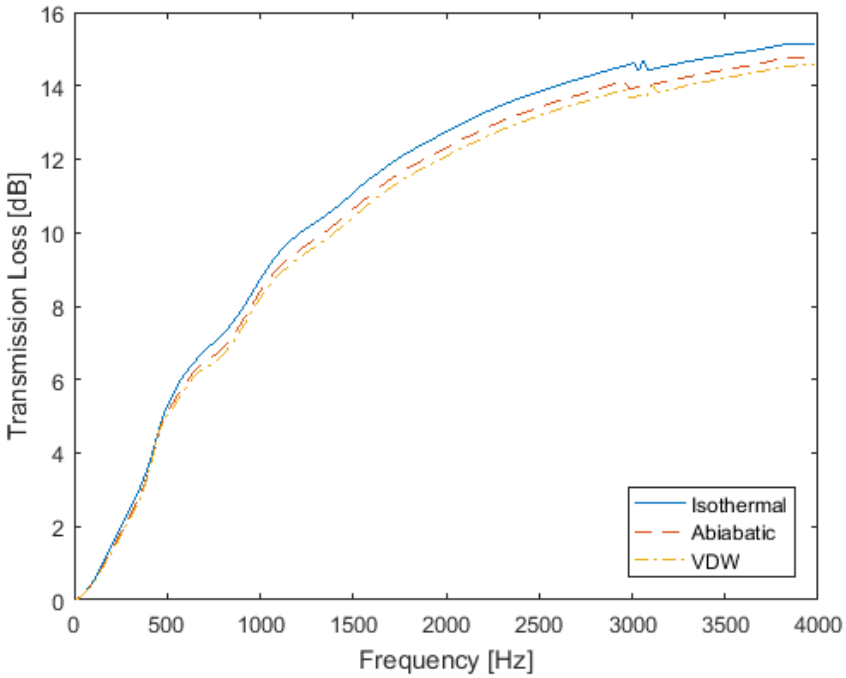

Figure 3-38: Transmission loss prediction for multiple gas compression assumptions, system pressure 25 MPa

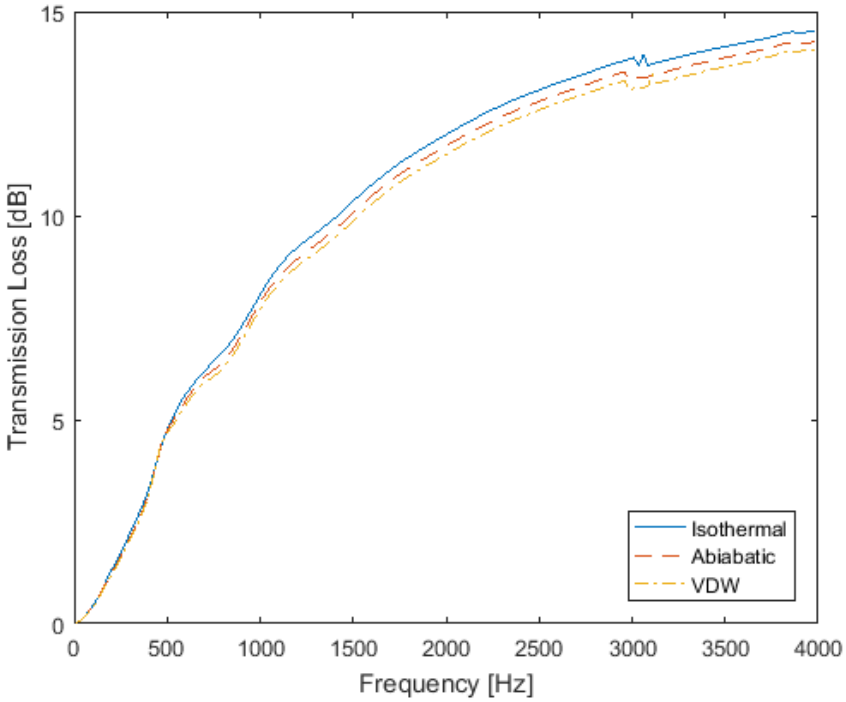

Figure 3-39: Transmission loss prediction for multiple gas compression assumptions, system pressure 35 MPa

CHAPTER 4

SYNTACTIC FOAM COMPOSITION AND FABRICATION

The syntactic foam used for hydraulic noise control is fabricated from a two-part polymer and properly prepared microspheres. A two-part polymer is manufactured from two constituent phases being mixed together and allowed to cure; the relative fraction of each constituent allows for some control over material properties. The most common fabrication method is to use a two part polymer and mix the microspheres into the polymer constituents before combining the polymer constituents together and casting into a mold. A benefit to this method is any foam geometry can be achieved for usage throughout the entire hydraulic system. The host polymer is responsible for interfacing directly with the hydraulic oil environment which requires chemical resistance and toughness as well as providing the loss characteristics for the composite. Collapsed microspheres create voids within the polymer which add compliance to the foam driving the primary noise control method.

4.1 Desired Host Polymer Properties

The host polymer makes up a significant fraction of the composite foam especially at elevated pressure and its properties must be considered when designing an optimal foam. The properties under consideration are mechanical moduli and its robustness. First, the modeling techniques will be used to determine the optimal bulk modulus of a host material. The effective bulk modulus of a composite is calculated by the composite spheres method, presented in Section 3.2, and given by the relation

$$K^* = K_m + (K_i - K_m)\frac{(4G_m + 3K_m)c}{4G_m + 3K_i + 3(K_m + K_i)c}, \tag{4.1}$$

where K is the bulk modulus, G is the shear modulus, c is the volume fraction and subscripts m and i represent the matrix – host polymer – and inclusions – voids or microspheres depending on pressure, respectively. For the purpose of hydraulic noise control, it is desirable for the foam to obtain the lowest effective bulk modulus. The purpose of the following analysis is to find the optimal bulk modulus for the host polymer, i.e. what value of host bulk modulus leads to the lowest effective bulk modulus and least amount of transmitted noise. The extrema of the effective bulk modulus are found by taking the derivative of the effective bulk modulus with respect to the host bulk modulus and setting the derivative equal to zero,

$$\frac{\partial K^*}{\partial K_m} = 0\,. \tag{4.2}$$

Before conducting the differentiation several variable substitutions can be made to facilitate analysis by reducing the optimization variables to parameters which have been previously considered. The previously considered parameters are system pressure, volume fractions, Poisson's ratio and internal microsphere pressure (IMP). System pressure is at the discretion of the operator and the task trying to be accomplished. In general, a higher IMP and microsphere fraction in the composite treat noise more effectively. Also, the Poisson's ratio of the host has been determined to be most effective for noise control when very high. The bulk modulus and shear modulus of the host can be related through a parameter β,

$$\frac{G_m}{K_m} = \beta\,. \tag{4.3}$$

Commonly β will be a linear material relation between the two moduli. The bulk modulus of the gaseous inclusions is proportional to the gas pressure, which is the same as the system working pressure because the foam is hydrostatically loaded,

$$K_i = \gamma P \,, \tag{4.4}$$

where γ is a constant of proportionality, depending on which thermodynamic assumption is made regarding the compression of the gas. For an isothermal compression, γ is 1, and for an adiabatic compression, γ is 1.4. These values represent the limiting bounds, and in general the difference does not affect a large change in the optimal host modulus. The effective bulk modulus is also a function of volume fraction of inclusion, c, which changes at different system pressures. The volume fraction is calculated by

$$c = \frac{V_i}{V_i + V_m}, \tag{4.5}$$

where V_i is the volume of the inclusion and V_m is the volume of the host matrix. At elevated pressures, the volume of a gaseous inclusion changes in accordance with Boyle's law,

$$V_{i,f} = \frac{P_g V_{i,i}}{P}, \tag{4.6}$$

where P_g is the initial pressure of the gas and the trailing subscripts i and f denote initial and final volume respectively. This optimization does assume ideal gas behavior in order to arrive at a closed form solution. The optimization may be updated with non-ideal behavior, as discussed in Section 3.8; however, the non-ideal gas behavior does not make a large difference as discussed. The compressed volume of the host polymer is found through

$$V_{m,f} = V_{m,i} - \frac{P V_{m,i}}{K_m} . \tag{4.7}$$

equation (4.6) and (4.7) are then substituted into equation (4.5) to find the volume fraction at elevated pressure. By substituting equations (4.2) through (4.7) into equation (4.1), a new relation for effective bulk modulus is found by

$$K^* = \frac{K_m P \left(4 K_m P_g \beta \gamma V_{i,i} + 4 K_m^2 \beta V_{m,i} - 4 K_m P \beta V_{m,i} + 3 K_m P \gamma V_{m,i} + 9 K_m P_g \gamma V_{i,i} - 3 P^2 \gamma V_{m,i}\right)}{4 K_m^2 P \beta V_{m,i} + 4 K_m^2 P_g \beta V_{i,i} - 4 K_m P^2 \beta V_{m,i} + 3 K_m P^2 \gamma V_{m,i} + 6 K_m P P_g \gamma V_{i,i} - 3 P^3 \gamma V_{m,i} + 3 K_m^2 P_g V_{i,i}} . \tag{4.8}$$

equation (4.8) can now be differentiated with respect to the bulk modulus of the host,

$$\frac{\partial K^*}{\partial K_m} = \frac{P \left(4 K_m P_g \beta \gamma V_{i,i} + 4 K_m^2 \beta V_{m,i} - 4 K_m P \beta V_{m,i} + 3 K_m P \gamma V_{m,i} + 9 K_m P_g \gamma V_{i,i} - 3 P^2 \gamma V_{m,i}\right)}{4 K_m^2 P \beta V_{m,i} + 4 K_m^2 P_g \beta V_{i,i} - 4 K_m P^2 \beta V_{m,i} + 3 K_m P^2 \gamma V_{m,i} + 6 K_m P P_g \gamma V_{i,i} - 3 P^3 \gamma V_{m,i} + 3 K_m^2 P_g V_{i,i}} +$$
$$\frac{K_m P \left(4 P_g \beta \gamma V_{i,i} + 8 K_m \beta V_{m,i} - 4 P \beta V_{m,i} + 3 P \gamma V_{m,i} + 9 P_g \gamma V_{i,i}\right)}{4 K_m^2 P \beta V_{m,i} + 4 K_m^2 P_g \beta V_{i,i} - 4 K_m P^2 \beta V_{m,i} + 3 K_m P^2 \gamma V_{m,i} + 6 K_m P P_g \gamma V_{i,i} - 3 P^3 \gamma V_{m,i} + 3 K_m^2 P_g V_{i,i}} -$$
$$\frac{K_m P \left(4 K_m P_g \beta \gamma V_{i,i} + 4 K_m^2 \beta V_{m,i} - 4 K_m P \beta V_{m,i} + 3 K_m P \gamma V_{m,i} + 9 K_m P_g \gamma V_{i,i} - 3 P^2 \gamma V_{m,i}\right)}{\left(4 K_m^2 P \beta V_{m,i} + 4 K_m^2 P_g \beta V_{i,i} - 4 K_m P^2 \beta V_{m,i} + 3 K_m P^2 \gamma V_{m,i} + 6 K_m P P_g \gamma V_{i,i} - 3 P^3 \gamma V_{m,i} + 3 K_m^2 P_g V_{i,i}\right)^2} *$$
$$\left(8 K_m P \beta V_{m,i} + 8 K_m P_g \beta V_{i,i} - 4 P^2 \beta V_{m,i} + 3 P^2 \gamma V_{m,i} + 6 P P_g \gamma V_{i,i} + 6 K_m P_g V_{i,i}\right)$$

. (4.9)

Setting the right hand side of equation (4.9) to zero and rearranging solves to

$$
\begin{aligned}
&\left(16P\beta^2 V_{m,i}{}^2 + 16P_g\beta^2 V_{i,i}V_{m,i} + 12P_g\beta V_{i,i}V_{m,i}\right)K_m^4 + \\
&\ldots\left(-32P^2\beta^2 V_{m,i}{}^2 + 24P^2\beta\gamma V_{m,i}{}^2 + 48PP_g\beta\gamma V_{i,i}V_{m,i}\right)K_m^3 + \\
&\ldots\left(\begin{array}{l}
-16P^2P_g\beta^2\gamma V_{i,i}V_{m,i} + 12P^2P_g\beta\gamma^2 V_{i,i}V_{m,i} + \\
\quad\ldots 24PP_g{}^2\beta\gamma^2 V_{i,i}{}^2 + 16P^3\beta^2 V_{m,i}{}^2 - 48P^3\beta\gamma V_{m,i}{}^2 + \\
\quad\ldots 9P^3\gamma^2 V_{m,i}{}^2 - 48P^2P_g\beta\gamma V_{i,i}V_{m,i} + 45P^2P_g\gamma^2 V_{i,i}V_{m,i} \\
\quad\ldots + 54PP_g{}^2\gamma^2 V_{i,i}{}^2 + 9P^2P_g\gamma V_{ii}V_{mi}
\end{array}\right)K_m^2 + \\
&\ldots\left(\begin{array}{l}
-24P^3P_g\beta\gamma^2 V_{i,i}V_{m,i} + 24P^4\beta\gamma V_{m,i}{}^2 \\
\quad\ldots - 18P^4\gamma^2 V_{m,i}{}^2 - 54P^3P_g\gamma^2 V_{i,i}V_{m,i}
\end{array}\right)K_m \\
&\ldots + 9P^5\gamma^2 V_{m,i}{}^2 = 0
\end{aligned}
\tag{4.10}
$$

The ratio between host moduli, β, in (4.3) can be a function of any remaining material property if a linear assumption is made; however, it is simplest to use Poisson's ratio,

$$
\frac{G_m}{K_m} = \beta = \frac{3(1-2\nu)}{2(1+\nu)}. \tag{4.11}
$$

The optimal Poisson's ratio for a host polymer can be seen from analysis of Figure 3-8 in section 3.2. Poisson's ratio values below 0.49 are not desirable as the effective bulk modulus of the resulting foam will increase too quickly in the low system pressure range.

An example optimization calculation is shown in Figure 4-1 for the parameters listed in Table 4-1; there are two zero crossings indicating possible optima for the host bulk modulus. However, the predicted optimal bulk modulus for host polymer is lower than the most compliant known material, an ideal gas. Therefore, it is desirable to have the softest host polymer possible. By changing the γ parameter for the analyzed case in Figure 4-1, the curve shifts to the right by 1 MPa. The preceding analysis considers the storage modulus of the polymer as an optimization variable; it did not consider the loss

modulus which contributes less to noise control in a hydraulic system. However, the loss modulus does contribute to noise control; therefore, it is still beneficial to have a high loss modulus if feasible.

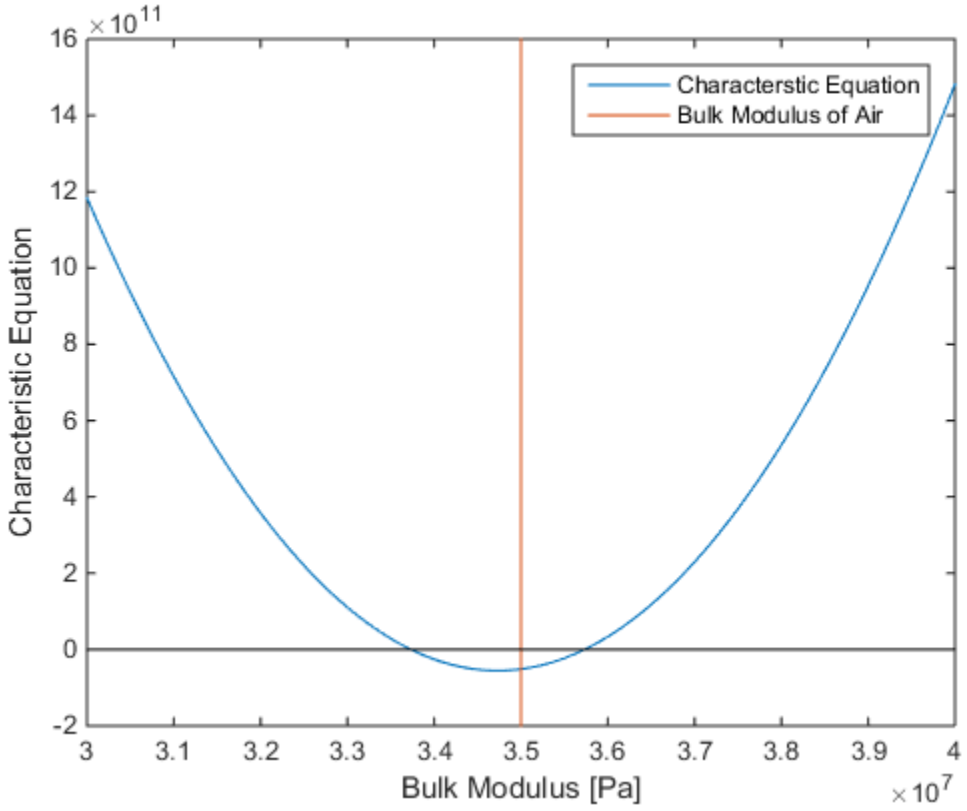

Figure 4-1: Characteristic equation for optimal bulk modulus

Table 4-1: Optimization Parameters

Parameter	Value
Initial Microsphere pressure	0.1 MPa
γ	1.4
β	0.001
Initial volume fraction of microspheres	50%

It is important to consider the limitations of equation (4.10). A limitation is that the optimization may predict a non-physical bulk modulus as the optimal modulus, as above. The material with the lowest known bulk modulus is an ideal gas with an isothermal compression assumption, meaning the bulk modulus is proportional to

pressure. Therefore, the lower bound of the bulk modulus is equivalent to system pressure. Furthermore, the derivation of the optimization makes a linear assumption for the behavior of the host material; if the material does not behave linearly, the model will need refinement. The refinements would be made in equation (4.7) by updating the material behavior of the compressed polymer and following the derivation forward.

In addition to having the optimal mechanical material properties, the host polymer directly interfaces with the hydraulic environment and must withstand its hazards. First, exposure to hydraulic oil will degrade some materials, which is unacceptable for a device which will be exposed to hydraulic fluid for long periods of time – on the order of decades. Second, hydraulic systems have operational temperature ranges from -40° C to 100° C, with localized heating above this. The temperature resistances as well as the aniline point for various polymers are shown in Figure 4-2. The aniline point of a material is a measure of how miscible the material is: a lower aniline point indicates the material will mix more readily, i.e. it will degrade. The blue shaded region indicates the typical range of a hydraulic system, both in aniline point and temperature. The material may change properties over this range, as discussed in Section 3.6, but it will not degrade. It is desirable that the properties do not change, allowing for the performance of the material to be independent of temperature. In addition, it is highly desirable to have a host with properties that are a weak function system pressure. However, if the properties do change with increasing system pressure, it is not criteria for rejection as the host is not the primary source of compliance.

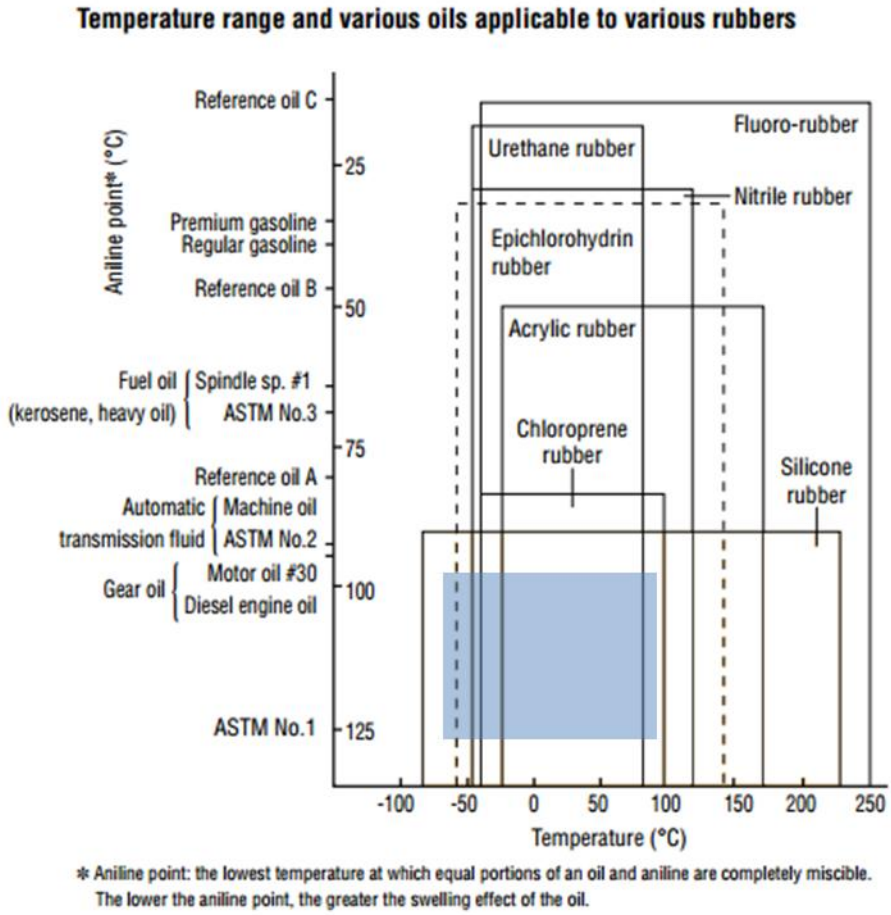

Figure 4-2: Temperature range and oil resistance of various polymers. Blue box indicated typical range of hydraulic systems. [51]

The polymer selected for the second generation of hydraulic noise control devices is a silicone rubber, shown in light orange in Figure 4-2. The only two polymers which cover the entire temperature range are silicone rubber and fluororubber. Fluororubbers have a much greater resistivity to the oil environment, as shown in Figure 4-2; however, fluororubbers generally come in pellet form, which must be screw-extruded, making it very difficult to achieve a homogenous mixing of the microspheres within the host polymer. Silicone rubber meets several important specifications to be a desirable host matrix. They are easy to obtain in two part components. Silicone rubbers can also be tuned in order to meet the desired material specifications. A two part, commercially

available silicone based polymer is Sylgard 184 produced by Dow Corning. Sylgard 184 is rated over the entire temperature range of hydraulic systems. Initial testing revealed a surface coating is necessary to prevent oil from being sorbed into the foam; surface coatings will be discussed in Section 4.4. If the oil is sorbed into the host polymer, it serves to stiffen the entirety of the foam which reduces its noise control effectiveness. Xiameter 3120 is another commercially available silicone based polymer which will be analyzed within.

4.2 Microsphere Inclusions

The voids, which are the main source of compliance of the syntactic foam, are created by the collapsed microspheres. The void leftover by the collapsed microsphere behaves as a gas bubble and therefore changes volume as predicted by Boyle's law, $PV=k$ where k is a constant or $P_1V_1=P_2V_2$, where 1 represents the initial state and 2 represents the final state of the gas. It is desirable to have the void retain its volume under increasing pressure; therefore, the initial pressure of the microsphere is increased. Figure 4-3, reproduced from Figure 2-13, shows the predicted volume fractions for three initial microsphere pressures (IMPs). As previously discussed in Section 2.3, a microsphere with atmospheric IMP rapidly compresses with increasing system pressure while microspheres with higher IMPs do not compress as drastically. The curves for the void fractions do not start at zero system pressure because the microspheres would not have collapsed at that pressure; therefore, the void fraction is undefined. In general, a larger void fraction means a more compliant foam which will increase noise control effectiveness.

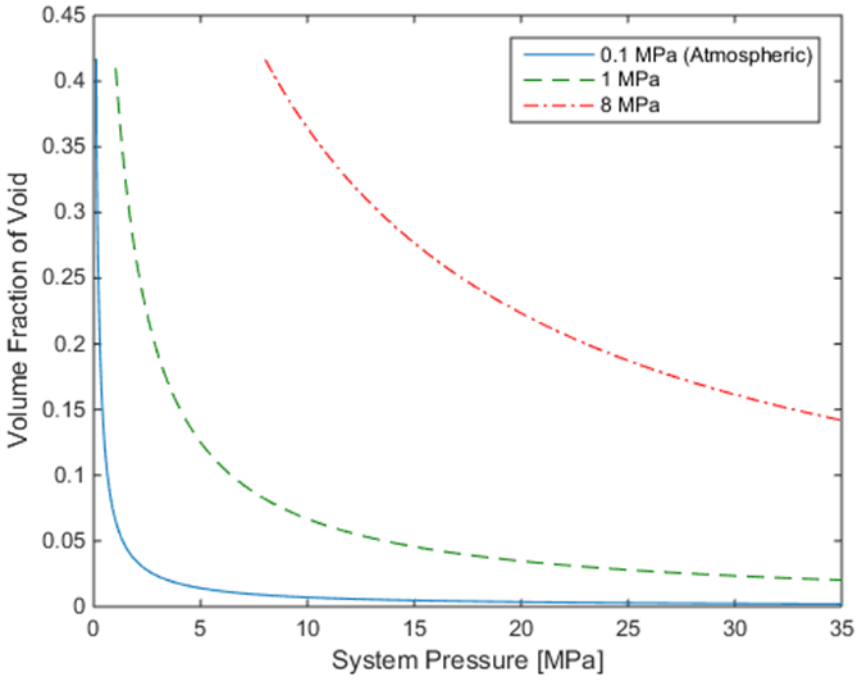

Figure 4-3: Void fractions for several IMPs over the pressure range of interest

4.2.1 Microsphere Material and Dimension

The utility of a microsphere in a hydraulic noise control sense is dictated by its collapse pressure and its burst pressure. The thin walled collapse equation, initially presented in equation (2.12) and reiterated here, is

$$P_{cr} = \frac{2Et^2}{r^2\sqrt{3\left(1-\nu^2\right)}} \tag{4.12}$$

where E is the Young's modulus of the microsphere material, ν is the Poisson ratio of microsphere material, t is the thickness of the microsphere and r is the radius of the microsphere. The model presented predicts a critical pressure which is higher than the critical pressure found through experimentation [52]. The actual microspheres are not perfect spheres: the small imperfections create local stress concentrations which lead to collapse at lower pressures than predicted, which is advantageous in this application.

A microsphere with a higher initial pressure will retain its volume more effectively at high pressure. Therefore, IMP should be as close to the burst pressure of the microspheres as possible to maximize void fraction within a composite foam for most effective noise treatment at elevated system pressures. The thin walled burst equation is

$$P_{burst} = \frac{2t\sigma_{yield}}{r}, \tag{4.13}$$

where t is the thickness of the microsphere, r is the radius of the microsphere and σ_{yield} is the yield stress of the microsphere material. The critical pressure is the pressure difference across the microsphere which causes collapse; the measured pressure on the exterior of the microsphere is the collapse pressure and will be the sum of the IMP and critical pressure. The previous relations assume thin-walled behavior and do not hold for thick walled microspheres; thick walled microspheres will be discussed in Section 4.2.3.

When analyzing equation (4.12) and equation (4.13), it is seen that both are functions of the thickness ratio, t/r. The critical pressure is a quadratic function of the thickness ratio and the burst pressure is a linear function. Since it is desirable to have low critical pressure and high burst pressure, it is beneficial to have a low thickness ratio. For a given thickness the critical pressure decreases faster than the burst pressure, as seen in Figure 4-4. Therefore, it is desirable to have a microsphere with a relatively large radius and then find the necessary thickness to contain the desired IMP.

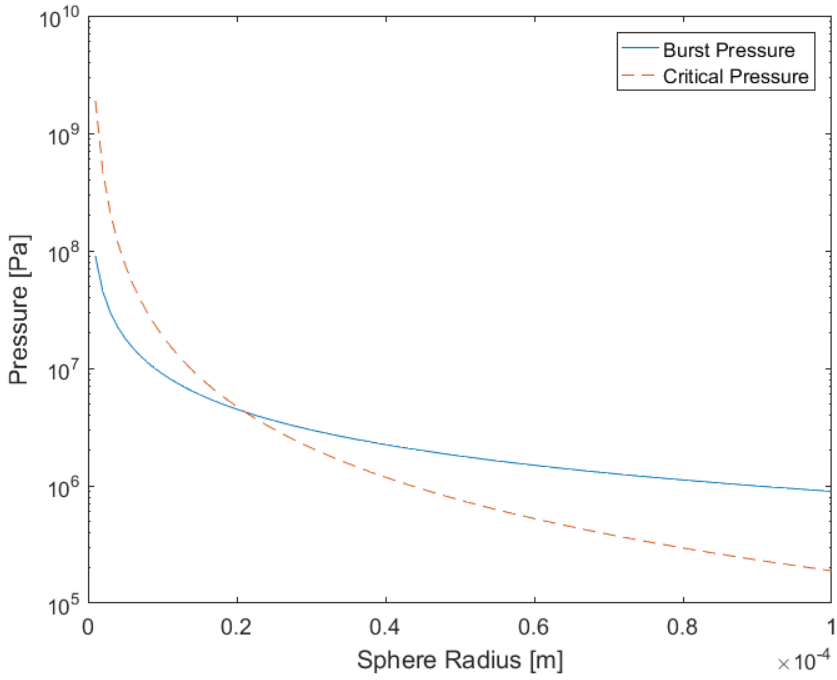

Figure 4-4: Burst pressure and critical pressure for a polystyrene sphere with fixed thickness, 0.8 µm, and varying radius.

The relevant material properties of the microsphere are the Young's modulus, Poisson's ratio and yield strength. It is necessary that the microspheres be constructed from a polymer to allow for preparation, which will be discussed in the following section, which bounds the Poisson's ratio between 0.3 and 0.5. However, it is desirable to have a material with lower Poisson's ratio in order to have a lower critical pressure. A low Young's modulus is also necessary for a low critical pressure. A low critical pressure is beneficial as the syntactic foam is effectively rigid at pressures lower than collapse pressure and ineffective at treating hydraulic noise. In order to increase the IMP for high pressure noise control, a high yield strength is desirable.

4.2.2 Microsphere Preparation

The microspheres are fabricated by the manufacturer at atmospheric pressure and therefore they have atmospheric IMP. As discussed above, the internal pressure of the

microsphere needs to be elevated in order to treat noise effectively. The internal pressure within the microsphere is increased by permeating a gas across the shell of the microsphere. Permeation is a combination of diffusion, molecules traveling through a barrier, and sorption, molecules entering and remaining in a barrier, as shown in Figure 4-5. Permeation is described mathematically by Fick's first and second laws; Fick's first law is

$$F = -D \, \partial C / \partial x \tag{4.14}$$

where F is the rate of transfer per unit area of section, C is the concentration of diffusing substance, in this case a gas, x is the space coordinate measured normal to the section and D is the diffusion coefficient [53]. equation (4.14) gives the permeation rate per area; therefore, for a given barrier a larger area will allow for greater permeation. Fick's second law, which relates the change in concentration of a substance over both time and space, is

$$\frac{\partial C}{\partial t} = D \frac{\partial^2 C}{\partial x^2}; \tag{4.15}$$

which can be transformed to spherical coordinates for easier use with microspheres

$$\frac{\partial u}{\partial t} = D \frac{\partial^2 u}{\partial r^2} \tag{4.16}$$

where $u=Cr$ [53]. The equations indicate that a thick membrane with a small area will slow permeation rate while a thin membrane with a large area will increase permeation rate. Furthermore, permeation coefficient, D, depends on the permeant, the gas for this

usage, and the membrane, the microsphere wall for this usage. For many polymers, nitrogen has the lowest permeation constant, i.e. the slowest permeation rate, which is desirable to ensure the pressure remains inside the microsphere for as long as possible [54]. In order to further extend the duration for which there is a high level of pressure within the sphere, the sphere wall is also chemically altered by exposing the membrane to fluorine after pressurization in order to slow the rate at which the gas permeates out of the microsphere after fluorination [55, 56].

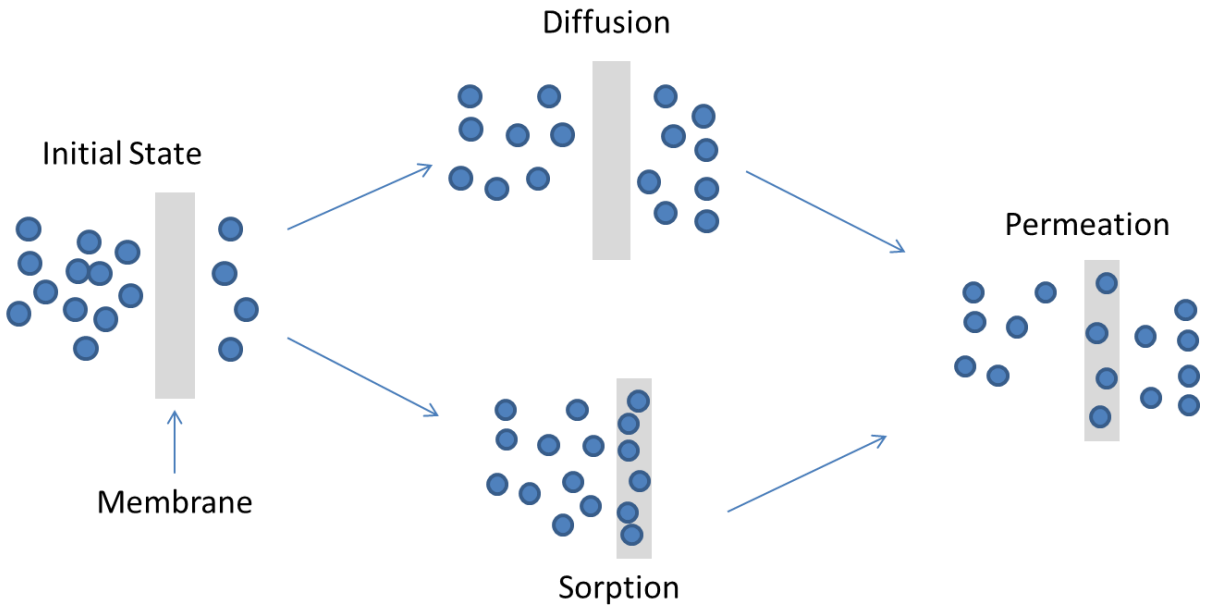

Figure 4-5: Diagram of diffusion, sorption and permeation

In order to assess if gas would permeate into microspheres and the rate of this permeation, a pressurization test fixture was constructed, shown in Figure 4-6. The first step in to pressurize microspheres is to increase the pressure within the pressure reaction vessel. The time trace of the pressure is known as the pressurization path. Several pressurization paths were analyzed but it was found exposure time was the most important variable for effective pressurization. Pressure inside the microspheres cannot be measured directly; instead, the pressure within the apparatus is lowered to atmospheric

pressure and then resealed to measure the gas which permeates out of the microspheres. The pressure is now higher within the microspheres and permeates out of them; the gas is trapped within the pressure reaction vessel and its pressure can be measured, this quantity is called the repressurization. Ideal gas relations and the measured depressurization value can be used to determine the pressure in the microspheres to determine the effectiveness of the pressurization. As expected from a first-order differential equation such as Fick's second law, the measured pressure changes exponentially over time. An example pressurization using a stair case pressurization path and associated repressurization is shown in Figure 4-7, Figure 4-8 and Figure 4-9.

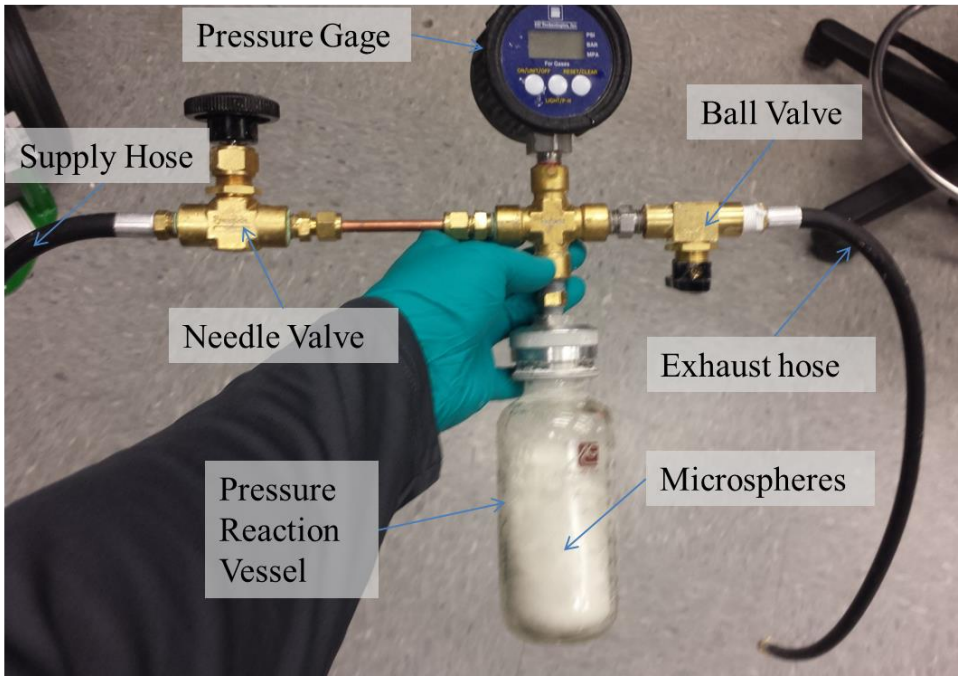

Figure 4-6: Picture of first version of pressurizer

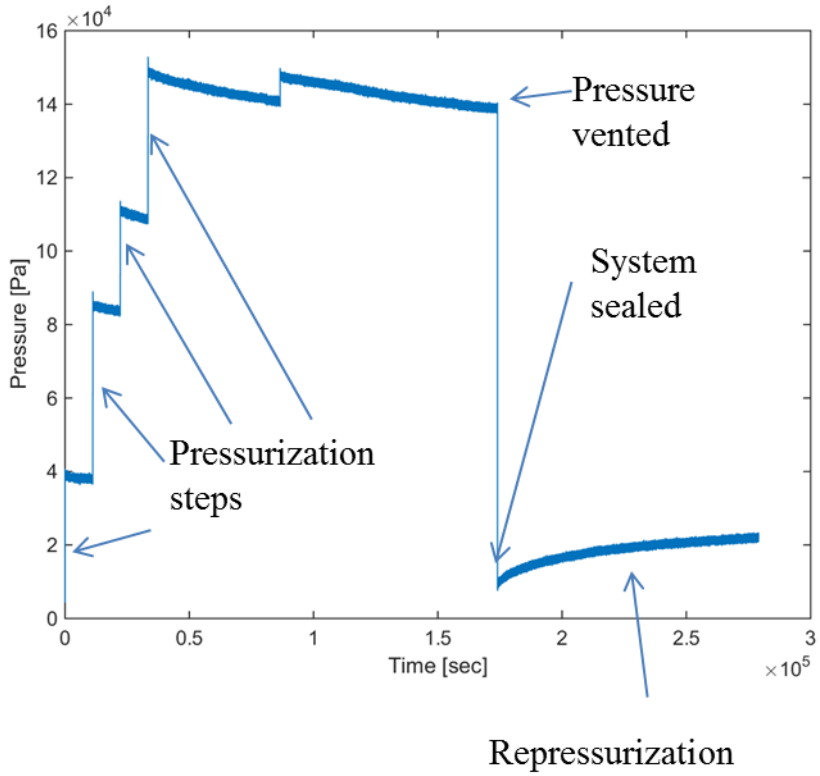

Figure 4-7: Pressurization of microspheres with staircase path

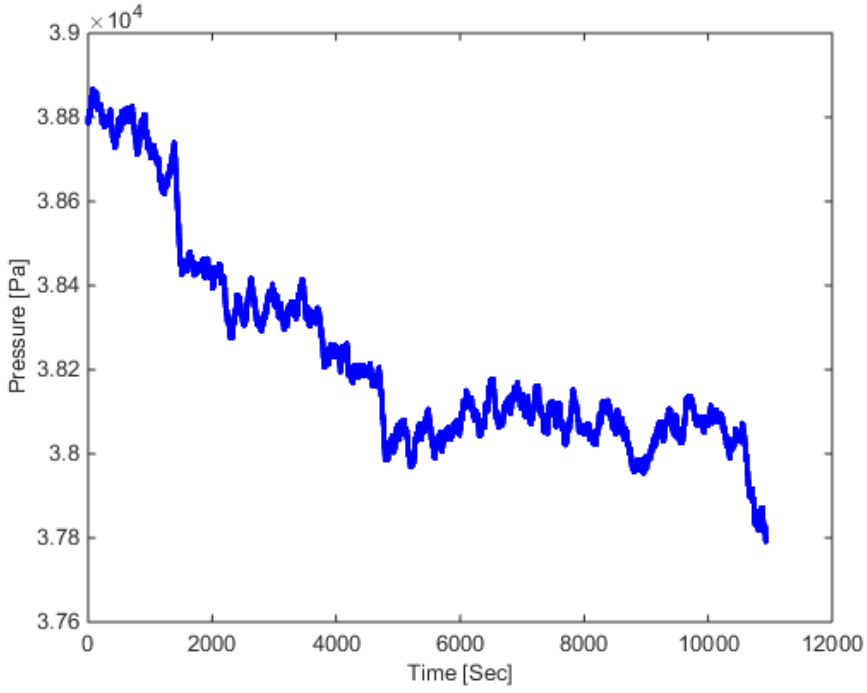

Figure 4-8: First step of pressurization

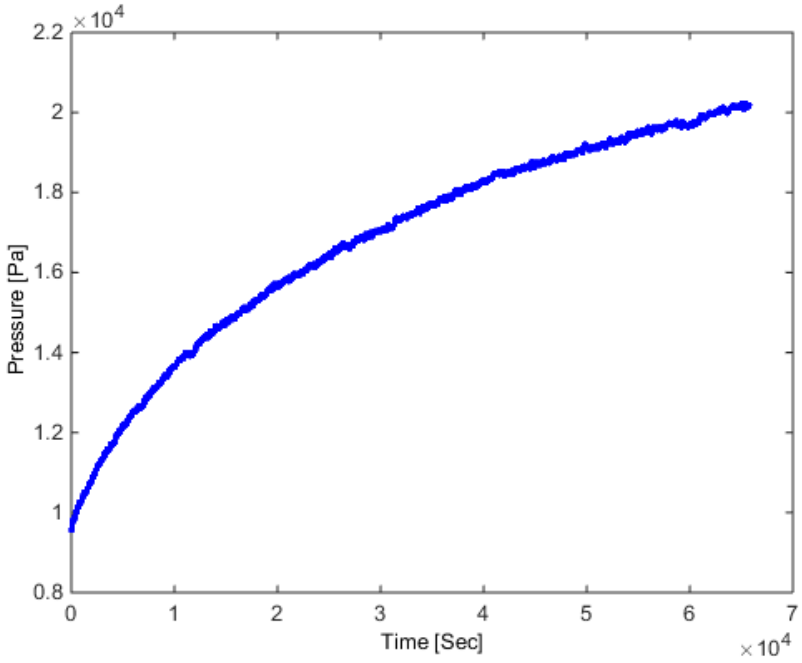

Figure 4-9: Repressurization

The amount of gas inside the system is fixed since the system is sealed; as gas permeates across the microsphere boundary the pressure within the apparatus decreases as seen after each time the pressure is increased in Figure 4-7 and more directly in Figure 4-8. The smallest and final pressurization was intended to accurately achieve the desired internal pressure within the microsphere. The decrease in pressure after each pressurization step could also be explained by a slow leak in the apparatus. The increasing pressure, shown in Figure 4-9, after the system pressure was vented and the system was resealed proves the decreasing pressure was not caused by a leak. The pressure is measured after the system was vented and resealed with the pressurized microspheres remaining within the chamber, shown in Figure 4-9. The increase in pressure is caused by gas permeating out of the microspheres; a system leak would not increase the pressure above atmospheric conditions.

The repressurization value can be used to determine the pressure within the microspheres before the system is vented by using isothermal ideal gas relations, the system volume and the volume of microspheres within the system. The relation is

$$P_{final} = \frac{P_{system,initial}V_{system} + P_{sphere,initial}V_{sphere}}{V_{system} + V_{sphere}}, \tag{4.17}$$

where P_{final} is the steady state pressure within the system; it is also important to note V_{sphere} is the total true volume of all microspheres interior. The true volume of microspheres is the apparent volume multiplied by the packing fraction of the microspheres. equation (4.17) can be algebraically manipulated to find initial microsphere pressure, $P_{sphere,initial}$.

A separate analysis was conducted to see if gas would permeate into collapsed microspheres by increasing the pressure within the test fixture above the collapse pressure of the microspheres and sealing the fixture. Over time the gas will permeate through the microsphere wall, which will narrow the pressure differential across the microsphere allowing the microsphere to regain its shape. This provides basis for microsphere pressurizations to be conducted at a given pressure without considering the collapse pressure of the microsphere, greatly decreasing the oversight necessary during pressurization.

Each pairing of permeant and membrane has a unique permeation coefficient. For two given polymer membranes, the order, in terms of fastest to slowest permeating, of permeation constants will necessarily not be the same for the same set of gases. Generally, nitrogen is one of the slowest permeating gases for almost every polymer [54]. One of the first permeation experiments ever conducted in 1866 found that a balloon

filled with pure nitrogen would expand after twenty-four hours because the oxygen in the surrounding environment was permeating into the balloon faster than the nitrogen was permeating out [57]. In addition, nitrogen is extremely abundant and relatively cheap which makes for an economical choice. Nitrogen has an additional benefit of being noncombustible, which is advantageous for two reasons. First, permeation rate increases with temperature; therefore, the rate of permeation into a microsphere can be increased if ambient temperature is increased, which may be advantageous for industrial level microsphere preparation. Second, the gas bubbles are wholly encapsulated within the foam may not be able dissipate heat which may auto-ignite a combustible gas. For commercial bladder-style suppressors and gaseous accumulators, nitrogen is the charging gas of choice because of its non-combustibility and long permeation time.

Permeation is a linearly reversible process; a permeant will goes into and out of a thin-walled microsphere at equal rates for similar boundary conditions. Therefore, it is highly desirable to have a process which can lock the pressure in the microsphere. Fluorination is one such process that chemically alters the composition of the microsphere material which prevents the gas from permeating out of the microsphere [55, 56]. Fluorination is a process where the electronegativity of fluorine is used to replace other atoms, particularly hydrogen, on the backbone of the polymer which makes up the microsphere wall. The strong bond and larger atom creates smaller gaps between atoms in the polymer chain which retard gas permeation through the microsphere wall. Each hydrogen bond is known as a replacement site; the fraction of engaged replacement sites determines the magnitude of reduction in permeation time. Commercial fluorination companies advertise that a successful fluorination can reduce the permeation constant by

a factor of 1000; however, this is for larger items where both sides of the barrier can be treated unlike the microspheres under analysis, where only the outer surface can be fluorinated. According to the manufacture, Expancel, the microspheres are fabricated from a polymer similar to poly-vinyl chloride (PVC). In order to achieve significant barrier improvement, approximately half of the hydrogen atoms on the PVC molecules need to be replaced by fluorine atoms. As the hydrogen replacement is an exothermic reaction, it is important to limit the reaction rate in order to prevent melting of the polymer. In two fluorination trials, a significant portion of the microspheres were melted and unable to be used in a syntactic foam. The permeation out of the microspheres is furthered extended once embedded within the host matrix which would provide a thicker barrier for the permeant to permeate through, extending the usage lifetime of the syntactic foam.

Fluorine will degrade most materials it comes in contact with; therefore, extreme precaution must be taken when fluorinating the microspheres. The first version of the pressurizer was not made of suitable materials for fluorine exposure. A second version was constructed; this version was constructed from Monel 405, a nickel alloy with extremely good chemical resistance including resistance to fluorine. The system has also been redesigned to allow for more effective handling of the microspheres and permeant gas; it is shown in Figure 4-10. The pressurization-fluorination chamber holds the microspheres for the duration of the microsphere preparation to be exposed to the permeant gas and then fluorinated. Needle valve 1 controls flow into the chamber while needle valve 2 controls flow out of the pressurization/fluorination chamber. Both ball valves are used to vent the system in an emergency blockage situation. For the

pressurization portion of the preparation, needle valve 1 is opened to allow the desired pressure into the chamber and then sealed for the length of the time necessary to allow the pressure inside the chamber to reach steady state. In order to fluorinate the microspheres both needle valves are slightly opened in order to induce flow through the chamber without reducing the pressure within the chamber. The fluorine regulator is set such that sufficient gas is supplied to the chamber. The exhaust out of the chamber flows through the scrubber. Within the scrubber, there is a limestone slurry in order to remove any remaining fluorine from the gas flow before being exhausted into a fume hood. The chemical reaction in the scrubber is given by

$$F_2 + 2H^+ + CaCO_3 \rightarrow CaF_2 + H_2O + CO_2 \tag{4.18}$$

The exhaust gas will primarily be made up of nitrogen and carbon dioxide, neither extremely dangerous to humans. The two ball valves are included for emergency exhausting of the gases into the scrubber. There is also a pressure relief valve to ensure the pressure within the chamber does not exceed the set value. The entire apparatus is used within a fume hood in case of leaks. The heating problem discussed above is further complicated by the optimal material for the preparation apparatus, Monel, which is an excellent heat insulator. In practice, purging the fluorination chamber with nitrogen intermittently will carry the heat out of the reaction chamber and prevent the microspheres from melting. A more detailed, step-by-step procedure is included in Appendix A.

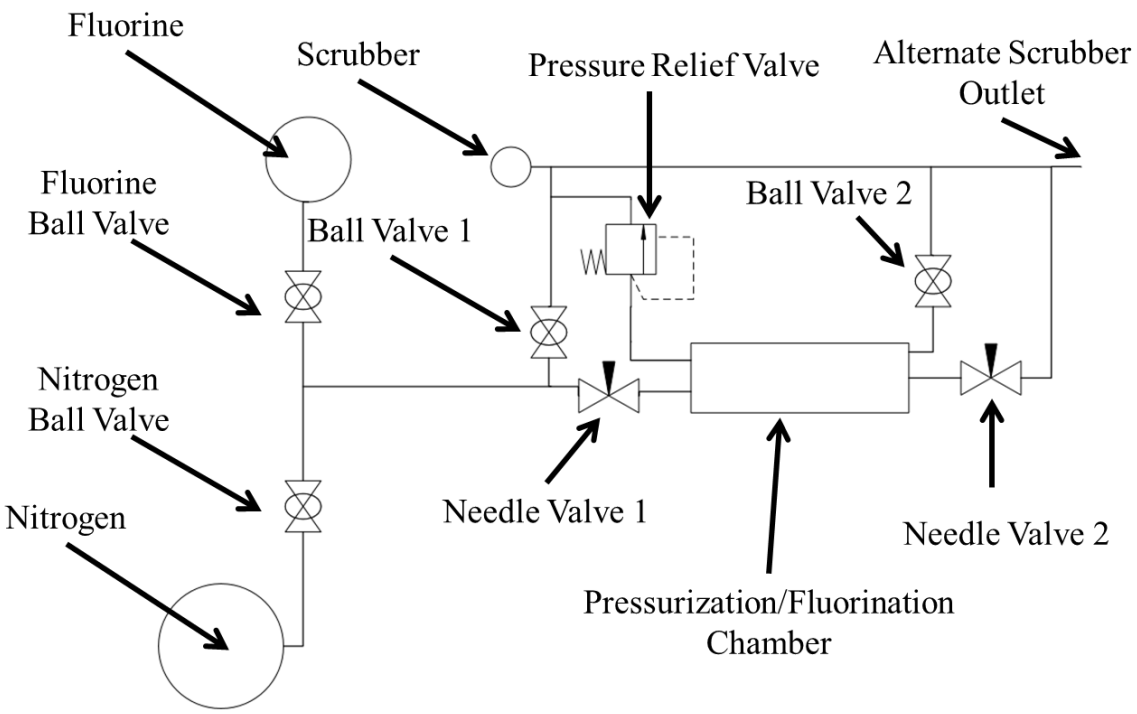

Figure 4-10: Schematic of fluorinator

4.2.3 Thick-Walled Microspheres

For a given sphere radius, a thicker sphere wall will have a higher burst pressure as well as increased permeation time with respect to thin-walled microspheres, which appears to be an improvement for this usage. At a certain thickness ratio, approximately 0.1, thin-walled assumptions no longer hold; therefore, equation (4.13) no longer accurately predicts the burst pressure and equation (4.12) no longer predicts the critical pressure of collapse. The closed-form solution to predict burst pressure of thick walled spheres is given by

$$P = \frac{2\sigma_y}{3}\left(1 - \frac{r_i^3}{r_o^3}\right) \tag{4.19}$$

where P is the burst pressure, σ_y is the yield strength, r_i is the inner radius and r_o is the outer radius, [58]. Figure 4-11 shows the predicted burst pressure for thin-walled and

thick-walled methods for thickness ratios from 0 to 1. The methods agree well at low thickness ratios but diverge at higher thickness ratios. Above a thickness ratio of 0.1, it is important to use the thick-walled criteria in order to accurately predict burst pressure. A closed-form solution for critical pressure has not been found in literature; however, an analytical solution is presented by Renton [59]. By applying the model to a polystyrene microsphere, the critical pressure can be predicted. The critical pressures for the thin and thick walled models for a polystyrene microsphere are shown in Figure 4-12. At a relatively low thickness ratio – approximately 0.1, the critical pressure exceeds that which is found in most hydraulic systems; therefore, thick walled microspheres will not collapse during usage, rendering them infeasible for noise control applications. Therefore, a thick-walled polystyrene spheres will not be useful for noise control. It follows logically that thick walled microspheres of other materials will also not be viable for usage, either. Thin-walled microspheres must be used in order for collapse to occur at a reasonably low pressure.

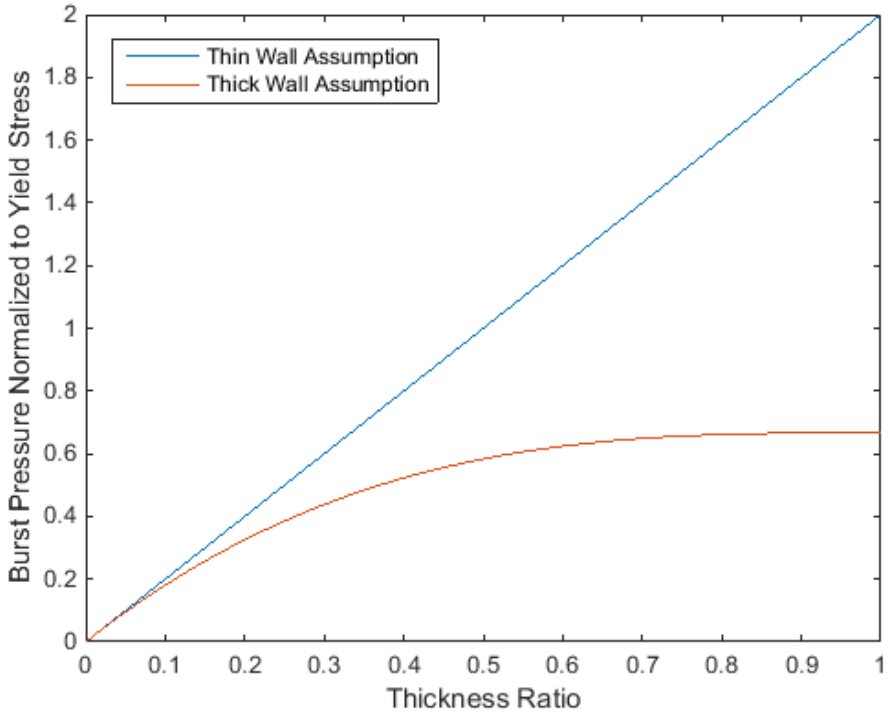

Figure 4-11: Comparison between thin walled and thick walled burst pressure prediction

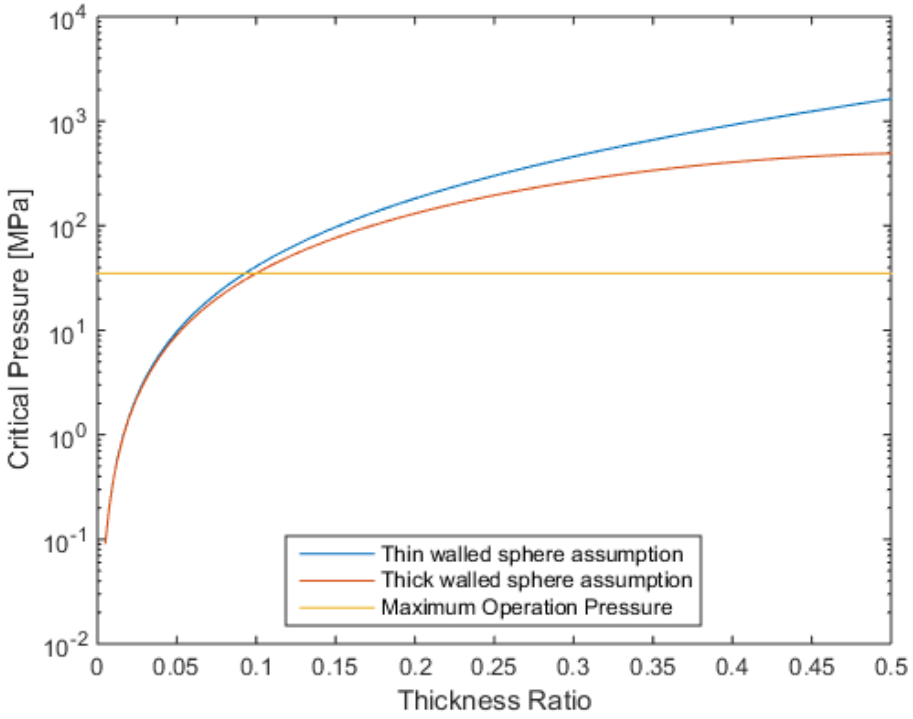

Figure 4-12: Comparison between thin walled and thick walled critical pressure prediction

4.3 Syntactic Foam Fabrication

Correct fabrication of the syntactic foam is essential for the foam to perform well and endure for its desired lifetime. Two silicone based polymers were selected for analysis: Xiameter 3120 and Sylgard 184 both produced by Dow Corning. A fully cured and crosslinked foam is essential for satisfactory long term performance in a hydraulic system. The hollow microspheres used are the 461 DE 20 d70 microspheres produced by AkzoNobel. The microspheres are primarily made from a PVC-like polymer which may be damaged during high temperature curing but can withstand the temperature range of the hydraulic circuit. In order to not damage the microspheres, the curing may be conducted at a lower temperature for longer. The volume of microspheres compared the polymer determines the effective volume fraction; a volume fraction of 50% microsphere is used for all foams considered within.

The fabrication of a syntactic foam is very similar regardless of the base polymer, microsphere type and microsphere volume fraction. The first step in fabricating the foam is to mix the constituents of the polymer and the microspheres together. For polymers with a 1:1 mixing ratio of constituents the appropriate amount of microspheres to achieve the final volume ratio should be mixed evenly into both constituents, i.e. the volume fraction of microspheres in each constituent should match the targeted volume fraction. After the microspheres are sufficiently mixed into both samples, the two constituents are then mixed together. For polymers with a based polymer and a curing agent with mixing ratios on the order of 10:1, the entirety of microspheres are mixed into the base. The curing agent will be mixed in after the microspheres are fully mixed into the base. The next step is to move the polymer into the mold, the mold used for the liner samples is shown in Figure 4-13. The method of transferring the polymer depends on the polymer;

Sylgard 184 mixes were transferred in a plastic bag and then injected into the mold. The sample is then cured, either at room temperature or elevated temperature depending on the host polymer requirements.

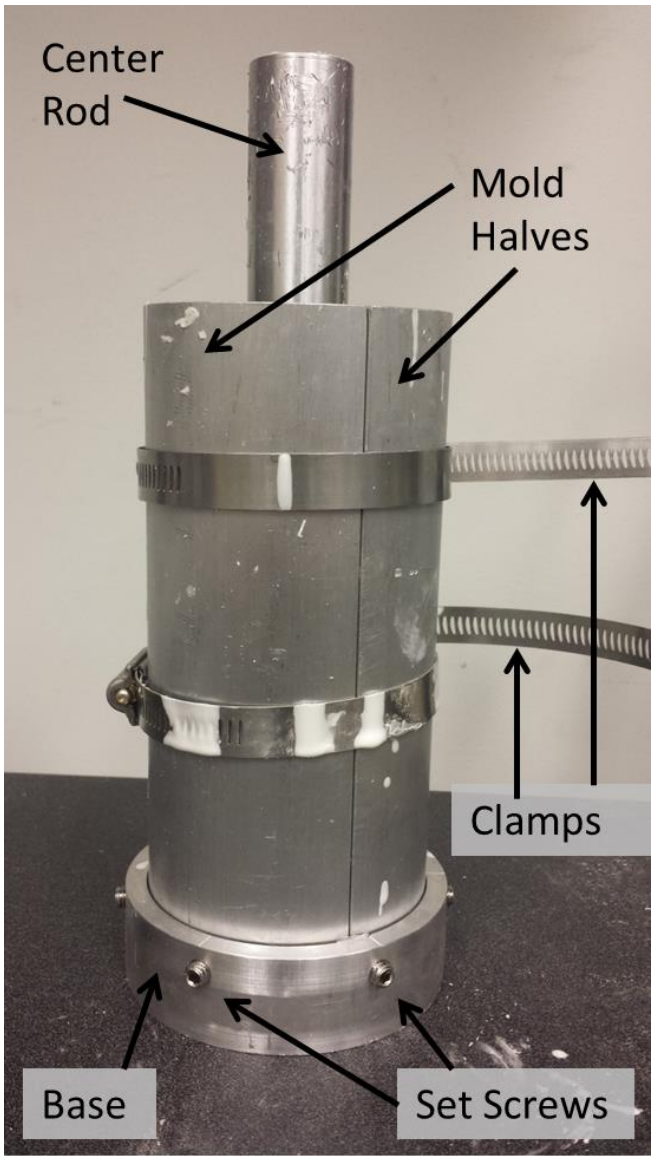

Figure 4-13: Prototype two-halved casing mold

4.4 Foam Surface Treatments

The hazards of a hydraulic environment necessitate a protective layer on the host material in order to prevent the foam from sorbing oil stiffens the foam as well as cause

degradation and shedding parts into the hydraulic system, which may cause component or system failure. Initial testing with the foams comprised of a Sylgard 184 host showed that oil would penetrate the outer layer which caused the foam to stiffen drastically which resulted in a reduction of noise control performance. In addition, modern hydraulic systems often have clearances on the order of the diameter of the microspheres under analysis; therefore, if microspheres enter the system, it may cause damage to the system by causing abrasive wear. In particular, problems will arise at sealing surfaces of moving components such as pistons and other actuators.

Another problem is if the selected polymer degrades when exposed to hydraulic oil over a long period of time. The first generation of foam did not show any degradation other than color change; initially the foam was white, but the edge became a brown color after being soaked in hydraulic fluid, as shown in Figure 4-14. However, neither version of foam has been rigorously tested for longevity. In order to increase the longevity of the syntactic foam, a layer of neat polymer may be applied to the surface. A neat polymer refers to a polymer which includes no inclusions. A neat layer of depth equivalent to the mean diameter of the microspheres will prevent most microspheres from shedding into the system.

Figure 4-14: First generation foam stained by oil

There are two general possibilities for skin layers: the first is to skin with the same polymer as the host; the second is to skin with a different polymer specifically selected to endure the hydraulic environment. Initial measurements showed that the oil was being sorbed into the Sylgard 184 without much resistance; an additional layer of the same polymer would not prevent sorption. PFTE, Teflon, was selected because it is resilient to the entire range of oils found in hydraulic usage as well having a maximum operating temperature well above the temperatures found in a hydraulic system. PTFE is also sold commercially in aerosol form, which is simple to apply to a foam annulus – care must be taken to ensure complete coverage of the entire annulus. The PTFE layer will also provide a barrier to prevent microspheres and other parts from being shed into the system.

CHAPTER 5

PRESSURE WAVEFIELD MEASUREMENT AND MODELING

To assess the acoustic performance of the foam the pressure fields of concern for hydraulic noise control can be broken down into two regions, the field upstream of the device and the field downstream of the device. Furthermore, each field has a forward and backward going wave. The waves are generalized to include all modes; however, it will be shown for the frequency range of interest that only the plane wave mode will propagate within the pipes. The waves are shown in Figure 5-1 and labeled A and B in the upstream section and E and F in the downstream section. Waves C and D denote the waves within the noise control device under examination both within the fluid and then foam; it is important to note these waves may be nonplanar. In addition, the solid foam liner will support acoustic shear waves.

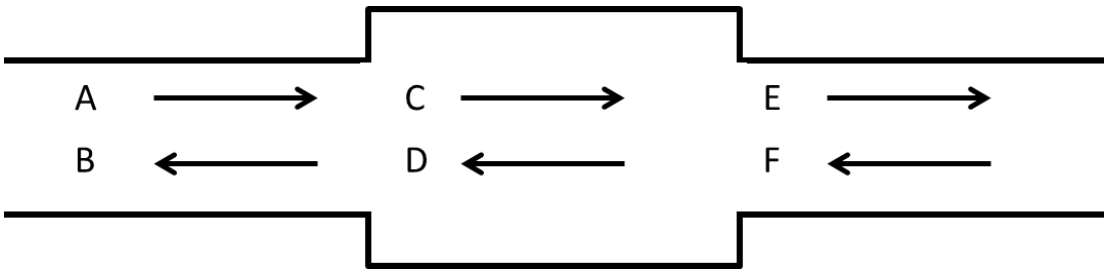

Figure 5-1: Wavefield upstream, downstream and within a noise control device

5.1 Wavefield Measurement

For hydraulic noise control devices, the wavefield is measured in accordance with the procedure described in the ISO-15086 standard [60-62]. A schematic of the test circuit is shown in Figure 5-2, along with acoustic waves upstream, waves A and B, and downstream, E and F. Both the upstream and downstream test sections are constructed from rigid walled tubing. Six pressure transducers are used to measure both wavefields,

three upstream and three downstream. Three transducers are used in each test section to prevent half-wavelength indeterminacy, a phenomena where two sensors measure the nulls of a standing wave and cannot accurately measure the signal. Three dissimilarly spaced transducers prevent half-wavelength indeterminacy from happening. The sensor spacing in the test section is shown in Figure 5-3. The pressure transducers can be located at any angle on the test section because the frequency range of interest is below the cut on frequency of the first non-planar mode; however, the pressure transducers are generally mounted at the top of the measurement pipe for simplicity. The cut-on frequency of the first radial mode is found from

$$\omega = \frac{j'_{ml}}{a} c \,, \tag{5.1}$$

where j'_{ml} is the extrema of $J_m(z)$, the Bessel function of the first kind, order m where m is the mode number, a is the radius of the cross-section and c is the speed of sound [21]. The speed of sound in hydraulic fluid is nominally 1400 m/s and the radius of the test section is 0.95 cm. For this test section, the first cut on mode occurs at 43,000 Hz which is far above the frequency range of interest, 0 to 4000 Hz. The pressure transducers are connected to signal conditioners and then a DAQ card in a PC.

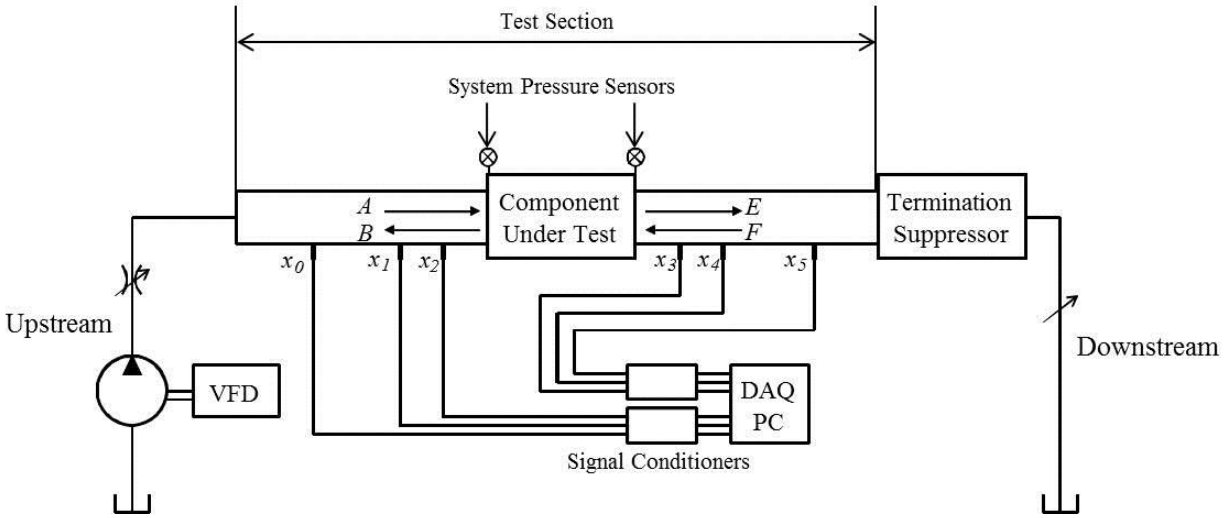

Figure 5-2: Schematic of test setup for measurement of fluid acoustic properties of a suppressor under test. [20]

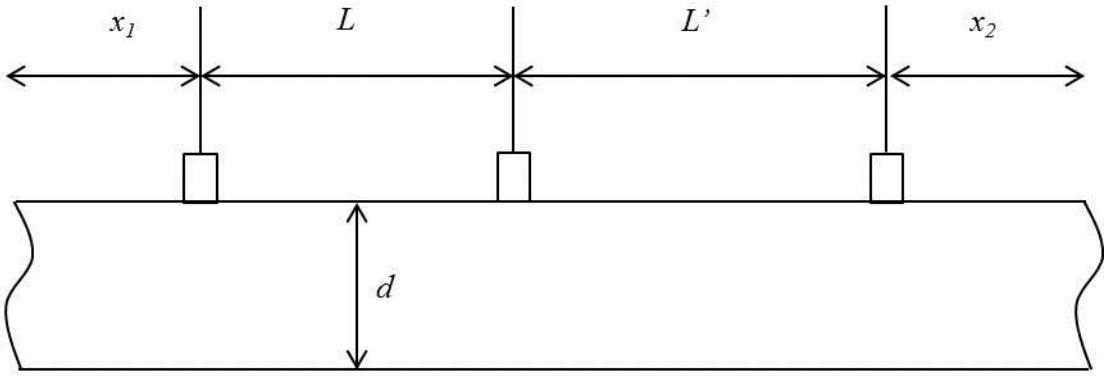

Figure 5-3: ISO 15086-2 dimensions, $x_1 \geq 10d$, $x_2 \geq 10d$, $L = 330 \pm 2mm$, $L' = 470 \pm 2mm$ [61]

Hydraulic flow is provided to the system by a pump which is spun by a variable frequency drive (VFD). The flow first passes through a partially closed needle valve in order to provide turbulent-flow broadband noise to the system. Static pressure sensors are located immediately upstream and downstream of the device under test. They are used to measure the static pressure loss across the device. The flow then passes through the termination suppressor. The termination suppressor is used to prevent noise from propagating in the opposite direction of flow into the system and contaminating the measurement. Before completing the hydraulic loop back to tank, the flow passes through

a second needle valve used to load the system. The orifice area of the needle valve is altered to control system pressure.

In order to be considered a valid test, ISO-15086-1 specifies the mean flow rate of the system needs to be less than a Mach number of 0.01 [60]. The Mach number is calculated by

$$M = \frac{V}{c} \tag{5.2}$$

where c is the speed of sound in the fluid, speed of sound is calculated for each test in both the upstream and downstream section; the speed of sound is nominally 1400 m/s in hydraulic systems. The mean flowrate, V, is calculated by

$$V = \frac{Q}{A} \tag{5.3}$$

where Q is the volume flow-rate and A is the cross sectional area of the pipe. For the test section employed, the flow diameter is 0.019 m and the volumetric flow rate is 37.85 liters/minute. The Mach number is 0.0016; almost an order of magnitude below the threshold. A larger diameter test rig would further reduce the Mach number for the same flow rate.

The wavefield with the test sections is found by using seven transfer functions to relate the six dynamic pressure transducers. The transfer functions in use are H_{01}, H_{21}, H_{31}, H_{41}, H_{51}, H_{34} and H_{54}, where H_{xy} is the transfer function between sensor x and y using the sensor notation in Figure 5-2, [63]. The acoustic pressure wavefield in the upstream section is

$$p_{upstream} = \left(A e^{-\gamma x} + B e^{\gamma x} \right) e^{j\omega t} \tag{5.4}$$

and the particle velocity is

$$Q_{upstream} = \frac{A e^{-\gamma x} - B e^{\gamma x}}{Z_0} e^{j\omega t} \tag{5.5}$$

where A and B are the complex wave amplitudes, γ is the complex wavenumber and Z_0 is the specific impedance. The upstream wave amplitudes are calculated by placing the measured acoustic pressures at each transducer into an over-determined matrix,

$$F = \begin{bmatrix} e^{-\gamma x_0} & e^{\gamma x_0} \\ e^{-\gamma x_1} & e^{\gamma x_1} \\ e^{-\gamma x_2} & e^{\gamma x_2} \end{bmatrix}. \tag{5.6}$$

The wave amplitudes are solved for using a pseudoinverse to compute the least-squares average of

$$X = Fb\,, \tag{5.7}$$

where

$$X = \begin{pmatrix} A/p_1 \\ B/p_1 \end{pmatrix}, \tag{5.8}$$

where p_1 is the acoustic pressure at sensor 1, and

$$b = \begin{pmatrix} H_{01} \\ 1 \\ H_{21} \end{pmatrix}. \tag{5.9}$$

The second entry in the right hand side of equation (5.9) is the H_{11} transfer function which is identically 1. The downstream pressure and particle velocity are given by

$$p_{downstream} = \left(E e^{-\gamma x} + F e^{\gamma x} \right) e^{j\omega t} \tag{5.10}$$

and

$$Q_{downstream} = \frac{E e^{-\gamma x} - F e^{\gamma x}}{Z_0} e^{j\omega t}. \tag{5.11}$$

Similarly to the upstream section, the wave amplitudes in the downstream section are calculated using

$$Y = G c \tag{5.12}$$

where

$$Y = \begin{pmatrix} C/p_1 \\ D/p_1 \end{pmatrix}, \tag{5.13}$$

$$G = \begin{bmatrix} e^{-\gamma x_3} & e^{\gamma x_3} \\ e^{-\gamma x_4} & e^{\gamma x_4} \\ e^{-\gamma x_5} & e^{\gamma x_5} \end{bmatrix}, \tag{5.14}$$

and

$$c = \begin{pmatrix} H_{31} \\ H_{41} \\ H_{51} \end{pmatrix}. \tag{5.15}$$

The acoustic pressure, p_1, and volume velocity, Q_1, at the upstream port are related to p_2 and Q_2 at the downstream ports by a transfer matrix with elements t_{ij},

$$\begin{pmatrix} p_1 \\ Q_1 \end{pmatrix} = \begin{bmatrix} t_{11} & t_{12} \\ t_{21} & t_{22} \end{bmatrix} \begin{pmatrix} p_2 \\ Q_2 \end{pmatrix}. \tag{5.16}$$

Pressure and velocity can be calculated from the wave amplitudes using the relations in equations (5.4), (5.5), (5.10) and (5.11). The transfer matrix in equation (5.16) can be simplified by assuming the test suppressor is geometrically symmetric end to end, and the system is assumed to be reciprocal, as seen in Pierce [64], resulting in

$$t_{11} = t_{22} \tag{5.17}$$

and

$$t_{21} = \frac{1 + t_{11}^2}{t_{12}}. \tag{5.18}$$

It can be shown from equation (5.16), (5.17) and (5.18) that the elements of the transfer matrix can be solved using

$$\begin{aligned} t_{11} &= \frac{p_1 Q_1 + p_2 Q_2}{p_2 Q_2 + p_1 Q_1} \quad & t_{12} &= \frac{p_2^2 - p_1^2}{p_2 Q_2 + p_1 Q_1} \\ t_{21} &= \frac{Q_2^2 - Q_1^2}{p_2 Q_2 + p_1 Q_1} \quad & t_{22} &= \frac{p_1 Q_1 + p_2 Q_2}{p_2 Q_2 + p_1 Q_1} \end{aligned}. \tag{5.19}$$

Using equations (5.4), (5.5), (5.10) and (5.11), the transfer matrix elements can be solved in terms of wave amplitudes

$$\begin{bmatrix} t_{11} = 1 & t_{12} = -Z_0 \dfrac{A^2 + 2AB + B^2 - F^2 - 2EF - E^2}{A^2 - B^2 - F^2 + E^2} \\ t_{21} = -\dfrac{A^2 - 2AB + B^2 - F^2 + 2EF - E^2}{Z_0\left(A^2 - B^2 - F^2 + E^2\right)} & t_{22} = 1 \end{bmatrix}. \quad (5.20)$$

The relation of the transfer matrix elements to the wave amplitudes will be useful when calculating the transmission loss in Section 5.3.

5.1.1 Coherence

The transfer functions measured must pass a coherence threshold of 0.95 to be considered valid data [60]. Coherence is a measure of two signals' dependence and its value can range from 0, meaning the two signals are completely unrelated, to 1, meaning the signals are perfectly linearly related. Coherence is calculated by

$$C_{xy} = \frac{\left|G_{xy}\right|^2}{G_{xx}G_{yy}} \quad (5.21)$$

where G_{xy} is the cross-spectral density between x and y, and G_{xx} and G_{yy} are the respective autospectral densities. The threshold value of 0.95 ensures that all data considered valid is a result of strongly related signals instead of randomness in the system. Excessive noise will reduce the coherence value; therefore, if a device treats the incident acoustic energy sufficiently well enough that the transmitted energy is on the order of the system noise floor or below in the downstream test section, the coherence value will be low and the data will not be considered valid. Normally, low coherence would be undesirable; however, in this case it may be indicative of noise being treated beyond the ability of the test rig to measure the noise.

5.1.2 Calibration

The pressure transducers are periodically calibrated relative to one another rather than as an absolute measurement. Calibration is conducted by mounting four sensors at a time in the calibration block shown in Figure 5-4. The calibration block is a rectangular prism purposely built such that none of its three dimensions are identical to diminish the impact of the vibratory resonant frequencies of the block on sensor measurements. The sensor ports are located at the same height on the block. Ideally, each sensor will detect the same magnitude and phase of the acoustic wave within the hydraulic fluid. In order to compare the measurements transfer functions are used to relate the sensor measurements. ISO-15086 specifies that any magnitude difference of 5% and a phase difference of ±5 degrees must be corrected [60]. However, for data presented within, any derivation from the ideal transfer function is corrected when calculating the wavefield. A sample of some calibration graphs are shown in Figure 5-5. This calibration set shows very good behavior of all transfer functions. Most frequencies would not require correction to be in accordance with the standard, but as stated previously, the difference is accounted for within the transmission loss processing code, shown in Appendix B.4.

Figure 5-4: Calibration block without sensors

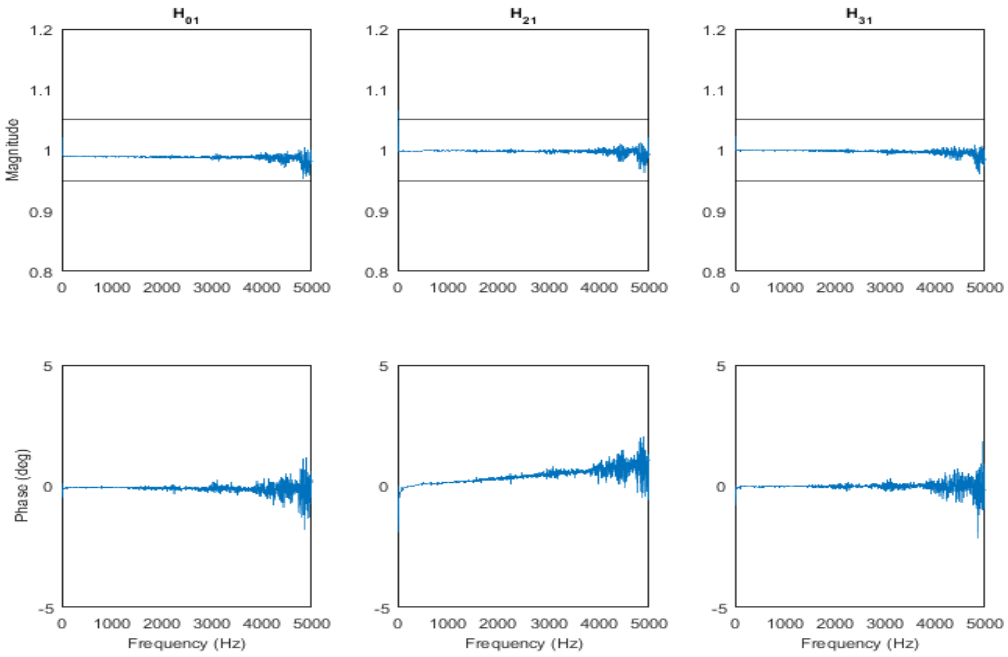

Figure 5-5: Example Calibration plots, black lines on magnitude plots indicate limit for correction to be necessary

5.2 Wavefield Modeling

Predictive models for the noise control devices have been developed. In particular, models to predict the acoustic performance of devices employing syntactic foam have been developed. As discussed preciously, a suppressor presents the most

effective noise control solution in terms of broadband effectiveness. A model for predicting the transmission loss behavior of a liner-style suppressor has been developed by Marek [3, 12]. The model calculates the wavefield adjacent to the suppressor by establishing boundary conditions within the device as well as upstream and downstream of the device. The wavefield as well as the relevant dimensions for the model are shown in Figure 5-6. Within the pipes upstream, region 1, and downstream, region 3, of the device, there is assumed to be a rigid boundary condition,

$$u_{1,3}\left(r_{pipe}\right)\vec{r} = 0\ , \tag{5.22}$$

where u is particle velocity. Within the device, all device walls are assumed to be rigid, i.e. the acoustic particle velocity is zero on the boundary,

$$u_{2}\left(r_{shell}\right)\vec{r} = 0 \tag{5.23}$$

and

$$u_{2}\left(r > r_{pipe}\right)\Big|_{x=0,L_{shell}}\vec{l} = 0\ . \tag{5.24}$$

At the interface between foam and oil, continuity of both pressure,

$$P_{foam}\left(r_{i}\right) = P_{oil}\left(r_{i}\right) \tag{5.25}$$

$$P_{foam}\left(r_{o}\right) = P_{oil}\left(r_{o}\right), \tag{5.26}$$

and particle velocity

$$u_{foam}\left(r_{i}\right) = u_{oil}\left(r_{i}\right) \tag{5.27}$$

$$u_{foam}(r_o) = u_{oil}(r_o), \tag{5.28}$$

are enforced. In the pipe sections upstream and downstream of the device plane wave behavior may be assumed as discussed in the previous section. However, inclusion of the foam within the device prevents such an assumption from being made within the device. Therefore, the radial and angular modes inside section two must be considered. The acoustic pressure and particle velocity can be found from the displacement potential in both the oil,

$$\nabla^2 \varphi_f = \frac{1}{c_f^2} \ddot{\varphi}_f, \tag{5.29}$$

and syntactic foam regimes,

$$\nabla^2 \varphi_l = \frac{1}{c_l^2} \ddot{\varphi}_l, \tag{5.30}$$

$$\nabla^2 \vec{\psi}_f = \frac{1}{c_f^2} \ddot{\vec{\psi}}_f, \tag{5.31}$$

where the speed of sound is represented by c, c_f represents the speed of sound in the fluid,

$$c_f = \sqrt{\frac{\lambda_f}{\rho_f}}, \tag{5.32}$$

the longitudinal speed of sound in the liner is

$$c_l = \sqrt{\frac{\lambda_l + \mu_l}{\rho_l}}, \tag{5.33}$$

and the shear wave speed of sound is

$$c_T = \sqrt{\frac{\mu_l}{\rho_l}}. \tag{5.34}$$

It is important to note the syntactic foam will support shear waves. At the boundaries between foam and oil the shear stress and displacement will be zero to match the pertinent quantities in the oil. By applying the boundary conditions to the pressure and velocity equations then solving them simultaneously, the pressure field upstream, within and downstream of the device can be calculated in reference to the incident wave upstream of the device. This solution takes into account the properties of the foam and its volume under compression. The wavefield simulation allows for transmission loss to be predicted, as discussed in Section 5.3. Development of the acoustic models for other noise control devices will not be discussed here but can be found in the work done by multiple authors [4, 13, 18, 19, 21].

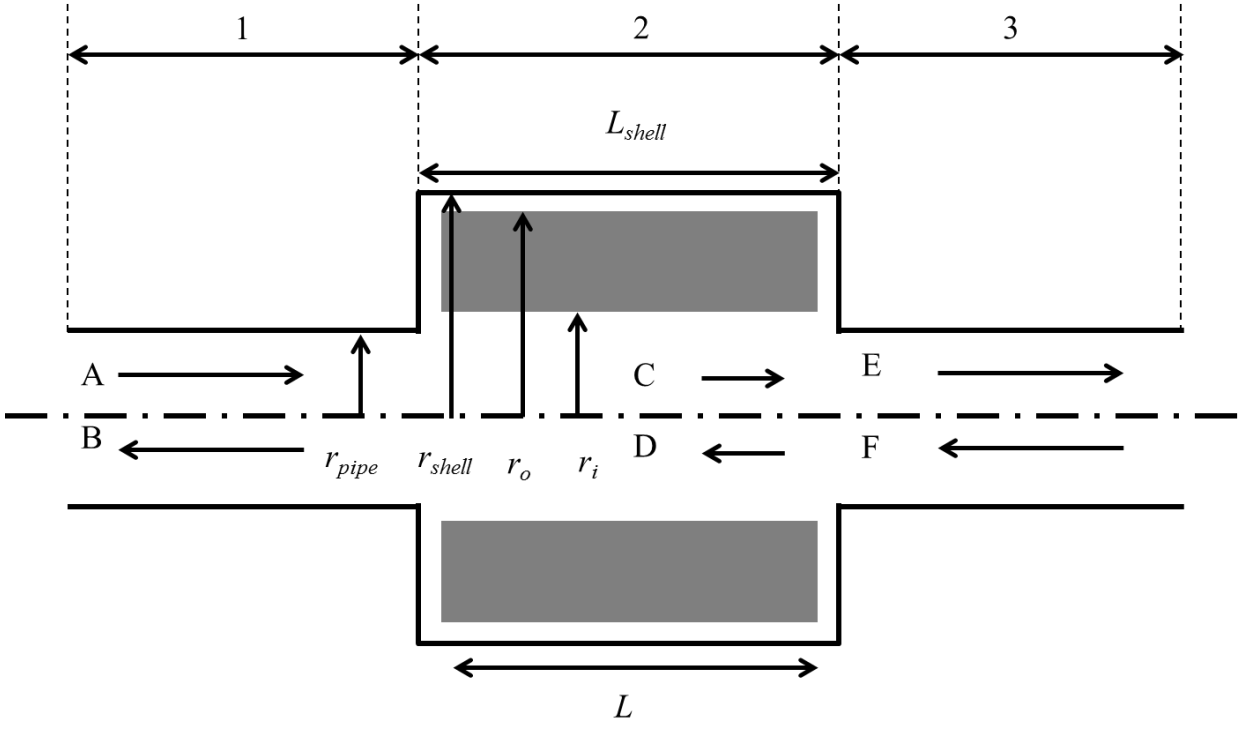

Figure 5-6: Schematic of suppressor with acoustic waves and relevant dimensions

5.3 Transmission Loss Calculation

A common way to measure noise control effectiveness in hydraulic systems is transmission loss. Transmission loss is the ratio of incident acoustic energy to transmitted acoustic energy,

$$TL = 10 \log_{10} \left(\frac{\Pi_i}{\Pi_t} \right) = 10 \log_{10} \left(\frac{1}{T_\Pi} \right), \tag{5.35}$$

where Π_i is incident acoustic power, Π_t is the transmitted acoustic power and T_Π is the acoustic power transmission coefficient. Transmission loss varies on a frequency-by-frequency basis, and a higher magnitude indicates more effective noise control. Furthermore, transmission loss is a device property rather than a system property, like insertion loss. A device will have the same transmission loss regardless of system architecture, which is advantageous when analyzing new system configurations or comparing devices. The elements of the transfer matrix, equation (5.16), can be used to calculate *TL*, using

$$\mathrm{TL} = 20 \log_{10} \frac{1}{2} \left| t_{11} + \frac{t_{12}}{Z_0} + Z_0 t_{21} + t_{22} \right|. \tag{5.36}$$

The elements of the transfer matrix can be related to the wave amplitudes by equation (5.20), allowing transmission loss to be directly related to the wavefield shown in Figure 5-2 by

$$TL = 10 \log_{10} \left| \frac{A^2 - F^2}{AE - BF} \right|, \tag{5.37}$$

this reduces to the traditional form of transmission loss if the termination is anechoic, *F=0*,

$$TL = 10 \log_{10} \left| \frac{A}{E} \right|. \tag{5.38}$$

Therefore, measurement and modeling of the wavefield upstream and downstream of a noise control device is sufficient to determine its noise control effectiveness. The magnitude of transmission loss which qualifies as effective noise control depends on the untreated level of noise within the system; a louder system requires more noise control.

CHAPTER 6

EXPERIMENTAL MEASUREMENTS

Foam samples were fabricated as described in Chapter 4 with a silicone polymer host, multiple IMPs and a PTFE coating; the samples were then tested by the wavefield measurement technique as described in Section 5.1. Sylgard 184 and Xiameter 3120 were selected for their low bulk modulus and silicone backbone as silicones generally have very good resistance to hydraulic fluids as discussed in section 4.1. The measurements were conducted over the whole range of system pressures from 0 to 35 MPa. A discussion pertaining to other polymers notwithstanding the hydraulic environment can be found in Appendix D.

6.1 Material properties

Both the static and dynamic material properties of second generation of foam are measured. The static material properties are measured by placing a sample of foam in the bulk modulus tester shown in Figure 6-1. The static bulk modulus is found by filling the cavity with oil, which has a known and well defined bulk modulus, and gradually reducing the volume in the chamber by rotating the plunger and using the threaded pitch to decrease volume. Figure 6-1 A) shows the initial state of the device with the plunger fully retracted and Figure 6-1 B) shows the plunger at a fully depressed state; the length of travel multiplied by the cross-sectional area of the o-ring carriage is the maximum volume which can be reduced. The resulting pressure increase from each plunger turn is recorded by the pressure sensor at the left-hand side. By knowing both the change in volume and pressure as well as the initial volume the effective bulk modulus of the entire

cavity can be found; a rule of mixture relation is then used to determine the static bulk modulus. The bulk modulus relates the volumetric strain to change in pressure,

$$\Delta P = K \frac{\delta V}{V}; \tag{6.1}$$

in order to measure bulk modulus, the initial volume, change in volume and change in pressure must be known. The plunger at the right end of the fixture is used to reduce the volume within the cavity; the cross sectional area of the o-ring carriage is known, a specified turn of the plunger rod moves the carriage by a known distance providing the change in volume. The resulting pressure change is measured by the sensor at the left end. By knowing the initial volume the effective bulk modulus of the entire cavity can be found. The rule of mixtures in series is applied to the find the bulk modulus of the foam,

$$K_{foam} = \frac{V_{foam}}{\left(\frac{V_{total}}{K_{total}} - \frac{V_{oil}}{K_{oil}} \right)}, \tag{6.2}$$

because the initial volumes and the bulk modulus of the oil are known. The volume quantities in equation (6.2) are updated at each discrete turn to match what is physically transpiring in the tester. In addition, the bulk modulus of the oil, K_{oil}, has been well studied over pressure and the pressure-dependent modulus is used [65]. Using this methodology the bulk modulus of the foam can be measured over the entire system pressure range. The code used to process this data can be found in Appendix A.2. The dynamic material properties are determined from the wavefield measurements by the technique described in section 5.1. The desirable material properties are low effective bulk modulus on the entire range of system pressures.

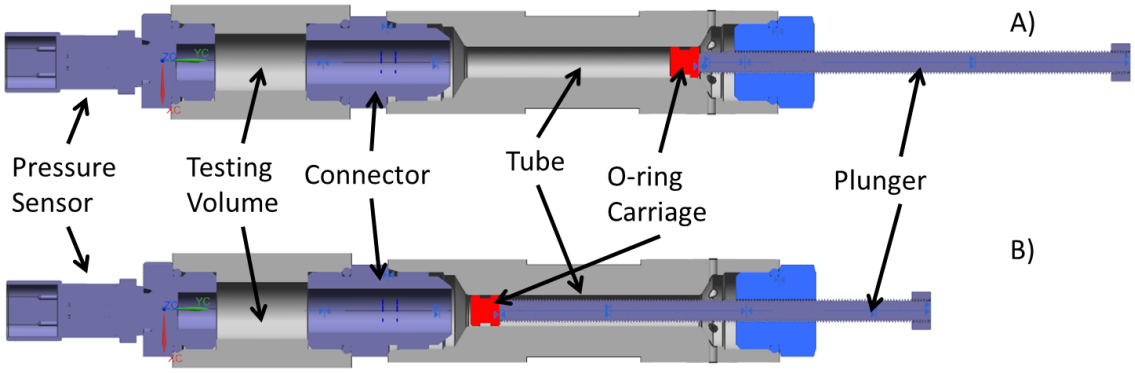

Figure 6-1: Bulk modulus testing apparatus

The static properties of a syntactic foam provide good insight into the general performance of the syntactic foam. Figure 6-2 shows the bulk modulus of the host polymer. Sylgard 184, the host polymer, shows little change in the bulk modulus with increasing system pressure which is desirable for noise control. Figure 6-3 shows the measured bulk modulus for two IMPs with a Sylgard 184 host. The increased IMP reduces the effective bulk modulus of the foam especially at higher pressures, which is highly desirable for effective noise control. The nature of the measurement lends itself to some error within the measurements; most are due to imprecise turns of the plunger. Figure 6-3 shows some of this bad data, most notably at a system pressure of 13 MPa for the elevated IMP case. In order to offset this, multiple data sets were taken of each IMP and presented together as a single set.

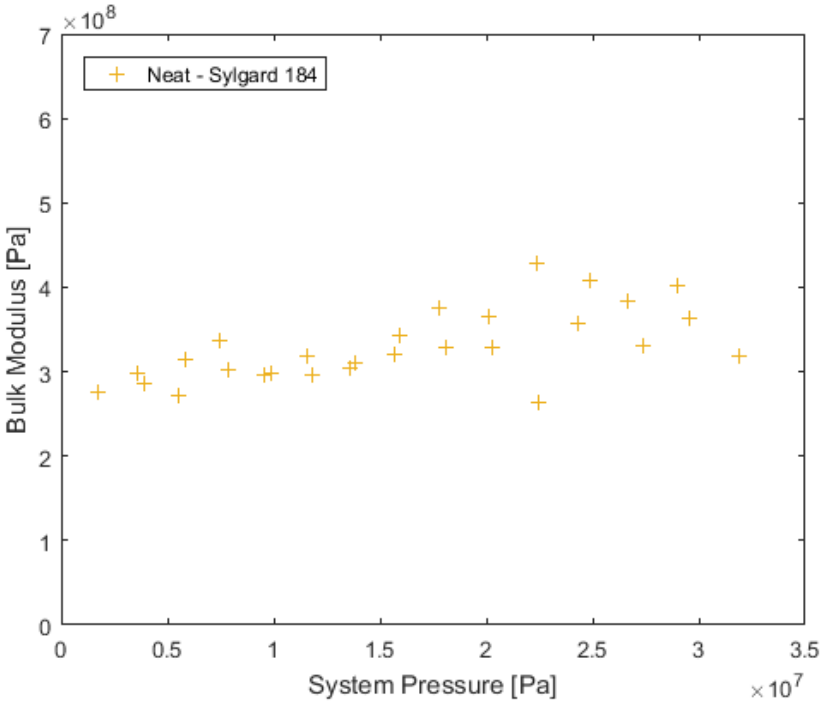

Figure 6-2: Bulk Modulus of neat host polymer, Sylgard 184

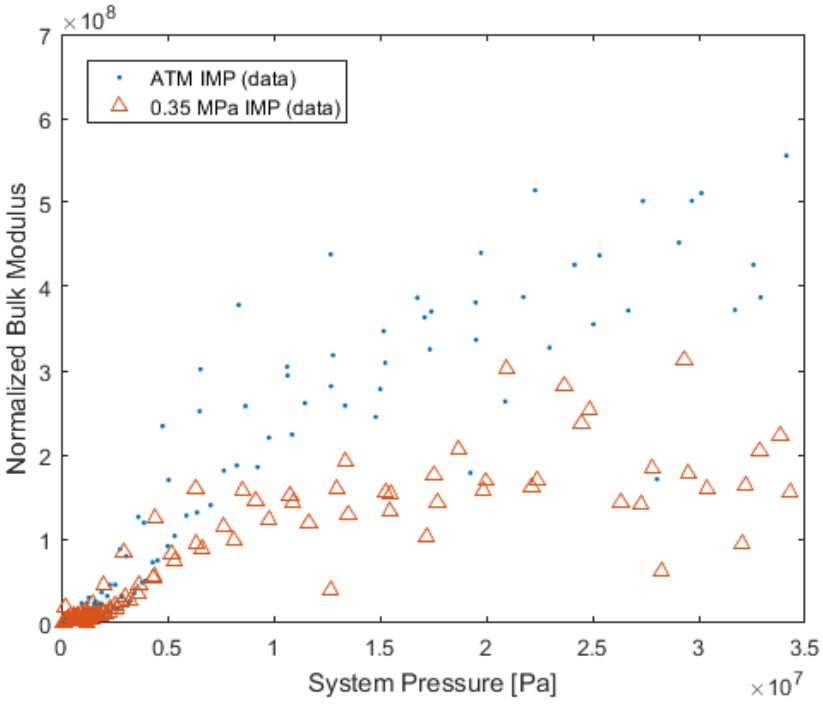

Figure 6-3: Measured bulk modulus data for a 50% by volume foam with a Sylgard 184 host and two IMPs

An additional set of samples in a Xiameter host matrix with two different IMPs were also prepared and measured; an additional difference is the microspheres at elevated IMP for the Xiameter host were also fluorinated. The measured bulk moduli up to 35 MPa of the two samples are shown in Figure 6-4. The foam sample with 0.4 MPa IMP has a lower effective bulk modulus over the entire range of system pressure further supporting the conclusion that elevated IMP can soften a foam which will lead to improved noise control. In addition, the data shows that microspheres which have been both pressurized and fluorinated can be mixed into a foam and cured into a form. The bulk modulus data for the pressurized and fluorinate microspheres, shown in Figure 6-4, supports the hypothesis that increasing the initial pressure within a microsphere will reduce the effective bulk modulus of the foam over the entire pressure range. Furthermore, the data shows that the microspheres may be fluorinated in a way that does not damage them and reduce their effective on the composite bulk modulus of the foam.

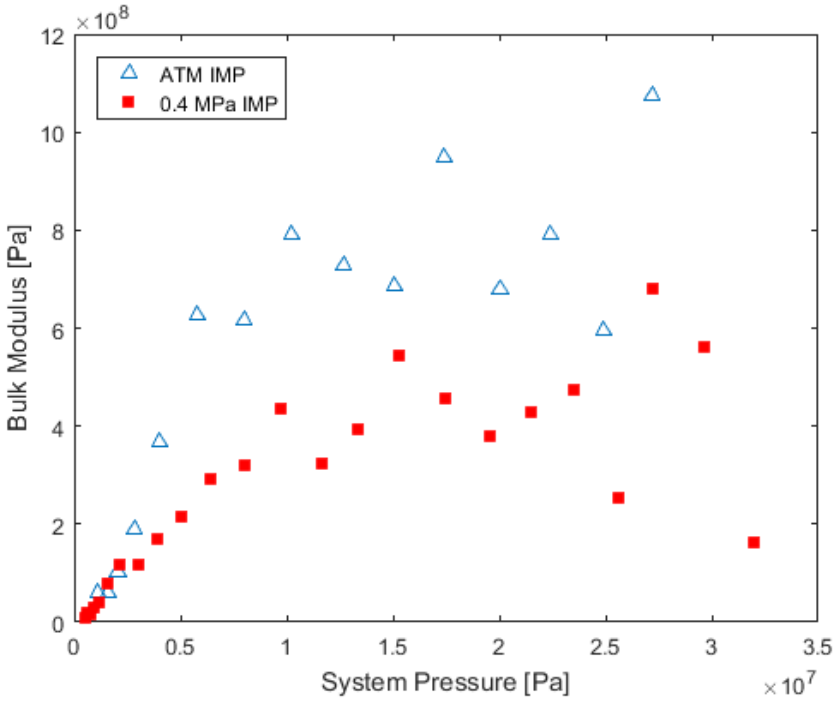

Figure 6-4: Measured bulk modulus data for a 50% by volume foam with a Xiameter 3120 host and two IMPs, microspheres with 0.4 MPa IMP were also fluorinated

6.1.1 Model Verification

The measured material properties were compared with the model to determine its accuracy. A comparison of the measured bulk modulus and predicted bulk modulus is shown in Figure 6-5. In general, the model matches well with data; however, there is a divergence between the model and measure data at higher pressures. The atmospheric IMP foam is measured at a higher bulk modulus than predicted while the elevated IMP is measured at below predicted bulk modulus at elevated pressure. The measured divergence is beneficial from a noise control perspective but troublesome from a modeling perspective as there is no known or hypothesized explanation for the divergence between the two measured data sets. In general, the model does agree with the measured data especially at pressures less than 15 MPa, which lends credence to its veracity. The bulk modulus is also modeled for the Xiameter based samples; the

prediction is shown in Figure 6-6. In general, the model matches the measured data well for the entire system pressure range with some deviation at higher pressure.

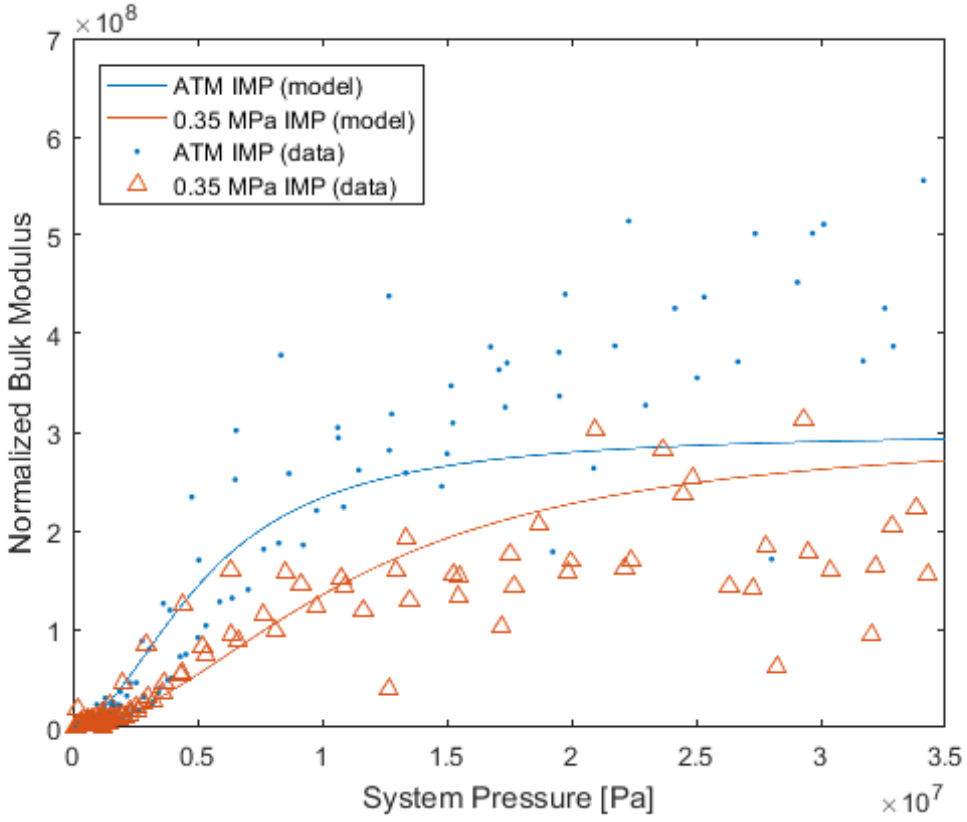

Figure 6-5: Difference in bulk moduli for ATM IMP and elevated IMP, Sylgard 184 host

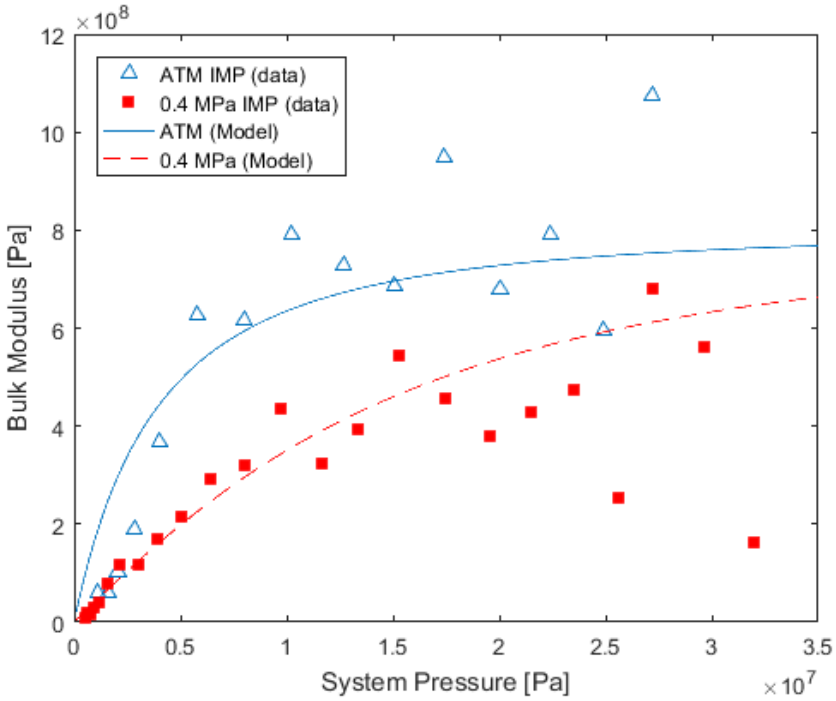

Figure 6-6: Difference in bulk moduli for ATM IMP and elevated IMP, Xiameter host

6.2 Transmission Loss

The transmission loss of the new generation of foams was measured by the technique described in Section 5.3 and calculated by equation (5.37). Transmission loss is the most direct way to characterize the noise control effectiveness of a device for comparison with another noise control device. It is important to consider the size of the device when comparing transmission loss. The dimensions of the annular syntactic foam liner are listed in Table 6-1, they are the same dimensions are those used in Earnhart allowing for direct comparison across generations of foam [4]. The same expansion chamber housing is used as the previous devices for further consistency. Measured transmission loss data is presented in Figure 6-7 and Figure 6-8 for a Sylgard 184 host with 50% volume fraction of microspheres and atmospheric IMP. The transmission loss approaches constant performance for system pressure of 7 MPa and above; this follows from the measured bulk modulus data for this foam, shown in Figure 6-3; the effective

bulk modulus of the foam approaches the value of the constant value of bulk modulus for the host polymer in this pressure range.

Table 6-1: Liner Dimensions

Dimensions	Quantity
Length	95 mm
Outer Radius	31 mm
Inner Radius	13.5 mm

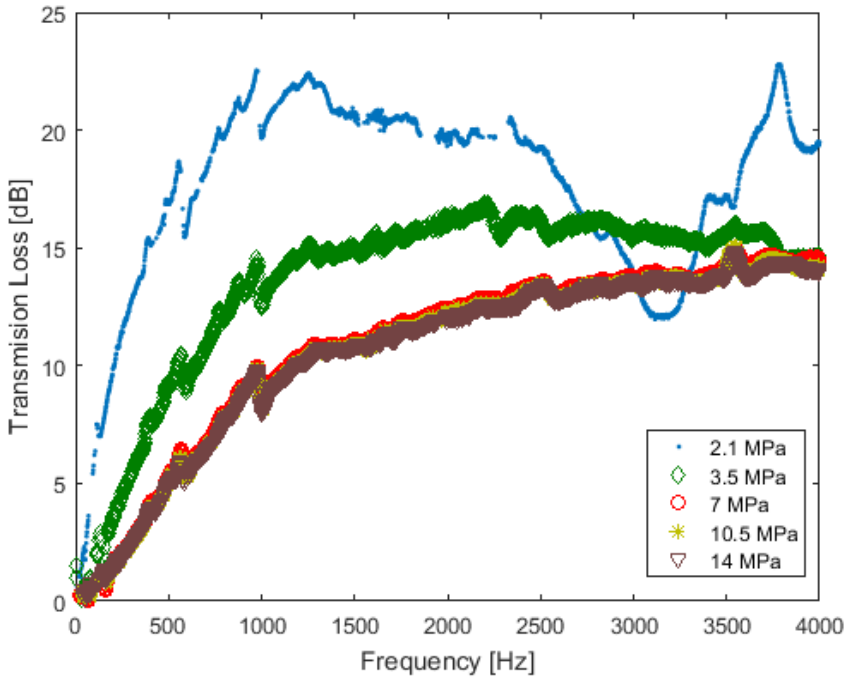

Figure 6-7: Transmission Loss of Sylgard 184 ATM IMP for low operating pressures

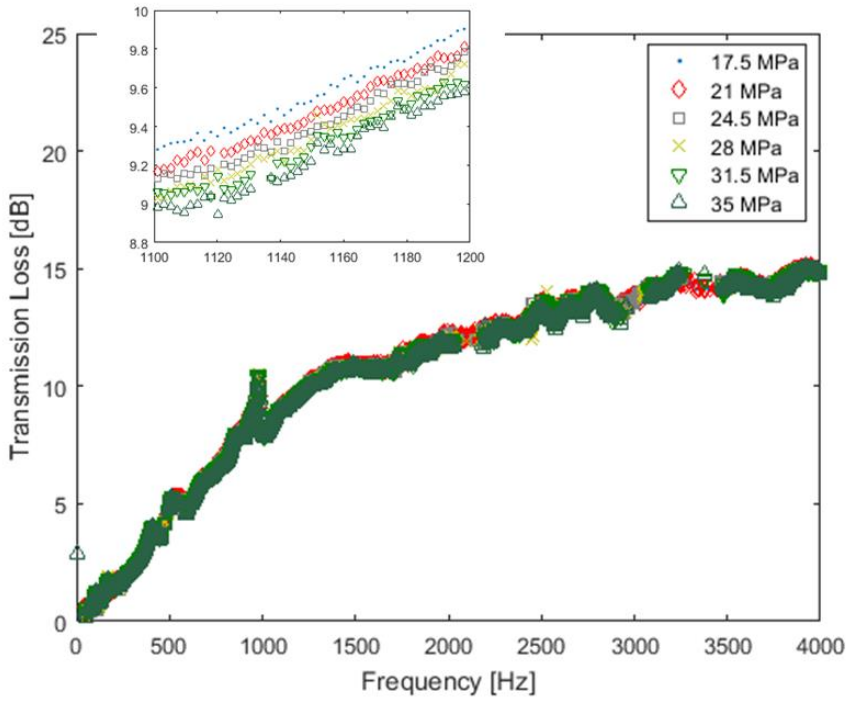

Figure 6-8: Transmission Loss of Sylgard 184 ATM IMP for high operating pressures

6.2.1 Comparison with Previous Generation

The first generation of syntactic foam does not perform well at high system pressure, generally in the system pressures above 10 MPa. The goal of this work was to develop a foam which treats noise effectively above 10 MPa; therefore, a direct comparison is an efficient way to determine the improvement in noise control effectiveness. As discussed previously, the acoustic energy at lower system pressures is lower; therefore, it is more necessary to treat noise at higher pressures. The transmission loss of Sylgard 184 and GR9-625 at pressures of 3.5 and 35 MPa are shown in Figure 6-9 and Figure 6-10, respectively. GR9-625 refers to a foam fabricated from the GR9 polymer and a targeted density of 625 kg/m^3 for the composite. The Sylgard 184 ATM IMP foam performs slightly worse at lower system pressure than the GR9-625 – the previous best performing foam at all system pressures; however, it does perform better at higher pressures [3, 4].

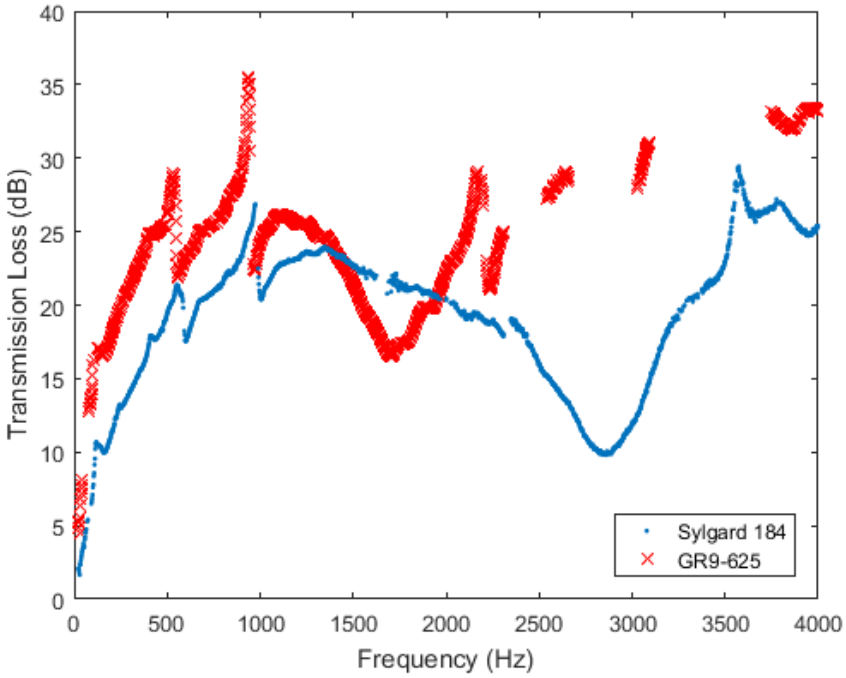

Figure 6-9: Transmission loss for GR9-625 and Sylgard 184 at 3.45 MPa. Both samples had initially 50% microspheres by volume.

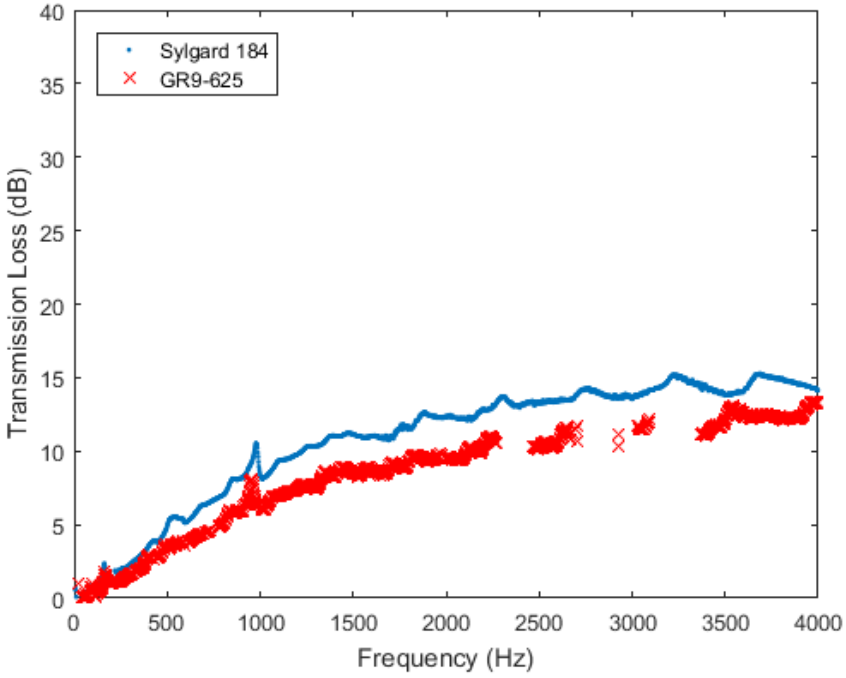

Figure 6-10: Transmission loss for GR9-625 and Sylgard 184 at 35 MPa. Both samples had initially 50% microspheres by volume.

Counterintuitively, a stiffer host may be part of a softer foam for specific Poisson's ratio combinations at low system pressures. The effective bulk modulus of a composite foam is calculated with varying Poisson's ratio for a host polymer with a bulk modulus of 1.2 GPa, equivalent to GR9. The results of the calculations are shown in Figure 6-11. The effective bulk modulus increases very sharply for Poisson's ratios under 0.45 for low system pressures. The predicted bulk modulus is concave down for the entirety of the pressure range. GR9 has a Poisson's ratio close to 0.4995 which is concave up for low pressures. The shape of the curve allows foams with a GR9 host to remain compliant to higher system pressures than lower Poisson's ratios.

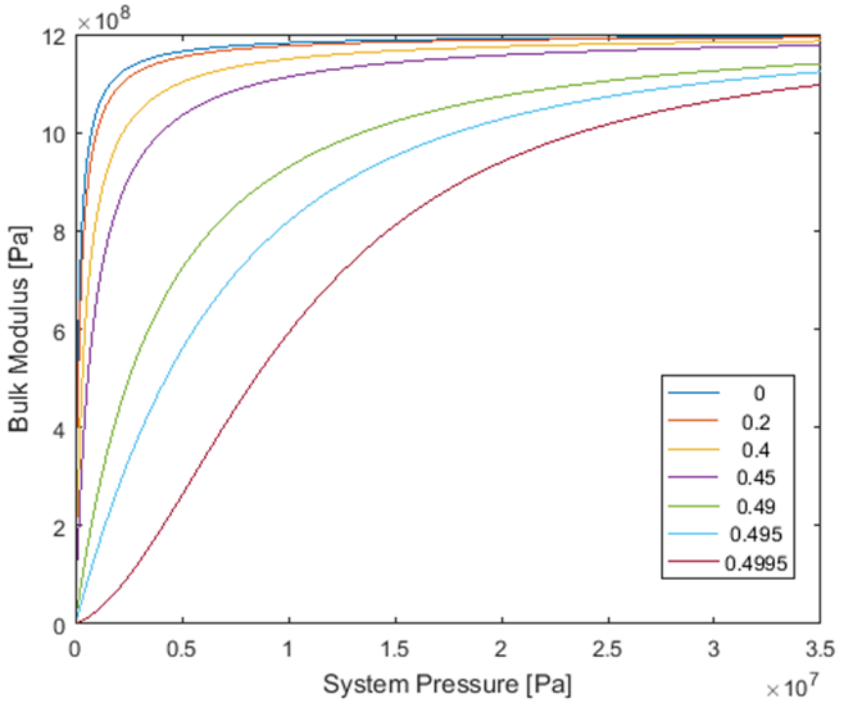

Figure 6-11: Effective bulk modulus for GR9 host varying Poisson's ratio. ATM IMP

The same Poisson's ratio sweep of effective bulk modulus was conducted with the Sylgard 184 host which has a bulk modulus of 300 MPa; the results of the calculation are shown in Figure 6-12. The predicted effective bulk moduli are not as sensitive to

changing Poisson's ratio as the foam with a GR9 host. The highest value of Poisson's ratio analyzed is concave up for some very low pressure but not to the same extent as a GR9 type host. The measured Sylgard 184 samples not have a concave up portion which suggests the Poisson's ratio is lower – approximately 0.49.

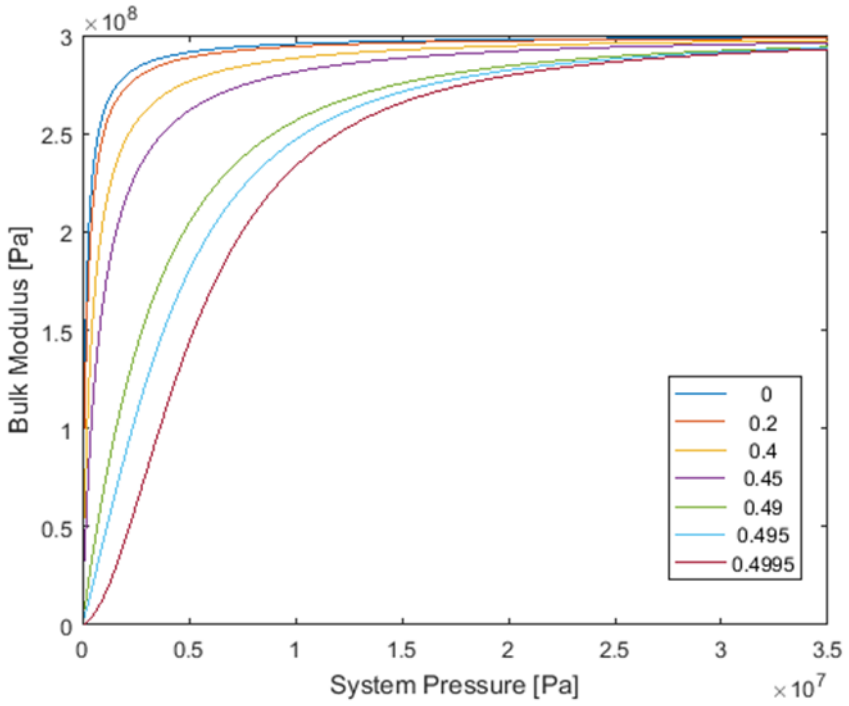

Figure 6-12: Effective bulk modulus for Sylgard host varying Poisson's ratio. ATM IMP

The predictions of the effective bulk moduli are directly compared in Figure 6-13 and Figure 6-14. GR9-625 is predicted to be softer at lower pressures, which agrees with the transmission loss measurements in Figure 6-7. In addition, there is a cross over point when the Sylgard 184 based foams become more compliant. The exact pressure of this cross-over point will be important for low pressure noise control, but that is not a primary concern for high pressure noise control where a softer host is significantly more effective than a stiffer host.

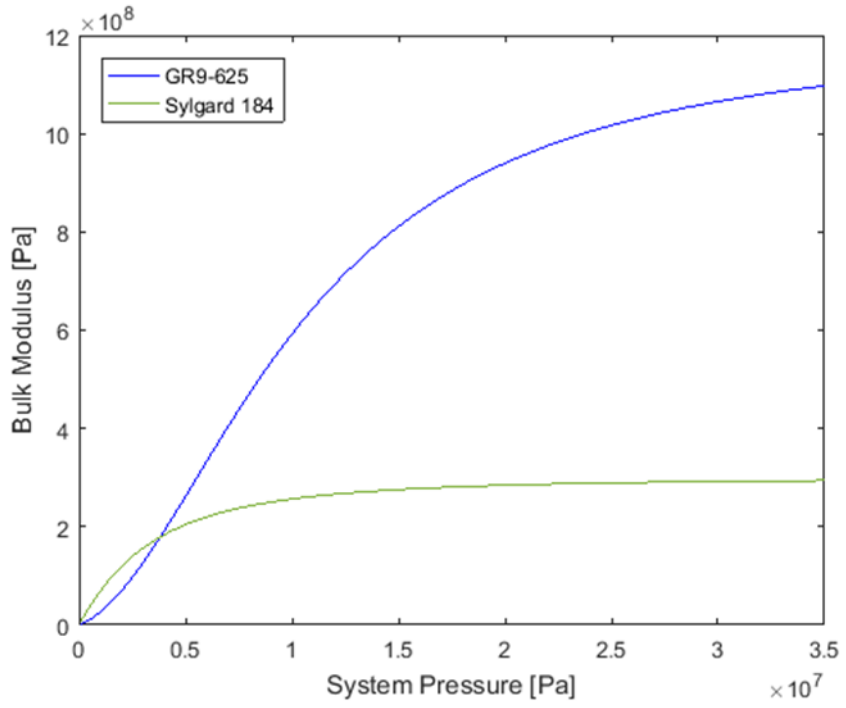

Figure 6-13: Bulk modulus comparison between GR9-625 and Sylgard 184

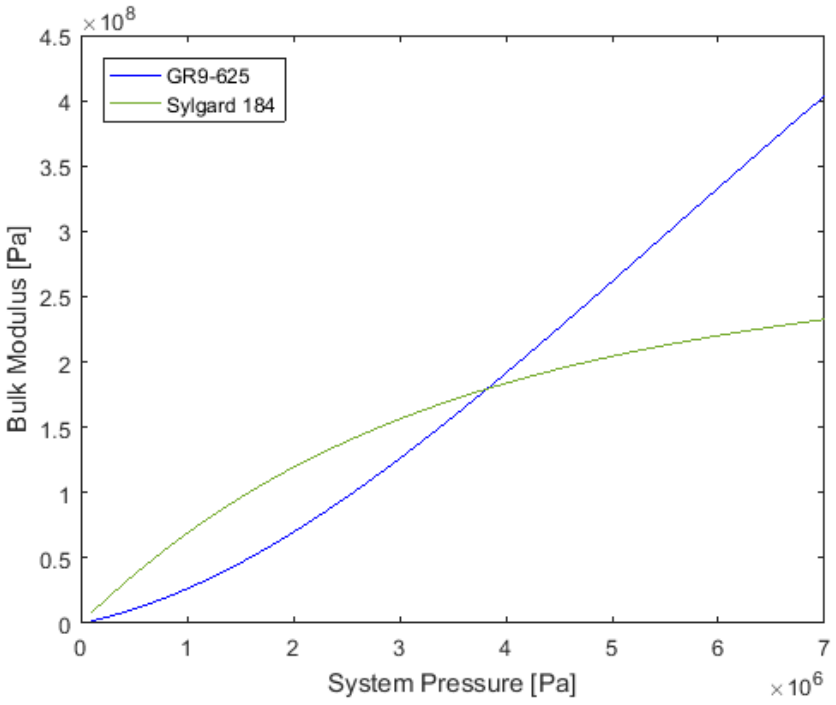

Figure 6-14: Bulk modulus comparison between GR9-625 and Sylgard 184, up to 7 MPa

CHAPTER 7

CONCLUSIONS

A method to design a syntactic foam which improves the effective bulk modulus across the entire range of system pressure, from atmospheric pressure to an elevated pressure of 35 MPa, has been presented. The improvement was measured to be significant reduced, some improvements up to a 200 MPa reduction, in bulk modulus over the entire range of system pressure. The method is a polymer with pressurized microsphere inclusions. The pressurization serves to ensure the voids created by the collapsed microspheres do not lose their volume as drastically with increasing system pressure. Since noise control effectiveness is a function of compliance and compliance is a function of void fraction, the voids retaining their size ensures compliance and effective noise control.

The pressurization process is conducted by increasing the pressure outside of the microsphere and allowing the gas, usually nitrogen, into the microsphere. A layer of fluorine is applied to the microspheres which alters its chemical structure and decreases the permeation rate of the gas out of the microsphere. The fluorination ensures that the gas will remain within the microsphere allowing it to continue being effective as a noise control treatment.

In addition, a model to predict the effective material properties over the pressure and frequency ranges of interest has been developed. The model allows for noise control effectiveness of a given foam to be predicted, which allows for the optimal set of parameters to be selected when fabricating the foam. The modeling will also be useful

moving forward if the foam is to be applied in other applications, such as water hammer arrestors, accumulators or a shock isolation measure.

The importance of the host polymer was also analyzed; both its mechanical properties and resistance to hydraulic oil. Desirable mechanical properties were found to be low bulk modulus and high Poisson's ratio. The polymer with such properties is Sylgard 184 produced by Dow Corning. This polymer needs a surface layer of PTFE in order to interface with the hydraulic environment for optimal noise control.

7.1 Future Work

The continuation of this work can be two-fold, furthering material development and pursuing alternate applications.

7.1.1 Constituent Material Development

Microsphere behavior and its influence on the noise control behavior of the composite foam is a function of microsphere geometry and material. The analysis conducted in Chapter 4 showed the optimal sphere size has a large radius with a reasonably thin wall. However, microspheres of this geometry are not currently commercially available. A large microsphere manufacture, Expancel, has stated a microsphere with these dimensions is possible. Furthermore, developments in polymer sciences may lead to a polymer which is better suited for use a microsphere wall. This polymer would have an extremely low Young's modulus with high yield strength; allowing a microsphere to have a low critical pressure and a high burst pressure, both highly desirable characteristics for hydraulic noise control. In addition, further analysis may be conducted into microsphere restoration pressure, i.e. the pressure where the microspheres regain their shape after collapse. The prior work concerning collapse of

both thin and thick walled microsphere was primarily concerned with structural usages of a sphere and therefore only covered collapse. However, it is possible that the collapse pressure is higher than the pressure where the microspheres regain their spherical shape. This difference can be exploited to improve noise control, as the collapsed microspheres drive noise control effectiveness. Therefore a startup procedure which spikes the pressure in the system may be beneficial for noise control purposes if there is a significant difference between collapse and restoration pressure.

Development and expertise in polymer sciences will also expand the selection domain for the host polymers allowing for a more suitable polymer to be found. The desirable characteristics for the host polymer are high compliance with a high Poisson's ratio and very good longevity in hydraulic oil. Two examples of polymers which may be considered are a fluorinated liquid silicone rubber (F-LSR) and a polyether MDI polyurethane. A commercial example of an F-LSR is the Silastic line of polymers from Dow Corning. These polymers have very good oil resistance and thermal ratings; however, the polymer is beyond the capabilities of our lab to safely handle. A commercially available polyether MDI polyurethane is Vibrathane produces by Chemtura. The feasibility of Vibrathane as a host polymer is currently being analyzed by a labmate.

It is also important to consider a polymer which can maximize the initial volume of microspheres within the host matrix as a higher initial volume fraction will improve noise control. Some of the polymers considered early in the research had trouble incorporating the microspheres into them especially at volume fractions above 50%.

From a materials fabrication standpoint, a polymer made from less viscous constituents is easier to manipulate and mix the microspheres into.

Currently, permeating the gas into the microspheres takes approximately five days to complete, which can be time prohibitive moving forward for large scale production. The permeation constant is a function of temperature; a higher ambient temperature will lead to a faster permeation rate. All permeations analyzed above were conducted at room temperature so even mild heating may cut down permeation time. Permeation time is also a function of the difference in concentration across the barrier. The microsphere barrier can be exposed to a higher amount of permeant than desired which will accelerate the permeation; as permeation nears completion the amount of free permeant will be reduced to the desired amount. Neither scheme is a perfect solution. In the increased temperature technique the pressure inside the microsphere would decrease as temperature is reduced. In the over-pressure scenario extra care would need to be taken to ensure the microsphere do not have a higher pressure than their burst pressure.

7.1.2 Alternate Applications

This dissertation analyzed syntactic foam with pressurized microspheres to be used within an annulus of foam as a liner; however, it is possible to use the foam – or similarly constructed foam – in other applications. First, the geometry of the foam, especially with respect to its fit within its housing, has not been deeply analyzed; there is a potential to improve the noise control effectiveness by altering the geometry of the foam. A current noise control methodology for hydraulics is to use dead volumes of oil – volumes of oil which do not propagate through the system – to treat noise. It would be possible to replace the dead volumes of oil, such as within a piston, with a significantly

smaller volume of foam instead of oil for the same compliance per volume resulting in an increase of noise control effectiveness. The syntactic foam may also be used to store potential energy in place of a charged bladder within an accumulator. The energy would be stored as strain energy through compression of the foam in the form of shear energy. The optimal composition, in terms of initial microsphere pressure and host polymer, may not be the same as the foam for hydraulic noise control. A foam-accumulator would have similar improvement over a bladder-style accumulator as the differences in suppressors – longevity and lack of maintenance contact.

An ongoing undergraduate research project is analyzing the feasibility of a syntactic foam, with a system-safe host polymer, as a water hammer arrestor for residential plumbing circuits. The syntactic foam device provides an upgrade over the current commercial solution as it will not degrade over a period of time. Analysis into the commercial viability of such a device has begun to be analyzed as well as its performance.

The foam can be designed to be used as a vibration isolation device for heavy components. The design characteristic being exploited here is the collapse of the microspheres. The IMP will be selected so the spheres do not collapse under common usage. However, a large shock event will exceed the collapse pressure of the microspheres and allow fragile components to avoid collisions. The compliance between objects will allow them to move independently and prevent them from causing damage.

APPENDIX A

PROCEDURES

A.1 Fluorination

Fluorination procedure

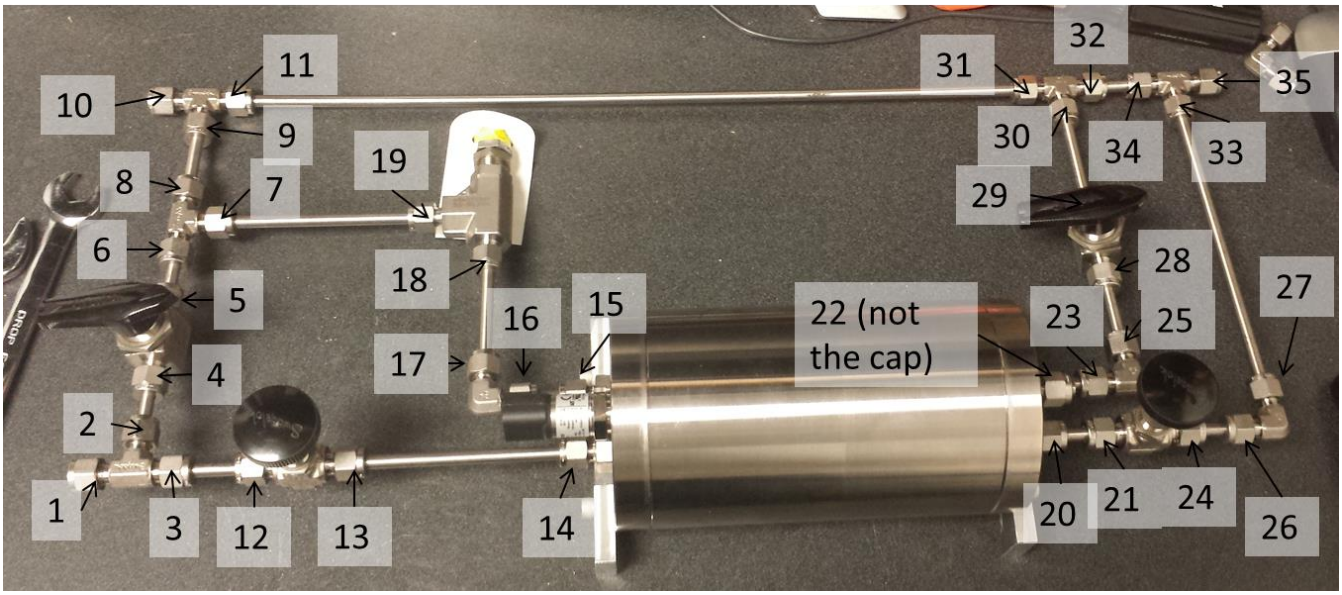

Figure 7-1: Fluorinator with connectors labeled

1. Pressurization
    1.1. Load microspheres into chamber
        1.1.1. Open connections 20, 22, 31, 14, 15
        1.1.2. Remove right hand cap (cap without pressure sensor)
            1.1.2.1. Remove gray screws and foot
            1.1.2.2. Remove blue screws
            1.1.2.3. Use four gray screws to push off cap
        1.1.3. Place desired volume of microspheres into chamber
            1.1.3.1. Place open chamber vertically in vice (use gravity to hold microspheres within chamber)
            1.1.3.2. Take care to not damage the pressure sensor
            1.1.3.3. Insert microspheres into chamber. In general prepare about 110% of desired spheres to make foam volume. A paper cup can be used to pour the microspheres in
                1.1.3.3.1. Pour slowly in order to avoid airborne microspheres

1.1.3.3.2. Clean face and sealing surface of chamber in order to prevent leakage

1.1.3.4. Cap chamber before removing from vice by replacing blue screws, also take care to align the cap correctly for easier assembly. Exercise care to not point the non-filter end downward as microspheres will spill out.

1.1.4. Reconnect open connections, be sure to fully tighten. At least ¾ turn, no more than a full turn past hand tight

1.2. Pressurize chamber

1.2.1. Ensure that all valves are in their closed position

1.2.2. Check pressure setting of PRV

1.2.2.1. Set pressure on regulator to desired pressure

1.2.2.2. Open upstream needle valve

1.2.2.3. Slowly open the PRV by unscrewing the top until it gas flow through it

1.2.2.4. Slightly retighten cap

1.2.3. Seal upstream needle valve

1.2.4. Ensure steady state pressure is as expected to ensure no leakage occurred.

1.2.4.1. Continuity of mass

1.2.4.2. Account for volume of walls

1.2.4.3. Will be difficult to determine exact

1.2.5. Allow sufficient time to reach study state within the chamber.

1.2.6. With the large volume of microspheres within the chamber, maintenance pressurization may be necessary. There is no way to tell if the system is leaking or if the gas is in the microspheres during the test.

1.2.6.1. If the steady state pressure is non-zero, the gas went into the microspheres

1.2.6.2. If the steady state pressure is zero, there is a leak. There may be pressure in the microspheres but the quantity is unknown. Based on experience, most leaks occur if a nut is not sufficiently tight on a ferrule. Exercise care to tighten nuts rather than loosen them. (right hand rule, “righty tighty, lefty loosey”)

1.3. Ensure seals outside of chamber are closed

1.3.1. Cap scrubber

1.3.2. Set regulator pressure to low pressure

1.3.3. Open upstream ball valve

1.3.4. Wait 12 hours and recheck pressure

1.3.5. If no change, open cap

1.3.6. If leakage occurred, check seals and repeat

2. Fluorination

2.1. Ensure scrubber is ready
    2.1.1. Cap is replaced
    2.1.2. Limestone slurry is inside
    2.1.3. pH of solution is correct
    2.1.4. There is sufficient space between the free level of the fluid and the top of the scrubber so the slurry will not be carried out by the gas bubbling through the slurry.
2.2. Set pressure of the fluorine slightly above desired pressure on regulator
2.3. Crack upstream needle valve
2.4. Crack downstream needle valve to create flow
2.5. Allow time to pass while monitoring scrubber pressure
    2.5.1. If pressure increases above atmospheric within scrubber stop fluorine supply immediately
    2.5.2. If pressure does not decrease, remove pressure sensor to allow for a second exhaust port. This is an emergency measure
2.6. Seal fluorine canister

3. Purge system
    3.1. Allow pressure within the entire system to reach atmospheric
    3.2. Open both needle valves
    3.3. Feed nitrogen to system at low pressure
    3.4. Open and close upstream ball valve
    3.5. Stop feed of nitrogen
    3.6. Wait to allow for and concentrations of fluorine to spread out
    3.7. Repeat steps 3.3 to 3.5 at least twice
4. Disassembly and storage
    4.1. Cap exhaust
    4.2. Check scrubber
        4.2.1. Remove cap from scrubber
        4.2.2. Exercise care to contain drips from down tube
        4.2.3. Check pH of solution, nitrile gloves should be worn for entirety of experiment but especially this step
        4.2.4. If pH approaches 7 dispose of solution or add more limestone
        4.2.5. Cap and seal scrubber
    4.3. Remove prepared microspheres and cast into foam
        4.3.1. Uncap with same procedure as above
        4.3.2. Remove desired volume of microspheres from PF chamber
    4.4. Occasionally check wear parts
        4.4.1. Stainless steel filters and retaining rings
        4.4.2. Pressure facing side of sensors
        4.4.3. O-rings (on caps of scrubber and chamber)

Data Acquisition set up

1. Ensure that the setting in NiMax or DaqMx are set correctly
    a. Input for channels ai0 and ai1 are RSE with an expected voltage between 0 and 5
    b. Output for channels ao0 and ao1 are 5 volts DC
    c. The task in the VI block diagram should not need to be changed
    d. Be careful about setting the sample rate, a high sample rate will generate more data however it will fill the memory quicker. A sample rate of approximately 10 Hz is suggestable.
    e. The Vi will start recording when the play button is pressed
    f. There are two ways to stop the VI
        i. Pressing the stop button on the front panel will stop recording and save data
        ii. Pressure the abort button on the tool bar will stop the program and not save data
    g. The file name needs to be appended with ".mat" in order to be correctly opened in Matlab
    h. The computer is set to not automatically restart to install updates but often does any. The best way to avoid this is force the updates to install before starting testing.

Emergency procedures

1. Chamber plugged
    1.1. Attempt to vent through upstream needle and valve
    1.2. Loosen pressure relief valve, will be time consuming
    1.3. Collapsed microspheres are not stopped by the filters, if necessary, spike pressure in PF chamber to collapse microspheres and open a release valve
    1.4. Open ball valve connected to non-filtered port. This will result in loss of microspheres and the need to clean the tubing. It is a last resort option.
2. Scrubber is plugged
    2.1. Stop flow of gas into system
    2.2. If pressure resolves itself
        2.2.1. If fluorine had entered system purge the system
        2.2.2. If not, disassemble and clean
    2.3. If pressure does not resolve
        2.3.1. Remove pressure sensor to open another exhaust port
        2.3.2. If fluorine has not entered system open top

2.3.3. If fluorine has entered system increase nitrogen pressure to try to clear the blockage. Be very careful when doing this and do not increase the pressure too high as to not blow out the system

2.3.4. Do not dump fluorine directly into atmosphere unless it is an absolute emergency. If it must be done, attempt to slowly leak as close to fume hood exhaust as possible.

3. Fluorine sensor triggers
   3.1. Stop flow of fluorine
   3.2. Open all valves to scrubber
   3.3. Let pressure drop as quickly as possible
   3.4. Pump nitrogen into system
   3.5. Depending on severity
      3.5.1. Pull fire alarm
      3.5.2. Seek medical attention
      3.5.3. Seek fresh air
   3.6. Once air is certified clean, analyze setup for leaks

A.2 Static Bulk Modulus Measurement

1. Load sample into chamber
2. Assemble system submerged in oil to prevent air from being trapped within test apparatus
   a. Seals do not need to be fully tight at this point
   b. If examining low end of pressure spectrum, depress plunger slightly and note initial volume
3. Fully tighten all seals
4. Connect sensor to DAQ
5. Determine turn fraction (usually half-turns)
6. Conduct pressure raising test to desired pressure
7. If possible, return plunger to initial pressure and repeat step 6
8. Find pressure peaks in data and process with code

A.2.1 Processing Code

```
clear all
close all
clc

%Inputs
% load del_P2 %Vector of delta pressures
% load P_avg2 %Vector of average pressures
load set3
del_V=(0.011/2)^2*pi*0.001*(0.5); %Area times pitch times turn fraction
Vi_oil=(18.54+1.77)*1e-6; %Initial volume of oil in m^3
Vi_foam=(0.019/2)^2*pi*(0.03); %Initial volue of foam in m^3
del_P=del_P*1e5;
P_avg=P_avg*1e5;
```

```
V_oil=Vi_oil;
V_foam=Vi_foam;
Vi_total=V_foam+V_oil;
B_oil=4.52.*(P_avg)+1868e6; %Bulk Modulus of oil

%Vector Initizlation
V_total=zeros(1,length(del_P)); %Total Volume
B_e=zeros(1,length(del_P)); %Effective Bulk Modulus
B_foam=zeros(1,length(del_P)); %Bulk Modulus of Foam
V_foam_list=zeros(1,length(del_P)); %Volume of foam as it is compressed


for x=1:length(del_P)
    V_total(x)=V_foam+V_oil;
    B_e(x)=del_P(x)*V_total(x)./del_V;
    B_foam(x)=V_foam./(V_total(x)*(1./B_e(x)-
V_oil./(B_oil(x)*V_total(x))));
    Strain_oil=del_P(x)./B_oil(x);
    V_oil=(1-Strain_oil)*V_oil;
    Strain_foam=del_P(x)/B_foam(x);
    V_foam=(1-Strain_foam)*V_foam;
    V_foam_list(x)=V_foam;
end

figure
plot(P_avg,B_e,'.',P_avg,B_foam,'^')
xlabel('System Pressure [Pa]')
ylabel('Bulk Modulus [Pa]')
legend('Effective Bulk Modulus','Foam Bulk
Modulus','location','northwest')
%
```

APPENDIX B

COMPUTER CODES

All codes are for Matlab unless otherwise specified.

B.1 Multiphase modeling

```
clear
% close all
clc

load GR9 %Loading host matrix properties

%Choosing which outputs

show_prop_graph=false;
show_prop_cont=false;
TL_calc=false;
barify=false;
MPaIfy=false;

% show_prop_graph=true;
% show_prop_cont=true;
% TL_calc=true;
% barify=true;
% MPaIfy=true;

maxFreqNum=47; %removing the Frequencies above a certain threshold
K_complex=K_complex(1:maxFreqNum,1); %Removing addition temperature and
frequency infromation
G_complex=G_complex(1:maxFreqNum,1);
Freq=Freq(1:maxFreqNum,1); %Frequency vector to predict material
properties
freq=10:25:4000; %Frequency vector to predict transmission
%Freq and freq do NOT need to be the same, there is an interpolation
%command later

%Removing data from double frequency measurements
K_complex(diff(Freq(:,1))==0,:)=[];
G_complex(diff(Freq(:,1))==0,:)=[];
Freq(diff(Freq(:,1))==0,:)=[];

P0=1e5; %intial pressure 1e5 Pa is ambient DO NOT CHANGE
Ptotal=350e5; %Target pressure in Pa sytem pressure
N=5e3; %number of steps
% Intialization of vectors, first entry is intial liner measurement
r_o=zeros(1,N+1);
r_o(1)=0.0381;%0.019525;%0.0241;
r_i=zeros(1,N+1);
r_i(1)=0.00965;%0.00965;%0.0173;
L=zeros(1,N+1);
```

```
L(1)=0.0254*3.874;%2;%0.1;%0.0447;
strain=zeros(1,N);
systemPressure=linspace(P0,Ptotal,N);

%Matrixes of mxn where m is the length of Freq and n is the length of
%system pressure. Therefore, each frequency and system pressure may
have a
%unique value
%UPDATE POTENTIAL: currently assumed (incorrectly) that the moduli of
the
%liner is pressure independent. This will require a merging of these
lines
%and above.
K_complex=K_complex*ones(1,length(systemPressure));
G_complex=G_complex*ones(1,length(systemPressure));

systemPressureMat=ones(length(Freq),1)*systemPressure;

%Initialization of physical parameters
host=struct('bulk',K_complex,'shear',G_complex,'poisson',0.4995);
insert=struct('youngs',3e9,'poisson',.34,'pressure',1e5,'radius',40e-
6,'thick',1.463e-07);%GR9-625 vs. desired Currently: GR9-625
volumeFractionIntial=0.4163;
gasAssump='adiabatic';%'isothermal';%

%BELOW WILL NEED TO BE UPDATED
rho_urethane=1051;
rho_air=1.21;
rho_poly=1050;
rho_iso=2150;%rho_air;%

volume_poly=4.7938e-15; %calculated from
thicknessWithBlowingAgentCalc.m in Wall Thickness folder
volume_air=2.6204e-13;
volume_iso=1.2531e-15;

volume_sphere=(volume_poly+volume_air+volume_iso);
volume_Total=volume_sphere./volumeFractionIntial;
volume_urethane=volume_Total-volume_sphere;

mass_urethane=(volume_urethane)*rho_urethane;
mass_air=volume_air*rho_air;
mass_poly=volume_poly*rho_poly;
mass_iso=volume_iso*rho_iso;

mass_total=mass_urethane+mass_air+mass_poly+mass_iso;

volume_air_elevated=volume_air*P0./Ptotal;
volume_iso_elevated=volume_iso*P0./Ptotal;
volume_total_elevated=volume_urethane+volume_poly+volume_air_elevated+v
olume_iso_elevated;

density_elevated=mass_total./volume_total_elevated;

insert=prop_Calc(insert);
```

```
gas.specificHeat=1.4; %Specific heat constant for nitrogen, which 80%
of atmosphere
BulkAdiabatic=gas.specificHeat.*systemPressure; %Adiabatic assumption
of ideal gas law
BulkIsothermal=systemPressure; %Isothermal assumption of ideal gas law
switch gasAssump
    case 'adiabatic'
        gas.bulk=ones(length(Freq),1)*BulkAdiabatic;
    case 'isothermal'
        gas.bulk=ones(length(Freq),1)*BulkIsothermal;
end
gas.shear=0; %Fluids cannot support shear
gas=prop_Calc(gas);
criticalPressure=2.*insert.youngs.*insert.thick.^2./(insert.radius.^2.*
sqrt(3.*(1-insert.poisson.^2)));
gas.volume=insert.radius.^3.*(4./3).*pi;
gas.area=insert.radius.^2.*4.*pi;
RVE.volume=gas.volume./volumeFractionIntial;
host.volume=RVE.volume-gas.volume;
volumeGasNew=(insert.pressure.*gas.volume)./systemPressureMat;
staticBulk=(ones(length(Freq),1)*host.bulk(1,:));
host.volumeComp=host.volume-
systemPressureMat.*(host.volume./staticBulk);
volumeFraction_collapsed=real((volumeGasNew./(host.volumeComp+volumeGas
New)));
volumeFraction_uncollapsed=volumeFractionIntial;

mass=626.2*pi*L(1)*(r_o(1)^2-r_i(1)^2);

%calculate effective bulk modulus for both collapsed and uncollapsed
cases
bulk_collapsed=host.bulk+(gas.bulk-
host.bulk).*(4.*host.shear+3.*host.bulk).*volumeFraction_collapsed./(4.
*host.shear+3.*gas.bulk+3.*(host.bulk-
gas.bulk).*volumeFraction_collapsed); %Composite spheres method,
equation 2
bulk_uncollapsed=host.bulk+(insert.bulk-
host.bulk).*(4.*host.shear+3.*host.bulk).*volumeFraction_uncollapsed./(
4.*host.shear+3.*insert.bulk+3.*(host.bulk-
insert.bulk).*volumeFraction_uncollapsed); %Composite spheres method,
equation 2

collapsePressure=criticalPressure+insert.pressure;

bulk_out=zeros(size(gas.bulk)); %Without this line, bulk_out will be an
incorrectly sized vector
%Assigning collapsed or uncollapsed values based on
bulk_out(systemPressureMat<=collapsePressure)=bulk_uncollapsed(systemPr
essureMat<=collapsePressure);
bulk_out(systemPressureMat>=collapsePressure)=bulk_collapsed(systemPres
sureMat>=collapsePressure);

composite.bulk=bulk_out;

%Calculate effective shear modulus for both collapsed and uncollapsed
cases
```

```
%collapsed case
n1c=(gas.shear./host.shear-1).*(49-
50.*gas.poisson.*host.poisson)+35.*(gas.shear./host.shear).*(gas.poisso
n-2.*host.poisson)+35.*(2.*gas.poisson-host.poisson);
n2c=5.*gas.poisson.*(gas.shear./host.shear-
8)+7.*(gas.shear+host.shear+4);
n3c=(gas.shear./host.shear).*(8-10.*host.poisson)+(7-5.*host.poisson);
Ac=8.*(gas.shear./host.shear-1).*(4-
5.*host.poisson).*n1c.*volumeFraction_collapsed.^(10./3)-
2.*(63.*(gas.shear./host.shear-
1).*n2c+2.*n1c.*n3c).*volumeFraction_collapsed.^(7./3)+252.*(gas.shear.
/host.shear-1).*n2c.*volumeFraction_collapsed.^(5./3)-
25.*(gas.shear./host.shear-1).*(7-
12.*host.poisson+8.*host.poisson.^2).*n2c.*volumeFraction_collapsed+4.*
(7-10.*host.poisson).*n2c.*n3c;
Bc=-4.*(gas.shear./host.shear-1).*(1-
5.*host.poisson).*n1c.*volumeFraction_collapsed.^(10./3)+4.*(63.*(gas.s
hear./host.shear-
1).*n2c+2.*n1c.*n3c).*volumeFraction_collapsed.^(7./3)-
504.*(gas.shear./host.shear-
1).*n2c.*volumeFraction_collapsed.^(5./3)+150.*(gas.shear./host.shear-
1).*(3-
host.poisson).*host.poisson.*n2c.*volumeFraction_collapsed+3.*(15.*host
.poisson-7).*n2c.*n3c;
Dc=4.*(gas.shear./host.shear-1).*(5.*host.poisson-
7).*n1c.*volumeFraction_collapsed.^(10./3)-
2.*(63.*(gas.shear./host.shear-
1).*n2c+2.*n1c.*n3c).*volumeFraction_collapsed.^(7./3)+252.*(gas.shear.
/host.shear-
1).*n2c.*volumeFraction_collapsed.^(5./3)+25.*(gas.shear./host.shear-
1).*(host.poisson.^2-7).*n2c.*volumeFraction_collapsed-
(7+5.*host.poisson).*n2c.*n3c;
x1c=(-Bc+sqrt(Bc.^2-4.*Ac.*Dc))./(2.*Ac);
x2c=(-Bc-sqrt(Bc.^2-4.*Ac.*Dc))./(2.*Ac);
shear1c=x1c.*host.shear;
shear2c=x2c.*host.shear;

shear_collapsed=shear1c;

%uncollapsed case
n1u=(insert.shear./host.shear-1).*(49-
50.*insert.poisson.*host.poisson)+35.*(insert.shear./host.shear).*(inse
rt.poisson-2.*host.poisson)+35.*(2.*insert.poisson-host.poisson);
n2u=5.*insert.poisson.*(insert.shear./host.shear-
8)+7.*(insert.shear+host.shear+4);
n3u=(insert.shear./host.shear).*(8-10.*host.poisson)+(7-
5.*host.poisson);
Au=8.*(insert.shear./host.shear-1).*(4-
5.*host.poisson).*n1u.*volumeFraction_uncollapsed.^(10./3)-
2.*(63.*(insert.shear./host.shear-
1).*n2u+2.*n1u.*n3u).*volumeFraction_uncollapsed.^(7./3)+252.*(insert.s
hear./host.shear-1).*n2u.*volumeFraction_uncollapsed.^(5./3)-
25.*(insert.shear./host.shear-1).*(7-
12.*host.poisson+8.*host.poisson.^2).*n2u.*volumeFraction_uncollapsed+4
.*(7-10.*host.poisson).*n2u.*n3u;
```

```
Bu=-4.*(insert.shear./host.shear-1).*(1-
5.*host.poisson).*n1u.*volumeFraction_uncollapsed.^(10./3)+4.*(63.*(ins
ert.shear./host.shear-
1).*n2u+2.*n1u.*n3u).*volumeFraction_uncollapsed.^(7./3)-
504.*(insert.shear./host.shear-
1).*n2u.*volumeFraction_uncollapsed.^(5./3)+150.*(insert.shear./host.sh
ear-1).*(3-
host.poisson).*host.poisson.*n2u.*volumeFraction_uncollapsed+3.*(15.*ho
st.poisson-7).*n2u.*n3u;
Du=4.*(insert.shear./host.shear-1).*(5.*host.poisson-
7).*n1u.*volumeFraction_uncollapsed.^(10./3)-
2.*(63.*(insert.shear./host.shear-
1).*n2u+2.*n1u.*n3u).*volumeFraction_uncollapsed.^(7./3)+252.*(insert.s
hear./host.shear-
1).*n2u.*volumeFraction_uncollapsed.^(5./3)+25.*(insert.shear./host.she
ar-1).*(host.poisson.^2-7).*n2u.*volumeFraction_uncollapsed-
(7+5.*host.poisson).*n2u.*n3u;
x1u=(-Bu+sqrt(Bu.^2-4.*Au.*Du))./(2.*Au);
x2u=(-Bu-sqrt(Bu.^2-4.*Au.*Du))./(2.*Au);
shear1u=x1u.*host.shear;
shear2u=x2u.*host.shear;

shear_uncollapsed=shear1u;

shear_out=zeros(size(gas.bulk));  %Without this line, shear_out will be
an incorrectly sized vector

shear_out(systemPressureMat<=collapsePressure)=shear_uncollapsed(system
PressureMat<=collapsePressure);
shear_out(systemPressureMat>=collapsePressure)=shear_collapsed(systemPr
essureMat>=collapsePressure);

composite.shear=shear_out;

K=composite.bulk(1,:); %static bulk modulus properties to determine
liner deformation

%volumeFractionCalc
volumeFrac_out=zeros(size(gas.bulk));
volumeFrac_out(systemPressureMat<=collapsePressure)=NaN;%volumeFraction
_uncollapsed;
volumeFrac_out(systemPressureMat>=collapsePressure)=volumeFraction_coll
apsed(systemPressureMat>=collapsePressure);

% calculate static deformation of the liner
for n=1:N %counter changed to allow for correct indexing
    strain(n)=(Ptotal/N)./((-1-(2*r_o(n).^2./(r_o(n)^2-
r_i(n)^2))+(2*r_i(n).^2./(r_o(n)^2-r_i(n)^2)))*real(K(n)));
    r_o(n+1)=r_o(n)*(strain(n)+1);
    r_i(n+1)=r_i(n)*(strain(n)+1);
    L(n+1)=L(n)*(strain(n)+1);
end

composite=prop_Calc(composite);
```

```
lambda_s=composite.lames(:,end);
mu_s=composite.shear(:,end);

%interpolating between material Freq vector to find the TL freq vector
%(note case)
lambda_s=interp1(Freq,lambda_s,freq);
mu_s=interp1(Freq,mu_s,freq);

if TL_calc==1
    datstruct =
shell4(lambda_s,mu_s,Ptotal,r_i(1),r_o(1),L(1),r_i(N+1),r_o(N+1),L(N+1)
,freq,density_elevated); %Need to use shell3 to accept correct inputs
    figure; plot(freq,datstruct.TL_1)
end

if barify==1 %Change units to bar
    composite.bulk=composite.bulk./1e5;
    composite.shear=composite.shear./1e5;
    systemPressure=systemPressure./1e5;
end

if MPaIfy==1 %Change units to bar
    composite.bulk=composite.bulk./1e6;
    composite.shear=composite.shear./1e6;
    systemPressure=systemPressure./1e6;
end

if show_prop_graph==1
    figure
    subplot(1,3,1)
    plot(Freq(:,1),real(composite.bulk))
    xlim([1,5000])
    subplot(1,3,2)
    plot(Freq(:,1),imag(composite.bulk))
    xlim([1,5000])
    subplot(1,3,3)
    plot(Freq(:,1),imag(composite.bulk)./real(composite.bulk))
    xlim([1,5000])
    figure
    subplot(1,3,1)
    plot(Freq(:,1),real(composite.shear))
    xlim([1,5000])
    subplot(1,3,2)
    plot(Freq(:,1),imag(composite.shear))
    xlim([1,5000])
    subplot(1,3,3)
    plot(Freq(:,1),imag(composite.shear)./real(composite.shear))
    xlim([1,5000])
end

if show_prop_cont==1
    figure
    subplot(1,2,1)

contourf(systemPressure,Freq,real(composite.bulk),40,'LineStyle','none'
)
```

```
    h1=gca;
    h1.FontSize=12;
%     title('Storage Modulus')
    colormap('jet')
    colorTitle=colorbar;
    if barify==1
        xlabel('System Pressure [Bar]')
    elseif MPaIfy==1
        xlabel('System Pressure [MPa]')
    else
        xlabel('System Pressure [Pa]')
    end
%     if barify==1
%         ylabel(colorTitle,'Modulus [Bar]')
%     elseif MPaIfy==1
%         ylabel(colorTitle,'Modulus [MPa]')
%     else
%         ylabel(colorTitle,'Modulus [Pa]')
%     end
    ylabel('Frequency [Hz]')
    subplot(1,2,2)

contourf(systemPressure,Freq,imag(composite.bulk),40,'LineStyle','none'
)
    h1=gca;
    h1.FontSize=12;
%     title('Loss Modulus')
    colormap('jet')
    colorTitle2=colorbar;
    if barify==1
        xlabel('System Pressure [Bar]')
    elseif MPaIfy==1
        xlabel('System Pressure [MPa]')
    else
        xlabel('System Pressure [Pa]')
    end
%     if barify==1
%         ylabel(colorTitle2,'Modulus [Bar]')
%     elseif MPaIfy==1
%         ylabel(colorTitle2,'Modulus [MPa]')
%     else
%         ylabel(colorTitle2,'Modulus [Pa]')
%     end
    ylabel('Frequency [Hz]')
%     figure
%     subplot(1,3,3)
%
contourf(systemPressure,Freq,imag(composite.bulk)./real(composite.bulk)
,40,'LineStyle','none')
%     h1=gca;
%     h1.FontSize=12;
%     title('tan \delta')
%     colormap('jet')
%     colorbar
%     if barify==1
%         xlabel('System Pressure [Bar]')
%     elseif MPaIfy==1
```

```
%         xlabel('System Pressure [MPa]')
%     else
%         xlabel('System Pressure [Pa]')
%     end
%     ylabel('Frequency [Hz]')
%     suptitle('Bulk Modulus')

    figure
    subplot(1,2,1)

contourf(systemPressure,Freq,real(composite.shear),40,'LineStyle','none
')
    h1=gca;
    h1.FontSize=12;
%     title('Storage Modulus')
    colormap('jet')
    colorbar
    if barify==1
        xlabel('System Pressure [Bar]')
    elseif MPaIfy==1
        xlabel('System Pressure [MPa]')
    else
        xlabel('System Pressure [Pa]')
    end
    ylabel('Frequency [Hz]')
    subplot(1,2,2)

contourf(systemPressure,Freq,imag(composite.shear),40,'LineStyle','none
')
    h1=gca;
    h1.FontSize=12;
%     title('Loss Modulus')
    colormap('jet')
    colorbar
    if barify==1
        xlabel('System Pressure [Bar]')
    elseif MPaIfy==1
        xlabel('System Pressure [MPa]')
    else
        xlabel('System Pressure [Pa]')
    end
    ylabel('Frequency [Hz]')
% %     figure
%     subplot(1,3,3)
%
contourf(systemPressure,Freq,imag(composite.shear)./real(composite.shea
r),40,'LineStyle','none')
%     title('tan \delta')
%     colormap('jet')
%     colorbar
%     if barify==1
%         xlabel('System Pressure [Bar]')
%     else
%         xlabel('System Pressure [Pa]')
%     end
%     ylabel('Frequency [Hz]')
%     suptitle('Shear Modulus')
```

```
end
```

B.2 Bulk modulus optimization

For use with Maple

```
> restart;
> with(plots) :
> Gm := beta·Km
```

$$Gm := \beta\, Km$$

```
> Vm[f] := Vm[i] - P·Vm[i]/Km
```

$$Vm_f := Vm_i - \frac{P\, Vm_i}{Km}$$

```
>
> Vi[f] := Pg·Vi[i]/P
```

$$Vi_f := \frac{Pg\, Vi_i}{P}$$

```
> Ki := gamma·P
```

$$Ki := \gamma P$$

```
> c := Vi[f]/(Vi[f] + Vm[f])
```

$$c := \frac{Pg\, Vi_i}{P\left(\frac{Pg\, Vi_i}{P} + Vm_i - \frac{P\, Vm_i}{Km}\right)}$$

```
> Kstar := Km + (Ki - Km)·(4·Gm + 3·Km)·c/(4·Gm + 3·Ki + 3·(Km + Ki)·c)
```

$$Kstar := Km + \frac{(P\gamma - Km)\,(4\,Km\,\beta + 3\,Km)\,Pg\,Vi_i}{P\left(\frac{Pg\, Vi_i}{P} + Vm_i - \frac{P\, Vm_i}{Km}\right)\left(4\,\beta\,Km + 3\,\gamma P + \frac{3\,(P\gamma + Km)\,Pg\,Vi_i}{P\left(\frac{Pg\, Vi_i}{P} + Vm_i - \frac{P\, Vm_i}{Km}\right)}\right)}$$

```
> KstarSim := simplify(Kstar)
```

$$KstarSim := \left(Km\,P\left(4\,Km\,Pg\,\beta\,\gamma\,Vi_i + 4\,Km^2\,\beta\,Vm_i - 4\,Km\,P\,\beta\,Vm_i + 3\,Km\,P\,\gamma\,Vm_i + 9\,Km\,Pg\,\gamma\,Vi_i - 3\,P^2\,\gamma\,Vm_i\right)\right) \Big/ \left(4\,Km^2\,P\,\beta\,Vm_i + 4\,Km^2\,Pg\,\beta\,Vi_i - 4\,Km\,P^2\,\beta\,Vm_i + 3\,Km\,P^2\,\gamma\,Vm_i + 6\,Km\,P\,Pg\,\gamma\,Vi_i - 3\,P^3\,\gamma\,Vm_i + 3\,Km^2\,Pg\,Vi_i\right)$$

```
> #latex( '(7)' )
> diff(KstarSim, Km)
```

$$\left(P\left(4\,Km\,Pg\,\beta\,\gamma\,Vi_i+4\,Km^2\,\beta\,Vm_i-4\,Km\,P\,\beta\,Vm_i+3\,Km\,P\,\gamma\,Vm_i+9\,Km\,Pg\,\gamma\,Vi_i\right.\right.$$
$$\left.-3\,P^2\,\gamma\,Vm_i\right)\Big)\Big/\left(4\,Km^2\,P\,\beta\,Vm_i+4\,Km^2\,Pg\,\beta\,Vi_i-4\,Km\,P^2\,\beta\,Vm_i+3\,Km\,P^2\,\gamma\,Vm_i\right.$$
$$+6\,Km\,P\,Pg\,\gamma\,Vi_i-3\,P^3\,\gamma\,Vm_i+3\,Km^2\,Pg\,Vi_i\Big)+\Big(Km\,P\left(4\,Pg\,\beta\,\gamma\,Vi_i+8\,Km\,\beta\,Vm_i\right.$$
$$\left.-4\,P\,\beta\,Vm_i+3\,P\,\gamma\,Vm_i+9\,Pg\,\gamma\,Vi_i\right)\Big)\Big/\left(4\,Km^2\,P\,\beta\,Vm_i+4\,Km^2\,Pg\,\beta\,Vi_i\right.$$
$$-4\,Km\,P^2\,\beta\,Vm_i+3\,Km\,P^2\,\gamma\,Vm_i+6\,Km\,P\,Pg\,\gamma\,Vi_i-3\,P^3\,\gamma\,Vm_i+3\,Km^2\,Pg\,Vi_i\Big)$$
$$-\Big(Km\,P\left(4\,Km\,Pg\,\beta\,\gamma\,Vi_i+4\,Km^2\,\beta\,Vm_i-4\,Km\,P\,\beta\,Vm_i+3\,Km\,P\,\gamma\,Vm_i+9\,Km\,Pg\,\gamma\,Vi_i\right.$$
$$\left.+3\,Km\,P^2\,\gamma\,Vm_i+6\,Km\,P\,Pg\,\gamma\,Vi_i-3\,P^3\,\gamma\,Vm_i+3\,Km^2\,Pg\,Vi_i\right)^2$$

>

> *simplify*(**(8)**)

$$\left(P\left(-16\,Km^2\,P^2\,Pg\,\beta^2\,\gamma\,Vi_i\,Vm_i+12\,Km^2\,P^2\,Pg\,\beta\,\gamma^2\,Vi_i\,Vm_i+24\,Km^2\,P\,Pg^2\,\beta\,\gamma^2\,Vi_i^2\right.\right.$$
$$-24\,Km\,P^3\,Pg\,\beta\,\gamma^2\,Vi_i\,Vm_i+16\,Km^4\,P\,\beta^2\,Vm_i^2+16\,Km^4\,Pg\,\beta^2\,Vi_i\,Vm_i-32\,Km^3\,P^2\,\beta^2$$
$$Vm_i^2+24\,Km^3\,P^2\,\beta\,\gamma\,Vm_i^2+48\,Km^3\,P\,Pg\,\beta\,\gamma\,Vi_i\,Vm_i+16\,Km^2\,P^3\,\beta^2\,Vm_i^2-48\,Km^2\,P^3\,\beta\,\gamma$$
$$Vm_i^2+9\,Km^2\,P^3\,\gamma^2\,Vm_i^2-48\,Km^2\,P^2\,Pg\,\beta\,\gamma\,Vi_i\,Vm_i+45\,Km^2\,P^2\,Pg\,\gamma^2\,Vi_i\,Vm_i$$
$$+54\,Km^2\,P\,Pg^2\,\gamma^2\,Vi_i^2+24\,Km\,P^4\,\beta\,\gamma\,Vm_i^2-18\,Km\,P^4\,\gamma^2\,Vm_i^2-54\,Km\,P^3\,Pg\,\gamma^2\,Vi_i\,Vm_i$$
$$\left.+9\,P^5\,\gamma^2\,Vm_i^2+12\,Km^4\,Pg\,\beta\,Vi_i\,Vm_i+9\,Km^2\,P^2\,Pg\,\gamma\,Vi_i\,Vm_i\right)\Big)\Big/\left(4\,Km^2\,P\,\beta\,Vm_i\right.$$
$$+4\,Km^2\,Pg\,\beta\,Vi_i-4\,Km\,P^2\,\beta\,Vm_i+3\,Km\,P^2\,\gamma\,Vm_i+6\,Km\,P\,Pg\,\gamma\,Vi_i-3\,P^3\,\gamma\,Vm_i$$
$$\left.+3\,Km^2\,Pg\,Vi_i\right)^2$$

> *#latex*(**(9)**)

> *KmZero* := *solve*(**(8)** = 0, *Km*)

$$KmZero := RootOf\Big(\left(16\,P\,\beta^2\,Vm_i^2+16\,Pg\,\beta^2\,Vi_i\,Vm_i+12\,Pg\,\beta\,Vi_i\,Vm_i\right)\_Z^4+\left(-32\,P^2\,\beta^2\right.$$
$$Vm_i^2+24\,P^2\,\beta\,\gamma\,Vm_i^2+48\,P\,Pg\,\beta\,\gamma\,Vi_i\,Vm_i\Big)\_Z^3+\Big(-16\,P^2\,Pg\,\beta^2\,\gamma\,Vi_i\,Vm_i$$
$$+12\,P^2\,Pg\,\beta\,\gamma^2\,Vi_i\,Vm_i+24\,P\,Pg^2\,\beta\,\gamma^2\,Vi_i^2+16\,P^3\,\beta^2\,Vm_i^2-48\,P^3\,\beta\,\gamma\,Vm_i^2+9\,P^3\,\gamma^2$$
$$Vm_i^2-48\,P^2\,Pg\,\beta\,\gamma\,Vi_i\,Vm_i+45\,P^2\,Pg\,\gamma^2\,Vi_i\,Vm_i+54\,P\,Pg^2\,\gamma^2\,Vi_i^2+9\,P^2\,Pg\,\gamma\,Vi_i\,Vm_i\Big)$$
$$\_Z^2+\Big(-24\,P^3\,Pg\,\beta\,\gamma^2\,Vi_i\,Vm_i+24\,P^4\,\beta\,\gamma\,Vm_i^2-18\,P^4\,\gamma^2\,Vm_i^2-54\,P^3\,Pg\,\gamma^2\,Vi_i\,Vm_i\Big)\_Z$$
$$\left.+9\,P^5\,\gamma^2\,Vm_i^2\right)$$

> *#latex*(*'***(10)**')

> *kmRoot* := *subs*({beta = 0.001, gamma = 1, *Vi*[*i*] = 2.6808e-13, *Vm*[*i*] = 2.6808e-13, Pg = 0.1 ·1e6, P = 35·1e6}, *KmZero*)

$$kmRoot := RootOf\left(1.266007071\,10^{-22}\_Z^4 + 2.122142916\,10^{-12}\_Z^3 + 0.02806022330\,\_Z^2 - 1.955272526\,10^{6}\,\_Z + 3.397125262\,10^{13}\right)$$

> $allvalues(kmRoot)$

$$3.453343285\,10^{7},\ 3.487385287\,10^{7},\ -8.415947968\,10^{9} + 1.232811289\,10^{10}\,I,\ -8.415947968\,10^{9} - 1.232811289\,10^{10}\,I$$

> $plot(op(kmRoot), \_Z = 0..\mathbf{(12)}[2]\cdot 1.5)$

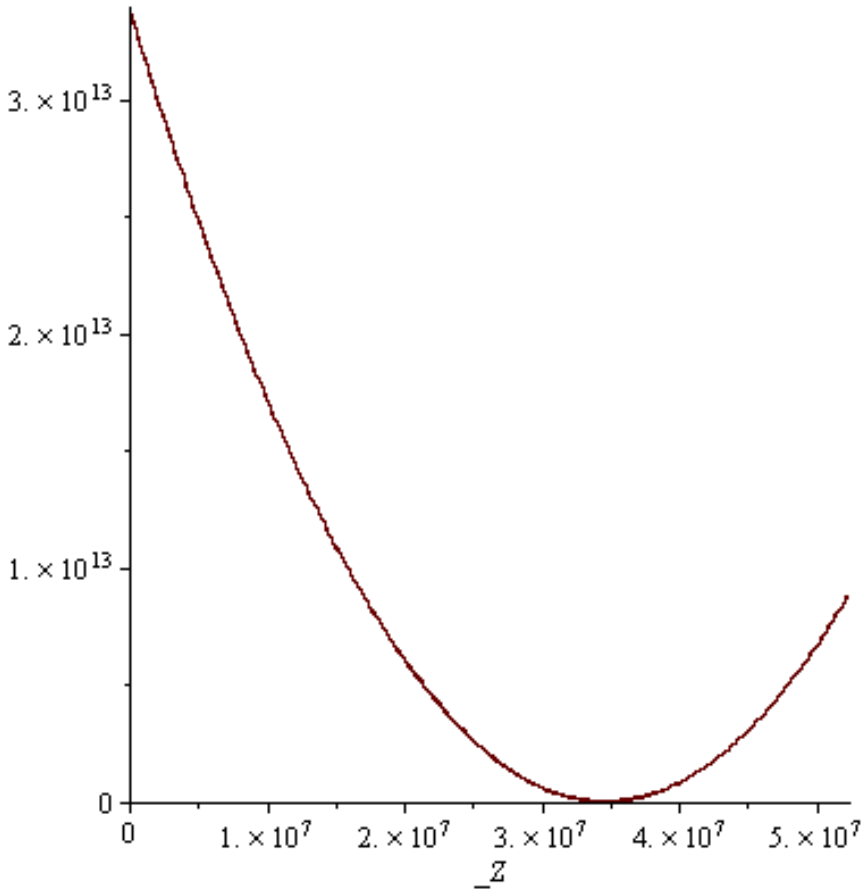

> $plot(subs(\{\text{beta} = 0.001, \text{gamma} = 1.4, Vi[i] = 2.6808\text{e-}13, Vm[i] = 2.6808\text{e-}13, \text{Pg} = 0.1\cdot 1\text{e}6, \text{P} = .44\cdot 1\text{e}6\}, Kstar), Km = 0..\mathbf{(12)}[2]\cdot 1.5)$

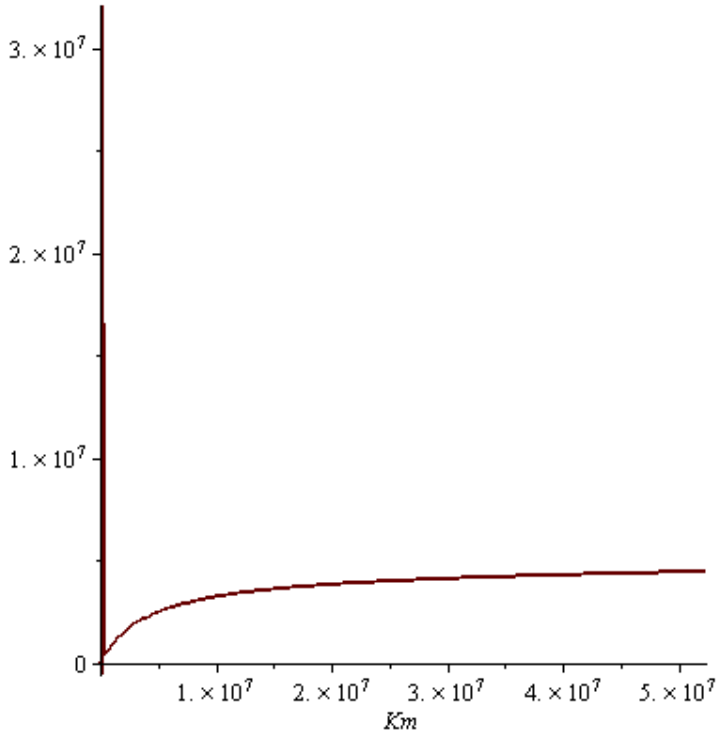


```
> #kmRoot:=subs({beta = 0.001, gamma = 1.4, Vi[i] = 0.5, Vm[i] = 0.5, Pg = 5·1e6, P = 35
      ·1e6}, KmZero)
> #allvalues(kmRoot)
> #plot(op(kmRoot), _Z = 0 ..??[2]·1.5)
```

B.3 Fluorine Requirement

The amount of fluorine necessary to prepare the microspheres depends on the volume of the chamber, the geometry of the microsphere and the depth of the fluorination. The volume of the chamber combined with the geometry of the microspheres determines the number of microspheres within the chamber. It is also important to consider the packing fraction of the microspheres. For regular arrangements of spheres, i.e. spheres with identical radii, the packing fraction ranges from 0.53 to 0.74. The microspheres do not have identical radii; their radii match a log-normal distribution; the packing fraction for this type of distribution ranges from 0.64 to 0.97 [66]. For the fluorinator shown in Figure 4-10 the approximate number of nominally 20 μm diameter

microspheres held within is 7.7 billion microspheres. The volume of microsphere material for an example microsphere is then found from

$$V_{wall} = \frac{4}{3}\pi\left(r^3 - (r-t)^3\right). \tag{6.3}$$

The total volume of microsphere material is now known; which allows the number moles of microsphere molecules to be found. The microspheres under examination within are made of polystyrene, chemical formula C_8H_8. Fluorination functions by replacing the hydrogen atoms on the polymer backbone with a fluorine atom; the replacement is one to one. The desired depth of fluorination determines how many moles of hydrogen must be replaced. Ideal gas relations can be used to find the necessary pressure reduction from a fluorine tank if they initial tank concertation is known. Code to calculate fluorine necessary to conduct a fluorination is given below.

```
clear
close all
clc

fluorine_tank_pressure_psi=1800; %intial pressure of fluorine tank,
[psi]
f2_depth_fraction=0.1; %fraction of wall desired to be fluorinated

fluorine_tank_pressure_Pa=fluorine_tank_pressure_psi*6894.75729;
%conversion to [Pa]
fluorine_tank_volume=0.0889^2*pi*0.5334; %Volume of tank [m^3]

R=8.3144598; %Universal Gas Constant
fluorine_tank_moles=0.03*fluorine_tank_pressure_Pa*fluorine_tank_volume
/(R*273.15+23); %moles of fluorine (only) in tank, 0.03 is fluorine
concentration

%Microsphere dimensions
r=10e-6;
t=0.146e-6;
V_sphere_wall_individual=4/3*pi*(r^3-(r-t)^3);
V_sphere_individual=4/3*pi*(r^3);

%Chamber dimensions
d=0.0635; %[m]
L=0.1524; %[m]
V_chamber=pi*L*(d/2)^2; %[m^3]
```

```
load_fraction=.95; %bulk level of spheres as a fraction
packing_fraction=0.7; %packing fraction of spheres

sphere_coeff=load_fraction*packing_fraction; %true fraction of chamber
made of microsphere

V_sphere_total_true=sphere_coeff*V_chamber;
number_of_spheres=V_sphere_total_true/V_sphere_individual;

V_sphere_wall_total=number_of_spheres*V_sphere_wall_individual;

rho_PS=1050; %Density of polystyrene
Mass_sphere_wall_total=rho_PS*V_sphere_wall_total;

moles_weight_PS=(12.011*8+1.008*8)./1000;
moles_PS=Mass_sphere_wall_total/moles_weight_PS;
moles_H_total=moles_PS*8;
moles_H_replace=moles_H_total*f2_depth_fraction;

change_fluorine_pressure=(moles_H_replace*fluorine_tank_pressure_Pa)./(
fluorine_tank_moles);
change_tank_pressure_psi=change_fluorine_pressure./6894.75729
```

B.4 Transmission Loss Measurement

```
%% Title Section
% Program to Determine:
% - The speed of sound in hydraulic fluid
% - The reflection coefficient and apparent transmission loss (3-mic)
% - The transmission loss through transfer matrix parameters
%
% By: Nicholas E. Earnhart
%
% Last Revision: 10/08/2010 (Later than this)
%-------------------------------------------------------------------------

% function [output5 header] = TL_func(runname)

% load(run01)


clear all
% close all
clc
%
newpath = '\twoSuppBig';
path(path,[pwd,newpath])

load run03
showplots = 0; % 1=Yes 0=No
coher = 0.95;%0.5;%
calset = 3;

% Pipe properties
```

```
I01 = 0.33; % [m] distance between sensors 0 and 1
I12 = 0.47; % [m] distance between sensors 1 and 2
I34 = 0.33; % [m] distance between sensors 3 and 4
I45 = 0.47; % [m] distance between sensors 4 and 5
d = 0.0381; % 0.0206; % [m] pipe inner diameter
r0 = d / 2; % [m] pipe inner radius
t = 0.0206; %0.0087376;   [m] Wall thickness of the pipe
Ew = 210e9; % [Pa] Young's modulus of the steel pipe wall

pipepropsup=struct('I01',I01,'I12',I12,'d',d,'r0',d/2,'t',t,'Ew',Ew);
pipepropsdown=struct('I01',I34,'I12',I45,'d',d,'r0',d/2,'t',t,'Ew',Ew);

% Fluid properties

% Conoco Megaflow AW ISO 46 Hydraulic Oil
% cSt @ 40degC = 46.0     (1 cSt = 10^-6 m^2/sec)
% cSt @ 100degC = 6.8
% Specific gravity @ 60degF 0.868
% Density @ 60degF = 7.23 lbs/gal

Oil_Temp = mean(TempArray0F(1:30));
Liner_Temp = mean(TempArray0C(1:30));

% kinematic viscosity
visc = 164.52e-6*exp(-0.032*Oil_Temp);
c0 = 1400; % [m/s] initial speed of sound guess
Df = 1724e6; % [Pa] Bulk modulus of the hydraulic oil
Rho = 868; % [kg/m^3] Density of hydraulic oil

fluidprops = struct('visc',visc,'Df',Df,'Ew',Ew,'Rho',Rho);
lastrow = length(TF(:,1));

Freq = transpose(Freq);
omega = Freq(:,1)*2*pi; % [rad/sec] radial frequency interval vector

% Calibrate Data
% Calibrate the transfer functions
[h01,h21,h31,h41,h51,h34,h54,ccup,ccacross,ccdown,cc] = ...
    CAL_func(TF,Power,coher);

% Compute Speed of Sound
fprintf('Upstream SOS\n')
cu = SOS_func(omega,h01,h21,pipepropsup,fluidprops,c0);

fprintf('Downstream SOS\n')
cd = SOS_func(omega,h34,h54,pipepropsdown,fluidprops,c0);


% Calculate, R, ATL, TL

% **********************************************************************
%
%_____________________________|            |_____________________________
%_____________________________              _____________________________
```

```
%  |       |        |       |___________|       |         |          |
%
%  0       1        2                           3         4          5
%  x0      x1       x2                          y0        y1         y2
%               x --------->|          |--------> y
%                          x=0       y=0
%**********************************************************************

% 0.139 is the distance from the test section to the resonator neck

x2 = -.455;
x1 = x2 - 0.47;
x0  = x1 - 0.33;

y0 = .380;
y1 = y0 + 0.33;
y2 = y1 + 0.47;
% Lp = 1.339 + 0.139 + .07; % Pipe length + resonator pipe + fitting to
                            % internals of termination silencer

H01(1,1,:) = h01(:,1);
H11(1,1,1:lastrow) = 1;
H21(1,1,:) = h21(:,1);

H31(1,1,:) = h31(:,1);
H41(1,1,:) = h41(:,1);
H51(1,1,:) = h51(:,1);

zeta = 1 + sqrt(visc./(r0^2*1i*omega)) + visc./(r0^2*1i*omega);

ku(1,1,:) = (omega / cu) .* zeta;   kd(1,1,:) = (omega / cd) .* zeta;

Z0u = (Rho * cu * zeta) / (pi * r0^2);
Z0d = (Rho * cd * zeta) / (pi * r0^2);

A = [exp(-1i*ku*x2) exp(1i*ku*x2);
     exp(-1i*ku*x1) exp(1i*ku*x1);
     exp(-1i*ku*x0) exp(1i*ku*x0)];
e = [H21; H11; H01];

G = [exp(-1i*kd*y0) exp(1i*kd*y0);
     exp(-1i*kd*y1) exp(1i*kd*y1);
     exp(-1i*kd*y2) exp(1i*kd*y2)];
h = [H31; H41; H51];

x = zeros(lastrow,2);
y = zeros(lastrow,2);
condx = zeros(lastrow,1);
condy = zeros(lastrow,1);

for p = 1:lastrow
    x(p,:) = transpose(pinv(A(:,:,p)) * e(:,:,p));
    condx(p,:) = cond(A(:,:,p));
    y(p,:) = transpose(pinv(G(:,:,p)) * h(:,:,p));
```

```
    condy(p,:) = cond(G(:,:,p));
end

% Preallocate matrices
Freq2 = zeros(sum(ccup),1); R = Freq2;
output2 = zeros(sum(ccup),4);

count = 1;
for ii = 1:lastrow
    if (ccup(ii) == 0);
    else
        Freq2(count,1) = Freq(ii);
        % Silencer entrance reflection coefficient
        R(count) = x(ii,2) / x(ii,1);
        output2(count,1:4) = [real(x(ii,1)),imag(x(ii,1)),...
            real(x(ii,2)),imag(x(ii,2))];
        count = count + 1;
    end
end

% Preallocate matrices
Freq4 = zeros(sum(ccdown),1);
output3 = zeros(sum(ccdown),4);

count3 = 1;
for ii = 1:lastrow
    if (ccdown(ii) == 0);
    else
        Freq4(count3,1) = Freq(ii);
        output3(count3,1:4) = [real(y(ii,1)),imag(y(ii,1)),...
            real(y(ii,2)),imag(y(ii,2))];
        count3 = count3 + 1;
    end
end

realR(:,1) = real(R);
imagR(:,1) = imag(R);
R2(:,1) = abs(R).^2; % Power reflection coefficient

Z = Rho*cu*((1 + R) ./ (1 - R)); % Silencer entrance impedance


% Generate the Transfer Matrix
p0 = x(:,1) + x(:,2); % Pressure at silencer entrance
q0 = (x(:,1) - x(:,2)) ./ Z0u; % Velocity at silencer entrance

pd = y(:,1) + y(:,2); % Pressure at silencer exit
qd = (y(:,1) - y(:,2)) ./ Z0d; % Velocity at silencer exit
% Velocity at silencer exit, different convention
% qd2 = (-y(:,1) + y(:,2)) ./ Z0d;

% pd = y(:,1);
% qd = y(:,1) ./ Z0d;

% Transfer matrix parameters
```

```
T11 = (pd .* qd + p0 .* q0) ./ (p0 .* qd + pd .* q0);
T12 = (p0.^2 - pd.^2) ./ (p0 .* qd + pd .* q0);
T21 = (q0.^2 - qd.^2) ./ (p0 .* qd + pd .* q0);
T22 = T11;

% T11 = (p0 .* qd + pd .* q0) ./ (pd .* qd + p0 .* q0);
% T12 = (p0 .* qd + pd .* q0) ./ (p0.^2 - pd.^2);
% T21 = (p0 .* qd + pd .* q0) ./ (q0.^2 - qd.^2);
% T22 = T11;

z11 = (pd.*qd - p0.*q0)./(qd.^2 - q0.^2); % = z22
z12 = (p0.*qd - pd.*q0)./(qd.^2 - q0.^2); % = z21

z11amp = abs(z11);
z11pha = angle(z11)*180/pi;
z12amp = abs(z12);
z12pha = angle(z12)*180/pi;

% Reflection coefficient at entrance of downstream pipe
Rd = y(:,2) ./ y(:,1);
% kd2 = (omega / cd) .* zeta;
% Termination silencer reflection coefficient
% Rt(:,1) = (y(:,2).*exp(-1i*kd2*Lp)) ./ (y(:,1).*exp(1i*kd2*Lp));
% Zt = Rho*cd*((1 + Rt) ./ (1 - Rt)); % Silencer entrance impedance
% Relationship btw C and D at downstream face of silencer under test
% Y(:,1) = abs(Rt .* exp(-2*1i*kd2*Lp));
% Y(:,1) = y(:,2) ./ y(:,1);

% Relative to amplitude of wave A
waveA = log10(abs(x(:,1))./abs(x(:,1)));
waveB = log10(abs(x(:,2))./abs(x(:,1)));
waveD = log10(abs(y(:,1))./abs(x(:,1)));
waveE = log10(abs(y(:,2))./abs(x(:,1)));

phaBA = angle(x(:,2)./x(:,1));
phaDC = angle(y(:,2)./y(:,1));
% diff = phaDC + phaBA;
waveratio = (x(:,2).*y(:,2))./(x(:,1).*y(:,1));
phadiff = angle(waveratio);

ccpha = ones(1,2560);%(phadiff < -.6) | (phadiff > .6);

Traveling_up = abs(x(:,1) - x(:,2).*exp(1i*phaBA));
Standing_up = abs(2*x(:,2).*exp(1i*phaBA));

Traveling_down = abs(y(:,1) - y(:,2).*exp(1i*phaDC));
Standing_down = abs(2*y(:,2).*exp(1i*phaDC));

% Preallocate matrices
Freq3 = zeros(sum(cc),1); TL = Freq3; TL1 = Freq3; TL2 = Freq3;
TL3 = Freq3; TL4 = Freq3; TL22 = Freq3;

count2 = 1;
for ii = 1:lastrow
    if (cc(ii) == 0) || (ccpha(ii) == 0)
```

```
    else
        Freq3(count2,1) = Freq(ii);

        T11(ii) = T11(ii) .* cc(ii);
        T12(ii) = T12(ii) .* cc(ii);
        T21(ii) = T21(ii) .* cc(ii);
        T22(ii) = T22(ii) .* cc(ii);

        t1 = sqrt(Z0d(ii)/Z0u(ii))*T11(ii);
        t2 = T12(ii)/sqrt(Z0u(ii)*Z0d(ii));
        t3 = sqrt(Z0u(ii)*Z0d(ii))*T21(ii);
        t4 = sqrt(Z0u(ii)/Z0d(ii))*T22(ii);

        % System-independent TL
        TL(count2,1) = 20*(log10((1/2)*abs(t1 + t2 + t3 + t4)));

        TL1(count2,1) = 20*log10((1/2)*abs(t1));
        TL2(count2,1) = 20*log10((1/2)*abs(t2));
        TL3(count2,1) = 20*log10((1/2)*abs(t3));
        TL4(count2,1) = 20*log10((1/2)*abs(t4));

        % System-dependent TL
        TL22(count2,1) = 20*log10((1/2)*abs(t1 + t2 + t3 + t4 + ...
            Rd(ii).*(t1 - t2 + t3 - t4)));

        count2 = count2 + 1;
    end
end

% figure(6);subplot(3,1,1);plot(Freq3,TL1,Freq3,TL);subplot(3,1,2);...
%     plot(Freq3,TL2,Freq3,TL);subplot(3,1,3);plot(Freq3,TL3,Freq3,TL)

% Transmission loss using impedance parameters
% TL_imped = 20*log10(0.5*abs(z11./z21 + z22./z21 + ...
%     (z11.*z22)./(z21.*Z0) + Z0./z21 - z12./Z0));%.* cc';

figure
plot(Freq3,TL,'.')
xlabel('Frequency (Hz)')
ylabel('Transmission Loss (dB)')
axis([0,4000,0,80])
% subplot(2,1,2)
% plot(Freq,phadiff)
% axis([0,4000,-pi-0.1,pi+0.1])
%% Typically Necessary Plot Commands

if showplots == 1;

    % Plot Power Spectra, Upstream Transfer Functions
    figure
    subplot(2,2,1)
    semilogy(Freq,Power1,Freq,Power2,Freq,Power3)
    grid on
    title('Power Vrms^2')
    legend('Power1','Power2','Power3')
```

```
subplot(2,2,2)
semilogy(Freq,Power4,Freq,Power5,Freq,Power6)
grid on
title('Power Vrms^2')
legend('Power4','Power5','Power6')

subplot(2,2,3)
plot(Freq,TF(:,2),Freq,TF(:,3))
grid on
title('TF 0/1')
legend('Real','Imag')

subplot(2,2,4)
plot(Freq,TF(:,5),Freq,TF(:,6))
grid on
title('TF 2/1')
legend('Real','Imag')


% Plot Coherence Vectors
figure
subplot(3,2,1)
plot(Freq,coher1)
grid on
title('Coherence of TF 0/1')

subplot(3,2,2)
plot(Freq,coher2)
title('Coherence of TF 2/1')
grid on

subplot(3,2,3)
plot(Freq,coher3)
title('Coherence of TF 3/1')
grid on

subplot(3,2,4)
plot(Freq,coher4)
title('Coherence of TF 4/1')
grid on

subplot(3,2,5)
plot(Freq,coher5)
title('Coherence of TF 5/1')
grid on

subplot(3,2,6)
plot(Freq,coher6,Freq,coher7)
title('Coherence of TF 3/4, 5/4')
grid on


% Plot Reflection Coefficient
```

```
    figure
    plot(Freq2,real(R),'.-',Freq2,imag(R),'.-',Freq2,abs(R),'.-')
    grid on
    xlabel('Frequency [Hz]')
    title('Reflection Coefficient of Silencer Entrance')
    legend('Real','Imag','Magnitude')

    figure
    plot(Freq3,TL,'.-')
    grid on
    xlabel('Frequency [Hz]')
    ylabel('TL [dB]')
    title('Transmission Loss')

    figure
    subplot(2,2,1)
    plot(Freq,real(T11),Freq,imag(T11))
    legend('Real','Imag')
    title('T11')

    subplot(2,2,2)
    plot(Freq,real(T12),Freq,imag(T12))
    legend('Real','Imag')
    title('T12')

    subplot(2,2,3)
    plot(Freq,real(T21),Freq,imag(T21))
    legend('Real','Imag')
    title('T21')

    subplot(2,2,4)
    plot(Freq,real(T22),Freq,imag(T22))
    legend('Real','Imag')
    title('T22')

    figure
    plot(Freq,phadiff,Freq,zeros(1,length(Freq)))
end

%% Extraneous plot commands
% figure(5)
% subplot(2,2,1)
% plot(Freq,real(T11),Freq,imag(T11))
% title('T11')
% xlabel('Frequency [Hz]')
%
% subplot(2,2,2)
% plot(Freq,real(T12),Freq,imag(T12))
% title('T12')
% xlabel('Frequency [Hz]')
%
% subplot(2,2,3)
% plot(Freq,real(T21),Freq,imag(T21))
% title('T21')
% xlabel('Frequency [Hz]')
```

```
%
% subplot(2,2,4)
% plot(Freq,real(T22),Freq,imag(T22))
% title('T22')
% xlabel('Frequency [Hz]')
%
% figure(6)
% subplot(2,2,1)
% plot(Freq,real(z11),Freq,imag(z11))
% title('Z11')
% xlabel('Frequency [Hz]')
%
% subplot(2,2,2)
% plot(Freq,real(z12),Freq,imag(z12))
% title('Z12')
% xlabel('Frequency [Hz]')
%
% subplot(2,2,3)
% plot(Freq,real(z21),Freq,imag(z21))
% title('Z21')
% xlabel('Frequency [Hz]')
%
% subplot(2,2,4)
% plot(Freq,real(z22),Freq,imag(z22))
% title('Z22')
% xlabel('Frequency [Hz]')

% Clear unwanted variables

% clear coher1 coher2 coher3 coher4 coher5 coher6 coher 7
% clear Power1 Power2 Power3 Power4 Power5 Power6
% clear re1 re2 re3 re4 re5 re6 re7 im1 im2 im3 im4 im5 im6 im7
clear Rate index loopindex

% Output Data
% output1 = [Freq2 realR imagR R2 real(ATL)];
output5 = [Freq3 TL];
% output3 = [real(T11) imag(T11) real(T12) imag(T12) real(T21)...
%     imag(T21) real(T22) imag(T22)];

header = [Oil_Temp Liner_Temp];


rmpath([pwd,newpath])
```

APPENDIX C

EXTRA FIGURES AND DATA

C.1 Non-ideal Gas Behavior

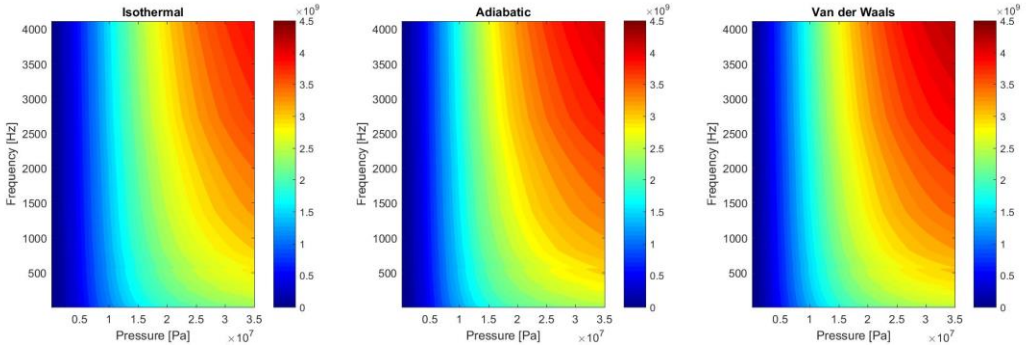

Figure C-1: Absolute bulk modulus for atmospheric IMP microspheres at 25 °C for three gas compression assumptions

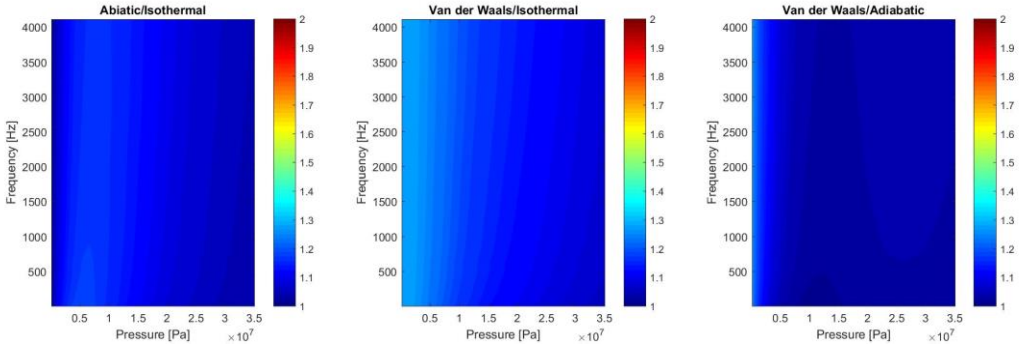

Figure C-2: Relative bulk modulus for atmospheric IMP microspheres at 25 °C for three gas compression assumptions

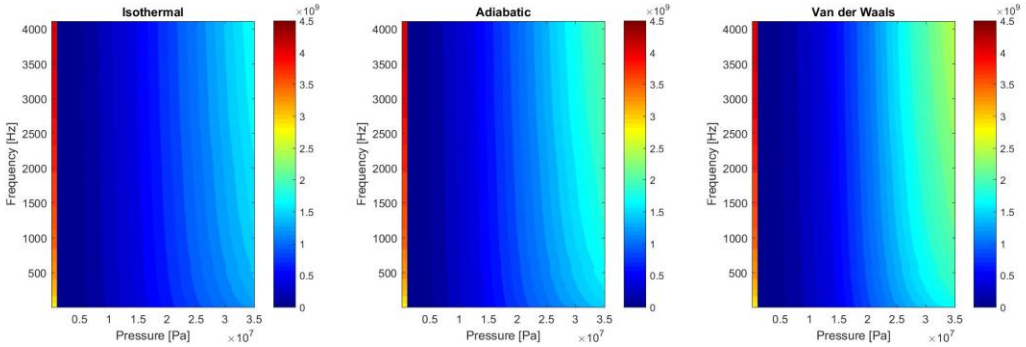

Figure C-3: Absolute bulk modulus for 1 MPa IMP microspheres at -40 °C for three gas compression assumptions

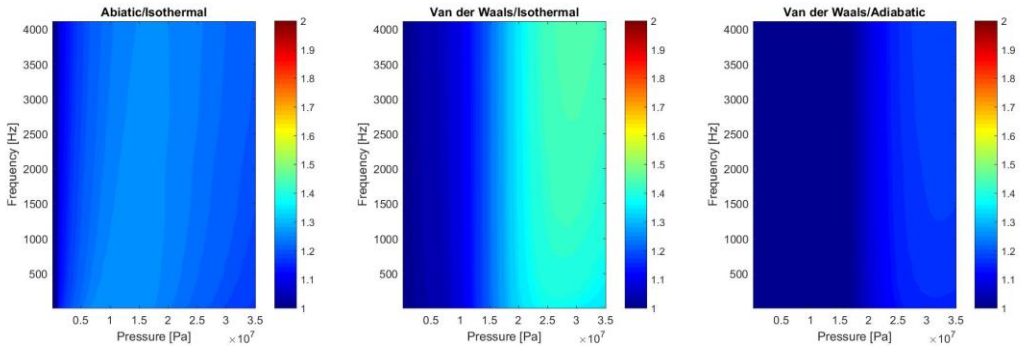

Figure C-4: Relative bulk modulus for 1 MPa IMP microspheres at -40 °C for three gas compression assumptions

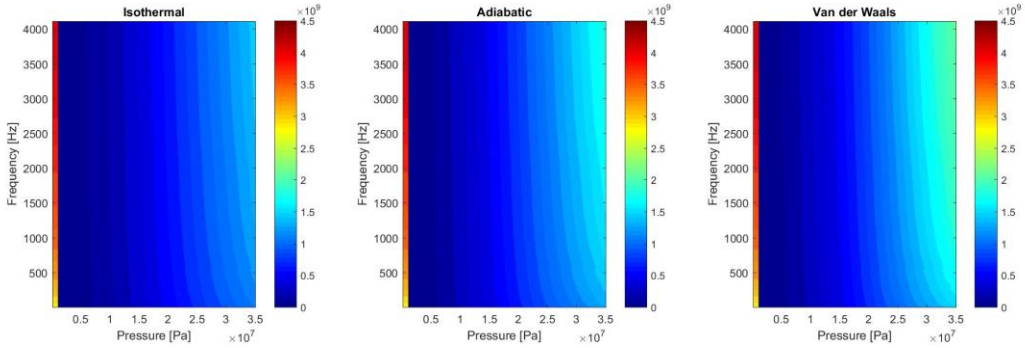

Figure C-5: Absolute bulk modulus for 1 MPa IMP microspheres at 25 °C for three gas compression assumptions

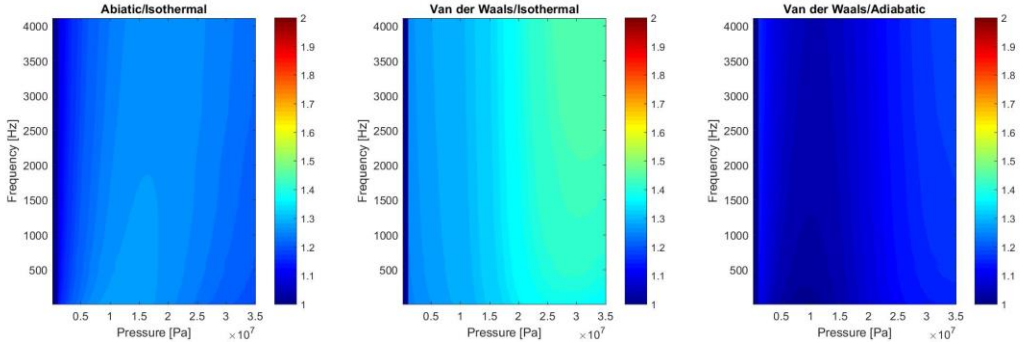

Figure C-6: Relative bulk modulus for 1 MPa IMP microspheres at 25 °C for three gas compression assumptions

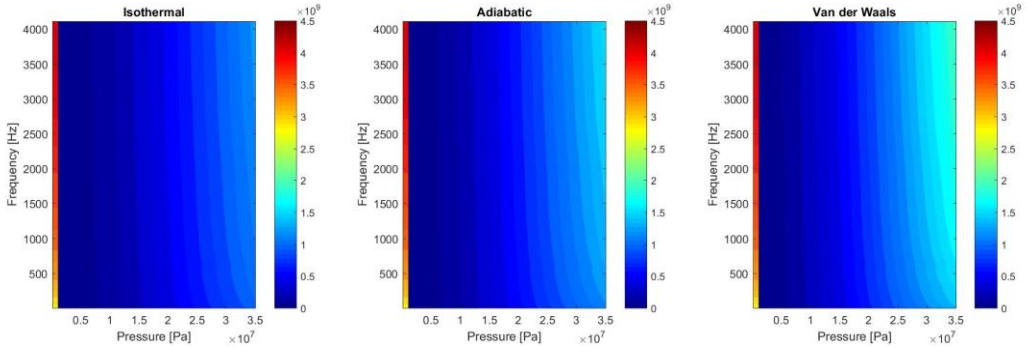

Figure C-7: Absolute bulk modulus for 1 MPa IMP microspheres at 100 °C for three gas compression assumptions

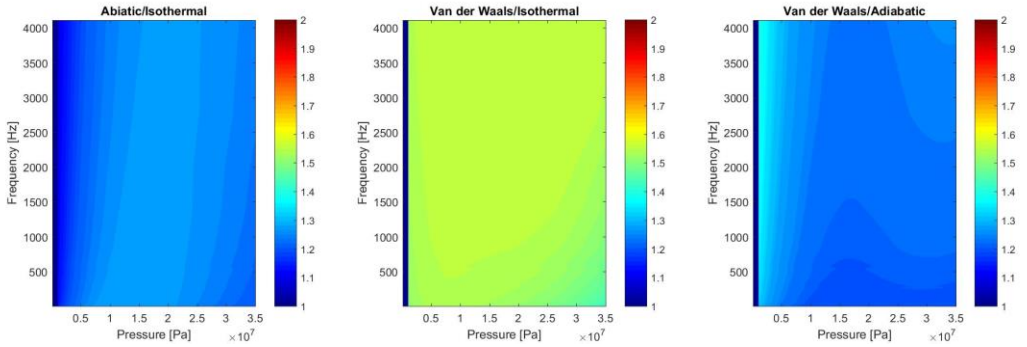

Figure C-8: Relative bulk modulus for 1 MPa IMP microspheres at 100 °C for three gas compression assumptions

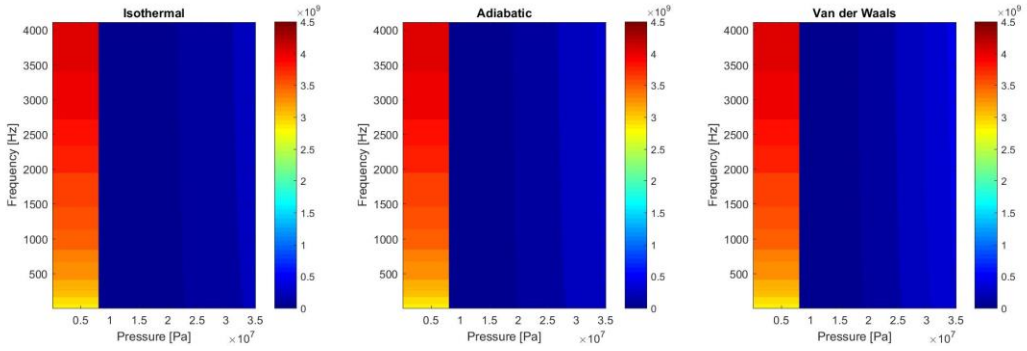

Figure C-9: Absolute bulk modulus for 8 MPa IMP microspheres at 25 °C for three gas compression assumptions

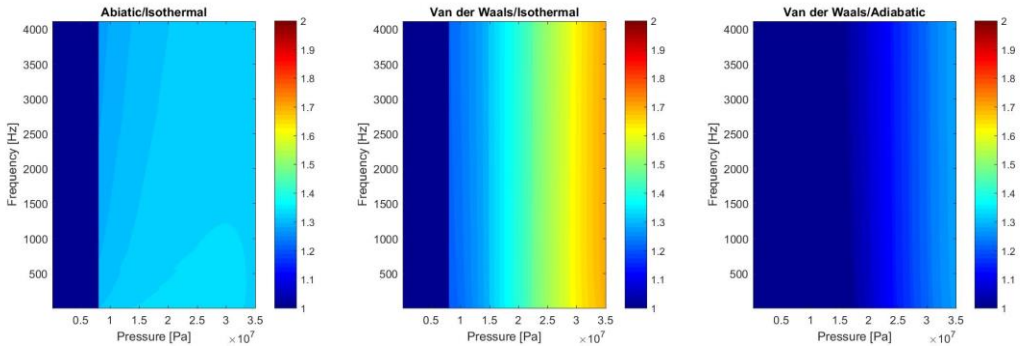

Figure C-10: Relative bulk modulus for 8 MPa IMP microspheres at 25 °C for three gas compression assumptions

APPENDIX D

Other polymers were tried for usage as the host but could not withstand the hydraulic environment well enough to provide satisfactory long-term noise control which fails the primary criteria for selecting a host polymer, as discussed in Section 4.1. Many suppliers provide an operational temperature range for their manufactured polymers but do not always provide data about resistance to fluids. Some manufactures provide volumetric swell for exposure to certain fluid exposures but this data does not cover mechanical property change. One polymer that was experimented on was a urethane-based polymer called Vytaflex 10 produced by Smooth-On. Another polymer considered for usage was a silicone based polymer called Sylgard 184 produced by Dow Corning. Neither polymer could interface with well enough with the hydraulic environment while accepting pressurized and fluorinated microspheres. In general, the composite foam would change properties after being exposed to elevated temperature or elevated pressure oil. The change in properties negatively affects the noise control performance of the foam and therefore will be referred to as ‘damaged foam’ within.

D.1 Vytaflex

Figure and Figure show the Vytaflex liner after transmission loss testing conducted similarly to the testing procedure in Section 6.2. The liner shrunk considerably during the test, it is not precisely known when the shrinkage occurred. Part of the liner also extruded into a port on the suppressor shell further indicating the material was not suitable for the environment, the port extrusion can be seen in Figure . In addition, gas

pockets formed under the surface of the liner; when some of the pockets were punctured with a knife a high-pitched squeak occurred indicating at least some of the pockets held residual pressure, the bubbles can be seen in Figure . It is currently unknown if the microsphere walls failed and the gas pockets were a result of the interior gases collecting, if the oil reacted with the host polymer or the heat of the system was enough to vaporize the polymer. The bulk modulus test plug, shown in Figure with another plug of the same initial dimensions, did show significant shrinkage but did not form any gas bubbles. The liner fabricated with a Vytaflex host also did not exhibit high transmission loss even at low pressures; therefore, Vytaflex is not a good candidate for usage in a hydraulic system.

Figure D-1: Damaged Vytaflex Foam after high pressure and temperature, port extrusion circled

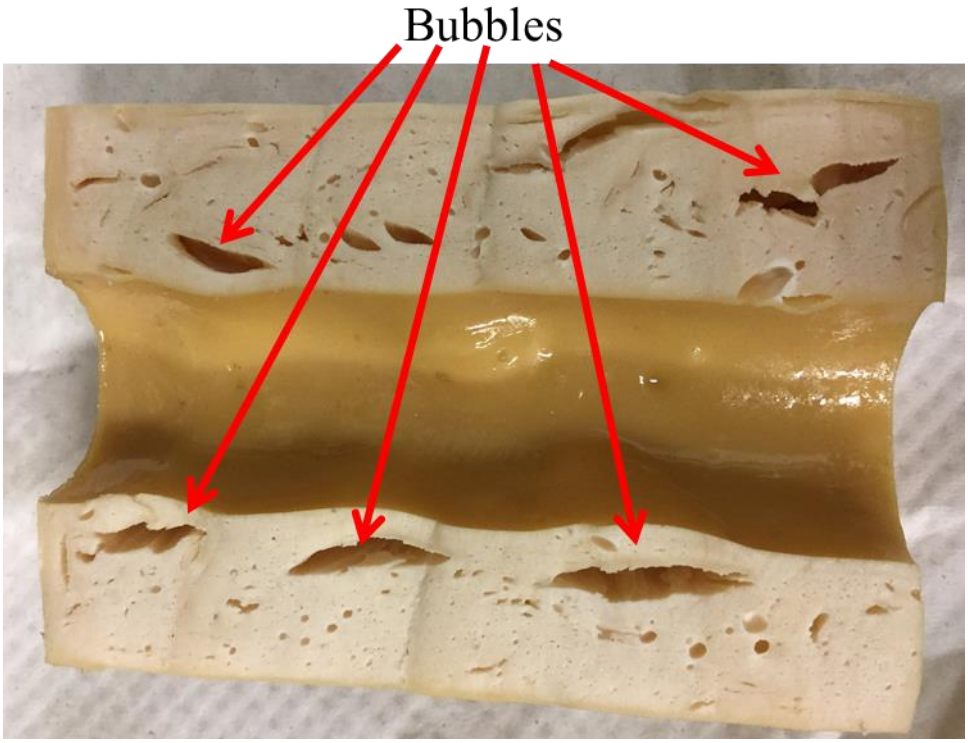

Figure D-2: Interior of failed Vytaflex liner

Figure D-3: Undamaged plug (left) damaged Vytaflex plug (right)

D.2 Sylgard 184

The foam samples with Sylgard 184 as the host matrix did not show the same degree of damage when being exposed to oil. Several of the bulk modulus plugs were tested without a skinned layer and showed no damage at all. However, a room-temperature cured liner also shrunk significantly when exposed to a transmission loss test, the shrunken liner is shown in Figure as compared to its initial size. The performance of bulk modulus plugs provided a basis that Sylgard could perform in the hydraulic environment; additional samples of Sylgard were cured at elevated temperature. Dow Corning, the manufacturer of Sylgard, lists curing times and temperatures up to 150 °C. However, the microspheres used within the foams become brittle above 125 °C, which limits their utility.

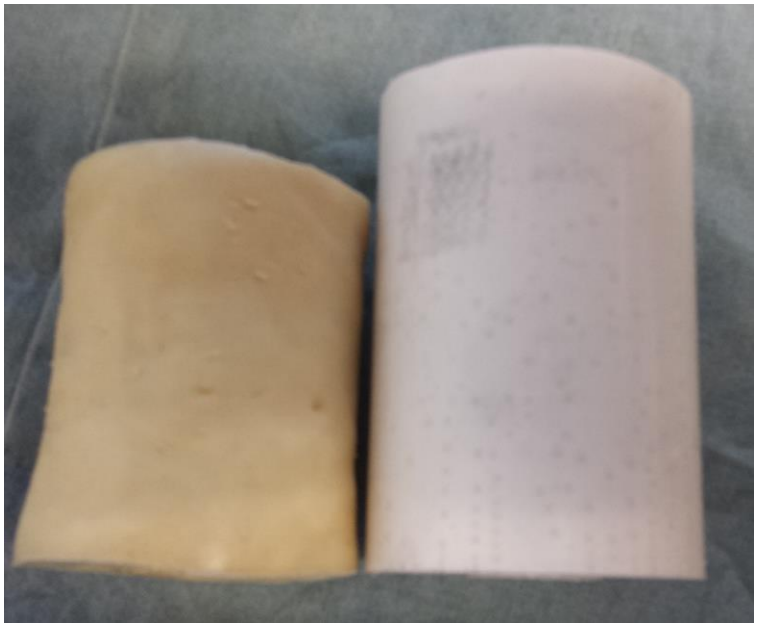

Figure D-4: Sylgard samples, after testing left before testing right

Figure shows a transmission loss comparison of three Sylgard foams: the first sample was cured at room temperature for 48 hours, the second sample was cured at 150 °C for two hours (the duration was short enough to not damage the microspheres) and the

third sample was cured at 100 °C for twenty hours as well as received a PTFE coating. The two elevated temperature cures had the highest transmission loss initially. The PTFE coated sample had a smaller drop-off in performance between the two test cases, which is why it was selected for usage going forward. In addition, the coating procedure was not refined for the sample analyzed; a more refined procedure will further reduce the noise control fall off. The transmission loss performance of the two heat cured samples at a system pressure of 2.07 MPa are compared in Figure . Again, the first run of the 150 °C cured foam exhibits the highest transmission loss but its second run exhibits the lowest transmission loss. The measured transmission loss for the two runs of the PTFE coated liner exhibit nearly identical transmission loss. The magnitude of the transmission loss may be slightly lower than the first run of the higher temperature uncoated foam, but the coated foam will exhibit better performance over its entire lifetime.

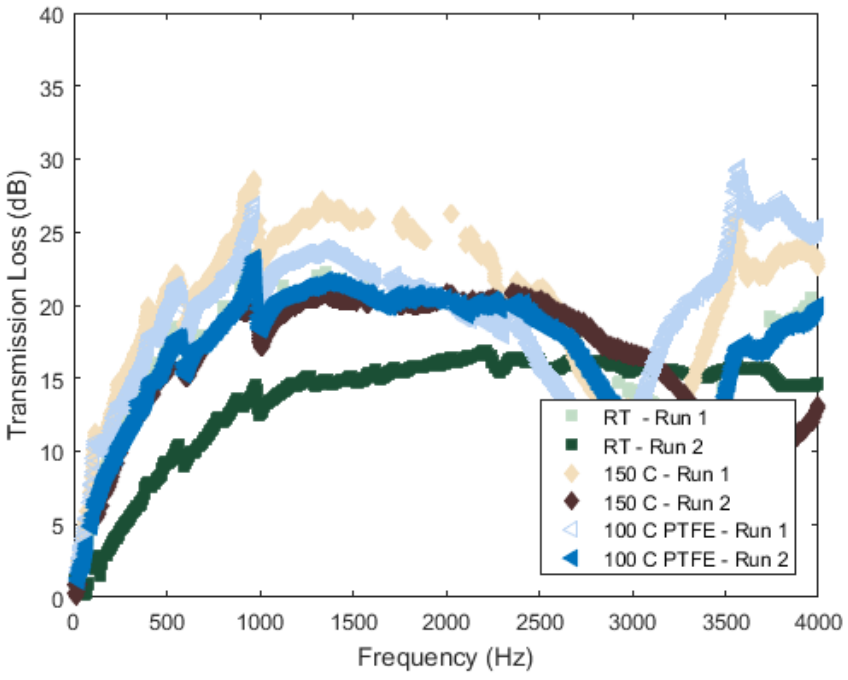

Figure D-5: Transmission loss differences between cure temperature and run numbers at a system pressure of 3.45 MPa

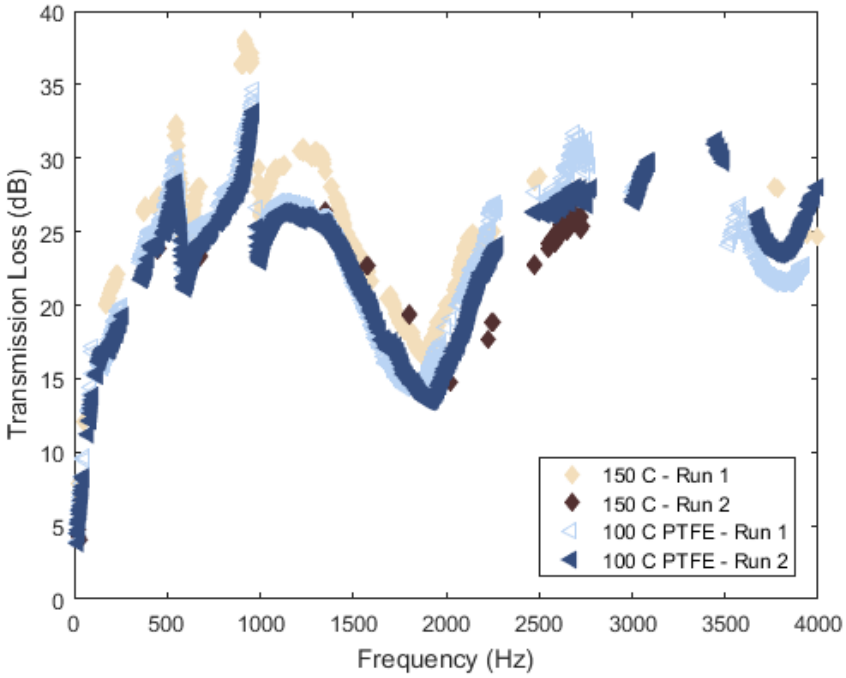

Figure D-6: Transmission loss differences between cure temperature and run numbers at a system pressure of 2.07 MPa

The bulk modulus of a sample of the room temperature cured foam which had been exposed to high temperature and pressure hydraulic oil was measured and compared to a sample which had not been exposed, the results of the measurement are shown in Figure . The bulk modulus of the exposed foam is significantly higher than the unexposed variant. In addition, the Poisson's ratio slightly reduces which increases the rate of bulk modulus increase with respect to system pressure. The change in properties after a single exposure to high pressure and high temperature oil prevent Sylgard 184 cured at room temperature from being a viable candidate for syntactic foam. However, elevated curing temperatures and coating prevent the mechanical property shift which allows Sylgard 184 to be used in the samples considered elsewhere in the dissertation.

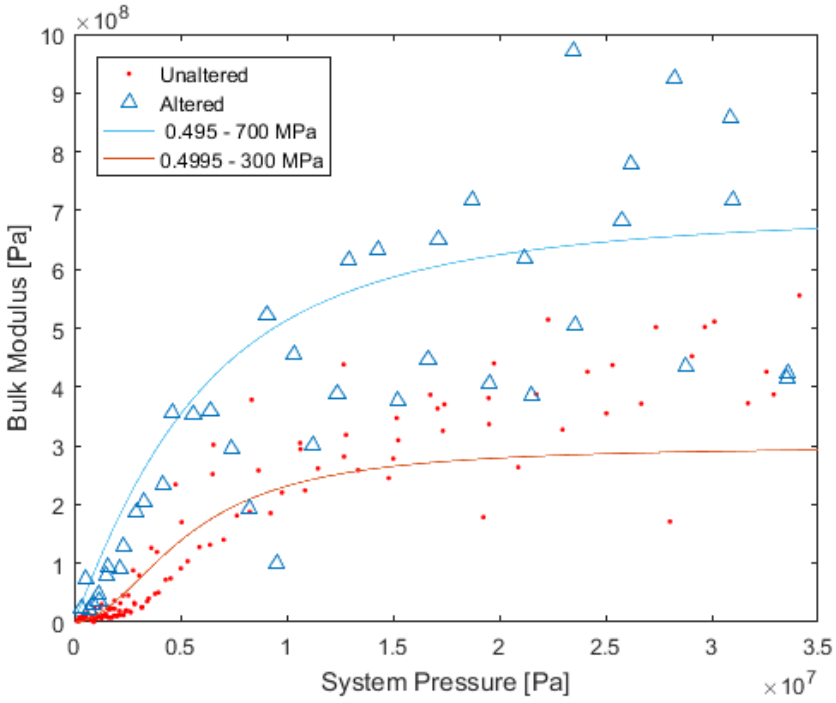

Figure D-7: Bulk modulus measurements of damaged and undamaged foam

It would seem that a heat-cured and PTFE coated Sylgard-based foam would be sufficient for usage in a hydraulic system; however, the heat curing at foam with pressurized and fluorinated microspheres causes the microspheres to expand and burst during curing. Figure shows the result of a failed cure. The right end has a smooth surface but is similarly porous to the sides when cut. The high number of pores increases the probability of shedding parts into the hydraulic test circuit increasing the likelihood of a system failure. The heat cure of a Sylgard-based foam is necessary for it to withstand the hydraulic environment but the pressurized and fluorinated microspheres cannot withstand a heat cure so Sylgard cannot be considered as a viable host polymer option.

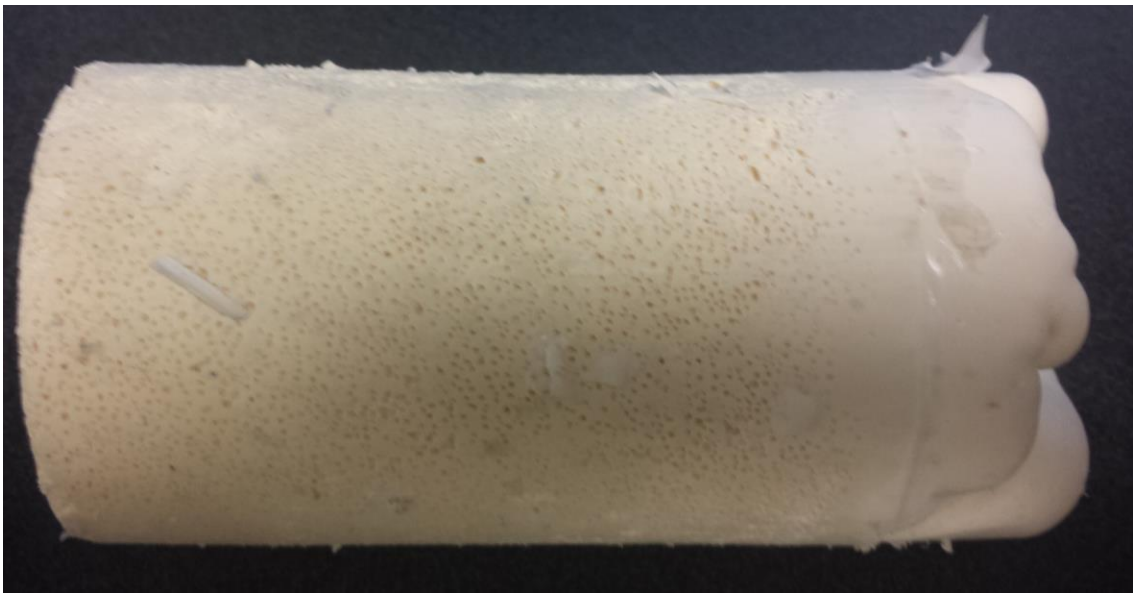

Figure D-8: Sylgard 184 foam with burst microspheres

REFERENCES

[1] E.R. Gruber, "Optimal Configuration of Adjustable Noise Suppressors," Master's of Science, Mechanical Engineering, Georgia Tech, 2013.

[2] K.A. Marek, E.R. Gruber, and K.A. Cunefare, *Linear Analytical Model for a Pressurized Gas Bladder Style Hydraulic Silencer*. International Journal of Fluid Power, 2013. **14**(2): p. 5-16.

[3] K.A. Marek, "The Modeling and Use of Syntactic Foams for Passive Control of Fluid-Borne Noise," Ph.D., Mechanical Engineering, Georgia Institute of Technology, Atlanta, GA, USA, 2014.

[4] N.E. Earnhart, "Modeling and validation of a syntactic foam lining for noise control devices for fluid power systems," Ph.D., Mechanical Engineering, Georgia Institute of Technology, Atlanta, GA, USA, 2012.

[5] N. Earnhart, K. Marek, and K. Cunefare. *The role of compliance in devices for reduction of fluid-borne noise*. in *7th FPNI PhD Symposium on Fluid Power*. 2012.

[6] S. Soveyni and R.B. Gillespie, *Cancellation of biodynamic feedthrough in vehicle control tasks.* Control Systems Technology, IEEE Transactions on, 2007. **15**(6): p. 1018-1029.

[7] O.S.H. Administration, *Occupational noise exposure: hearing conservation amendment*, in *Federal register*. 1983. p. 9738-9785.

[8] M. Monaghan, *Racket Busters.* SAE Off-Highway Engineering, 2014: p. 25-27.

[9] D.N. Johnston and K.A. Edge, *A Test Method for Measurement of Pump Fluid-Borne Noise Characteristics*, in *International Off-highway & Powerplant Congress and Exposition*. 1991: Milwaukee, WI.

[10] E.R. Gruber, et al., *Comparison of Noise Control Effectiveness Between Bladder-syle and Liner-style Hyrdaulic Noise Control Devices*, in *Internoise 2015*, C. Burroughs and G. Maling, Editors. 2015, Institute of Noise Control Engineering: San Francisco, CA, USA.

[11] R.D. Woodworth, J.F. Stoutamore, and P.S. Vanderhoek, *Digital fluid pressure flow rate and position control system*. 1985, Google Patents.

[12] K. Marek, N.E. Earnhart, and K. Cunefare, *Model and analysis of a cylinderical in-line hydraulic suppresor with a solid compressible liner.* Journal of Sound and Vibration, 2014. **333**: p. 6312-6331.

[13] L.L. Beranek and I. Ver, *Noise and Vibration Control Engineering Principles and Application*. 1992, New York, NY, USA: John Wiley & Sons.

[14] A. Einstein, *Investigations on the Theory of the Brownian Movement*. 1956: DoverPublications. com.

[15] J.D. Eshelby, *The Determination of the Elastic Field of an Ellipsoidal Inclusion, and Related Problems.* Proceedings of the Royal Society A: Mathematical, Physical and Engineering Sciences, 1957. **241**(1226): p. 376-396.

[16] Z. Hashin, *The Elastic Moduli of Heterogenous Materials.* Journal of Applied Mechanics, 1962. **29**: p. 143-150.

[17] R. Christensen and K. Lo, *Solutions for Effective Shear Properties in Three Phase Sphere and Cylinder Models.* Journal of the Mechanics and Physics of Solids, 1979. **27**: p. 315-330.

[18] C.C. Chen and M.C. Hastings, *Half-wavelength tuning cables for passive noise control in automotive power steering systems.* Active Control of Vibration and Noise, 1994. **75**(355-361).
[19] M.C. Hastings and C.C. Chen, *Analysis of tuning cables for reduction of fluidborne noise in automotive power steering hydraulic lines.* Journal of Passenger Cars, 1993. **P-264**: p. 1762-1767.
[20] N.E. Earnhart, K.A. Marek, and K.A. Cunefare, *Evaluation of Hydraulic Silences*, in *Noise-Con*. 2010: Baltimore, MD.
[21] L.E. Kinsler, et al., *Fundamentals of acoustics*. Fundamentals of Acoustics, 4th Edition, by Lawrence E. Kinsler, Austin R. Frey, Alan B. Coppens, James V. Sanders, pp. 560. ISBN 0-471-84789-5. Wiley-VCH, December 1999. Vol. 1. 1999.
[22] M. Ijas and T. Virvalo, *Experimental Verification of Pulsation Dampers and Their Simplified Theory*. Power Transmission and Motion Control, PTMC, 2000: p. 13-27.
[23] E. Arendt. *Pulsation Absorbing Devices*. USPTO Pat. No. 4,759,378 (1988).
[24] R.G. Wilkes, *Noise Reduction in Hydraulic Systems.* SAE Technical Paper 952154, 1995.
[25] G.T. Klees. *Attenuating device*. USPTO Pat. No. 3,323,305 (1967).
[26] J.G.M. Jenski and J.C. Shiery. *Noise Suppressor*. USPTO Pat. No. 5,735,313 (1998).
[27] J.C. Shiery. *Noise Suppressor*. USPTO Pat. No. 5,732,741 (1998).
[28] L.J. Eriksson, *Effect of inlet/outlet locations on hgiher order modes in silencers.* Journal of the Acoustical Society of America, 1982. **72**(4): p. 1208-1211.
[29] E.R. Gruber and K. Cunefare, *Optimization of Dissimilarly-Sized Dual In-line Suppressors*, in *International Fluid Power Exposition*. 2014, National Fluid Power Association: Las Vegas, NV, USA.
[30] E.R. Gruber and K. Cunefare, *Optimal Paired In-Line Bladder-Style Suppressors for Broadband Noise Control*, in *Scandinavian International Conference on Fluid Power*, K. Huhtala, Editor. 2015, Tampere University of Technology: Tampere, Finland.
[31] E.R. Gruber, et al., *Optimization of Single and Dual Suppressors Under Varying Load and Pressure Conditions.* International Journal of Fluid Power, 2013. **14**(3): p. 27-34.
[32] W.C. Young and R.G. Budynas, *Roark's formulas for stress and strain*. Vol. 6. 2002: McGraw-Hill New York.
[33] A. Grill, V.V. Patel, and S.M. Gates, *Multiphase low dielectric constant material*. 2001, Google Patents.
[34] J.D. Eshelby, *The Continuum Theory of Lattice Defects.* Solid State Physics, 1956. **3**: p. 79-144.
[35] W. Voigt, *Lehrbuch der kristallphysik:(mit ausschluss der kristalloptik)*. Vol. 34. 1910: BG Teubner.
[36] A. Reuss, *Berechnung der Fließgrenze von Mischkristallen auf Grund der Plastizitätsbedingung für Einkristalle.* ZAMM-Journal of Applied Mathematics and Mechanics/Zeitschrift für Angewandte Mathematik und Mechanik, 1929. **9**(1): p. 49-58.

[37] A. Einstein, *Eine neue bestimmung der moleküldimensionen.* Annalen der Physik, 1906. **324**(2): p. 289-306.
[38] A. Einstein, *Berichtigung zu meiner Arbeit:„Eine neue Bestimmung der Moleküldimensionen"* . Annalen der Physik, 1911. **339**(3): p. 591-592.
[39] D. Bruggeman, *Calculation of various physics constants in heterogeneous substances I Dielectricity constants and conductivity of mixed bodies from isotropic substances.* Annalen der Physik, 1935. **24**(7): p. 636-664.
[40] R. Roscoe, *The viscosity of Suspensions of Rigid Spheres.* British Journal of Applied Physics, 1952: p. 267-269.
[41] T.T. Mori, K., *Average Stress In Matrix and Average Elastic Energy of Materials with Misfitting Inclusions.* Acta Metallurgica, 1973. **21**: p. 571-574.
[42] Y. Benveniste, *A New Approach to the Application fo Mori-Tanaka's Theory in Composite Materials.* Mechanics of Materials, 1987. **6**: p. 147-157.
[43] Z. Hashin, *The elastic moduli of heterogenous materials.* Office of Naval Research, 1960.
[44] Z. Hashin and B.W. Rosen, *The Elastic Moduli of Fiber-Reinforced Materials.* Journal of Applied Mechanics, 1964: p. 223-232.
[45] Z. Hashin and S. Shtrikman, *A Variational Approach to the Theory of the Elastic Behaviour of Multiphase Materials.* Journal of the Mechanics and Physics of Solids, 1963. **11**: p. 127-140.
[46] R. Christensen, *A Critical Evaluation for a Class of Micro-Mechanics Models.* Journal of the Mechanics and Physics of Solids, 1990. **38**(3): p. 379-404.
[47] R.A. Salmon, "Development of a Second Generation Liner-Style Hydraulic Suppressor," Master's, Georgia Institute of Technology, 2015.
[48] M.L. Williams, R.F. Landel, and J.D. Ferry, *The temperature dependence of relaxation mechanisms in amorphous polymers and other glass-forming liquids.* Journal of the American Chemical Society, 1955. **77**(14): p. 3701-3707.
[49] M.J. Moran, et al., *Fundamentals of engineering thermodynamics*. 2010: John Wiley & Sons.
[50] *Compressibility Chart*. 2016 10-27-2016].
[51] S.-E. Silicone. *Characteristic properties of Silicone Rubber Compounds*. 2012 [cited 2016 February 4].
[52] Z. Bazant, *A correlation study of formulations of incremental deformation and stability of continuous bodies.* Journal of Applied Mechanics, 1971. **38**(4): p. 919-928.
[53] J. Crank, *The Mathematics of Diffusion*. 1979: Oxford University Press.
[54] J. Brandrup, et al., *Polymer handbook.* Vol. 89. 1999: Wiley New York.
[55] A.P. Kharitonov and Y.L. Moskvin, *Direct fluorination of polystyrene films.* Journal of Fluorine Chemistry, 1998. **91**: p. 87-93.
[56] R.J. Lagow and J.L. Margrave, *Direct fluorination: a "new" approach to fluorine chemistry.* Progress in Inorganic Chemistry, Volume 26, 1979: p. 161-210.
[57] T. Graham, *On the absorption and dialytic separation of gases by colloid septa.* Philosophical transactions of the Royal Society of London, 1866. **156**: p. 399-439.
[58] W.C. Young and R.G. Budynas, *Roark's formulas for stress and strain*. Vol. 7. 2002: McGraw-Hill New York.

[59] J.D. Renton, *On the Buckling of Thick Spherical Shells Under Normal Pressure.* International Journal of Solids and Structures, 1981. **17**: p. 145-153.
[60] ISO-15086-1, *Hydraulic fluid power - Determination of fluid-borne noise characteristics of components and systems*, in *Introduction*. 2001, International Standards Organization: Geneva, Switzerland.
[61] ISO-15086-2, *Hydraulic fluid power - Determination of fluid-borne noise characteristics of components and systems*, in *Measurement of speed of sound in a fluid in a pipe*. 2000, International Standards Organization: Geneva, Switzerland.
[62] ISO-15086-3, *Hydraulic fluid power - Determination of the fluid-borne noise characteristics of components and systems*, in *Measurement of hydraulic impedance*. 2008, International Standards Organization: Geneva, Switzerland.
[63] D.N. Johnston, D.K. Longmore, and J.E. Drew, *A Technique for the measrurement of the transfer matrix characteristices of two-port hydraulic components*, in *Fluid Power Systems and Technology*. 1994, ASME.
[64] A.D. Pierce, *Acoustics: An Introduction to Its Physical Properties and Applications*. 1989, Melville, NY: Acoustical Society of America.
[65] R. Haas, A. Tairych, and B. Manhartsgruber, *Adiabatic and Isothermal fluid bulk modulus-common theories and model verification*, in *The 7th FPNI PhD Symposium on Fluid Power*. 2012.
[66] R.S. Farr, *Random close packing fractions of lognormal distributions of hard spheres.* Powder technology, 2013. **245**: p. 28-34.